THE ROLE OF GLYCOGEN SYNTHASE KINASE-3 (GSK-3) PROTEIN IN THE DEVELOPMENT OF MYOCARDIAL HYPERTROPHY IN A RAT MODEL OF DIET INDUCED OBESITY AND INSULIN RESISTANCE

Tandekile Lubelwana Hafver

Dissertation presented in complete fulfilment of the requirements for the degree

Master of Science in Medical Sciences

Department of Biomedical Sciences

Division of Medical Physiology

University of Stellenbosch

Supervisor: Professor Barbara Huisamen

Co-supervisor: Professor Amanda Lochner

March 2012

Declaration

By submitting this thesis electronically, I declare that the entirety of the work contained therein is my own, original work, that I am the sole author thereof (save to the extent explicitly otherwise stated), that reproduction and publication thereof by Stellenbosch University will not infringe any third party rights and that I have not previously in its entirety or in part submitted it for obtaining any qualification.

Signature:..................................... Date:...

Confirmation of contributions by principal researchers and fellow researchers

I hereby declare that the work contained in this thesis is my own contribution. Dr Benjamin Loos at Stellenbosch University (main campus) assisted with the fluorescent microscopy experiments. Dr Neil Davies and Sarah-Kate Sharp at the University of Cape Town assisted with the echocardiography experiments.

Confirmation of contributions by principal researchers and fellow researchers

ABSTRACT

Introduction: The worldwide escalation in the incidence of obesity and its strong association with insulin resistance, type 2 diabetes and the cardiovascular complications that accompany these disease states have elicited interest in the underlying mechanisms of these pathologies. Preliminary data generated in our laboratory showed that obesity is associated with abnormalities in the insulin signalling pathway. Specifically, we found a down-regulation of protein kinase B (PKB/Akt), which is known to mediate the metabolic effects of insulin. One of the downstream targets of PKB/Akt is glycogen synthase kinase-3 (GSK-3), which is inhibited by this phosphorylation. Detrimental effects of unopposed activity of GSK-3 have recently been described. This may play a pivotal role in some of the adverse consequences of insulin resistance in the heart.

Hypothesis: Chronic inhibition of GSK-3 will induce myocardial hypertrophy or exacerbate the development of existing hypertrophy in a pre-diabetic model of diet induced obesity and insulin resistance.

Objectives: (1) Assess the extent of the development of myocardial hypertrophy in a rat model of diet induced obesity (DIO) and insulin resistance. (2) Assess the effect of inhibition of GSK-3 protein on the development of myocardial hypertrophy.

Methods: Two groups of age-matched male Wistar rats were used. Control animals received standard rat chow, while obese animals received a high caloric diet for 20 weeks. After 12 weeks, half of the animals in both groups received GSK-3 inhibitor treatment (CHIR118637, 30mg/kg/day, Novartis). At the end of 20 weeks, three series of experiments were conducted. (i) The animals were subjected to echocardiography to determine *in vivo* myocardial function, and biometric, metabolic and biochemical parameters were evaluated.

(ii) The ability of the cardiomyocytes to accumulate deoxy-glucose after stimulation with insulin was determined, and (iii) the localization of key proteins was monitored using fluorescence microscopy and cell size was determined using light microscopy and flow activated cell sorter analysis.

Results and discussion: The high caloric diet increased body weight ($p < 0.005$) and intra-peritoneal fat mass ($p < 0.01$) when compared to controls. Complications associated with obesity, such as impaired glucose tolerance ($p < 0.05$), hyperinsulinemia ($p < 0.0005$) and an increased HOMA-IR index ($p < 0.01$) were observed. Additionally, cardiomyocytes from the DIO animals had a significantly impaired response to insulin, specifically when 10nM ($p < 0.05$) and 100nM ($p < 0.05$) of insulin were used as stimulus. We also found a dysregulation in PKB/Akt, indicated by a down-regulation of phosphorylated PKB/Akt ($p < 0.01$). The diet promoted the development of myocardial hypertrophy, since the ventricular weight ($p < 0.05$) and ventricular weight to tibia length ratio were increased ($p < 0.01$). Echocardiography experiments showed an increase in end diastolic diameter in the DIO animals ($p < 0.05$). Additionally, there was an increase in the cardiomyocyte cell width in the DIO rats ($p < 0.0001$) and a tendency for peri-nuclear localization of NFATc3. GSK-3 inhibition promoted the development of insulin resistance in control animals, as indicated by an increase in the body weight ($p < 0.05$), serum insulin levels ($p < 0.01$) and HOMA-IR index ($p < 0.01$). In the DIO animals, the GSK-3 inhibitor treatment improved insulin resistance, as a decrease in serum insulin concentration ($p < 0.05$) was observed. The cardiomyocytes from the treated DIO animals also showed an increase in glucose uptake ($p < 0.05$) when stimulated with 100nM of insulin. The GSK-3 inhibitor promoted the development of myocardial hypertrophy in the control animals, indicated by an increase in ventricular weight ($p < 0.05$) and cardiomyocyte cell width ($p < 0.0001$), but did not exacerbate hypertrophy in the DIO animals.

Conclusion: Both the high caloric diet and the GSK-3 inhibitor promoted the development of insulin resistance and myocardial hypertrophy in the rats. In the DIO animals the GSK-3 inhibitor treatment ameliorated insulin resistance and did not promote the further development of myocardial hypertrophy.

OPSOMMING

Inleiding: Die huidige styging in vetsugtigheid en die sterk assosiasie daarvan met insulien weerstandigheid, tipe 2 diabetes en kardiovaskulêre komplikasies soos hipertrofie, het 'n belangstelling in die onderliggende meganismes van hierdie siektetoestande ontlok. Voorlopige data uit ons laboratorium het getoon dat vetsug geassosieerd is met abnormaliteite in die insulien seintransduksie-pad soos byvoorbeeld 'n afregulering van miokardiale proteïen kinase B (PKB/Akt), wat bekend is om die metaboliese effekte van insulien te medieer. Een van die proteïene wat deur PKB/Akt gefosforileer en daardeur geïnhibeer word, is glikogeen sintase kinase-3 (GSK-3). Negatiewe effekte van onge-opponeerde aktiwiteit van GSK-3 is beskryf en dit mag 'n sleutelrol speel in sommige van die nadelige gevolge van insulien weerstandigheid in die hart.

Hipotese: Chroniese onderdrukking van GSK-3 sal miokardiale hipertrofie ontlok of die bestaande hipertrofie in 'n pre-diabetiese model van dieet-geïnduseerde vetsug en insulien weerstandigheid vererger.

Doelstellings: (1) Om die omvang van die ontwikkeling van miokardiale hipertrofie in 'n rotmodel van dieet-geïnduseerde vetsug te ondersoek en (2) om die effek van inhibisie van GSK-3 op die ontwikkeling van hipertrofie te ondersoek.

Metodes: Ouderdomsgepaarde manlike Wistarrotte is in hierdie studie gebruik. Die diere is vir 'n periode van 20 weke aan verskillende diëte onderwerp, naamlik standaard kommersiële rotkos vir die kontrole diere en 'n hoë kalorie dieet vir die eksperimenteel vet diere (DIO). Helfte van elke groep diere is vir 8 weke met 'n GSK-3 inhibitor behandel (CHIR118637, 30mg/kg/day, Novartis). Na die 20 weke is 3 eksperimentele reekse uitgevoer: (i) Die diere is eggokardiografies ondersoek om *in vivo* miokardiale funksie te bepaal en biometriese, metaboliese en biochemiese parameters is evalueer.

(ii) Die vermoë van kardiomiosiete om de-oksiglukose na insulien stimulasie te akkumuleer, is bepaal, en (iii) die lokalisering van sleutelproteïene is met behulp van fluoressensie mikroskopie en die selgrootte met behulp van ligmikroskopie bepaal.

Resultate en bespreking: Die hoë kalorie dieet het gepaard gegaan met 'n beduidende toename in liggaamsgewig (p<0.005) en intraperitoneale vetmassa (p<0.01) in vergelyking met diere op die kontrole dieet. Newe-effekte geassosieerd met vetsug nl. onderdrukte glucose toleransie (p<0.05), hiperinsulinemie (p<0.0005) en 'n verhoogde HOMA-IR index (p<0.01) is ook waargeneem. Daar was ook 'n beduidend ingekorte respons van glukose opname deur kardiomiosiete van die vet diere na stimulasie met 10nM (p<0.05) en 100nM (p<0.05) insulien. Disregulering van PKB/Akt is gevind in die vorm van 'n afregulering van die fosforilering van die proteïen (p<0.01). Die dieet het ook gelei tot die ontwikkeling van miokardiale hipertrofie aangesien die ventrikulêre gewig (p<0.05) asook die verhouding van die ventrikulêre gewig teenoor tibia lengte beduidend toegeneem het (p<0.01). Eggokardiografie het 'n toename in ventrikulêre end-diastoliese dimensie in die DIO diere aangetoon (p<0.05). Tesame hiermee het die breedte van kardiomiosiete van die DIO diere toegeneem (p<0.0001) en daar was ook 'n peri-nukluêre lokalisering van NFATc3. Behandeling van kontrole diere met 'n GSK-3 inhibitor het insulienweerstandigheid ontlok soos afgelei uit 'n verhoging in liggaamsgewig (p<0.05), serum insulien-vlakke (p<0.01) en die HOMA-IR waarde (p<0.01). In teenstelling het behandeling van die DIO diere met die GSK-3 inhibitor tot 'n verbetering van insulienweerstandigheid gelei aangesien 'n verlaging in serum insulien konsentrasies gevind is (p<0.05). Kardiomiosiete vanaf die behandelde DIO diere het ook 'n verhoogde insulien-gestimuleerde glukose opname met 100nM insulien getoon (p<0.05).

Behandeling met die GSK-3 inhibitor het die ontwikkeling van miokardiale hipertrofie in die kontrole diere teweeggebring, soos aangetoon deur 'n toename in die ventrikulêre gewig (p<0.05) en 'n groter selwydte in kardiomiosiete terwyl dit geen invloed op die bestaande hipertrofie van die vet diere gehad het nie.

Gevolgtrekking: Die huidige studie het getoon dat die betrokke dieet asook behandeling met 'n GSK-3 inhibitor insulienweerstandigheid sowel as die ontwikkelling van miokardiale hipertrofie in rotte ontlok. In die DIO diere het die behandeling met die GSK-3 inhibitor bloedglukose en insulien-vlakke verlaag en het nie hipertrofie vererger nie.

ACKNOWLEDGEMENTS

TABLE OF CONTENTS

LIST OF ABBREVIATIONS

Units of measurement

%	Percentage
˚C	Degree Celsius
µg	Microgram
µl	Microlitre
µm	Micrometer
AU	Arbitrary Units
cm	Centimetre
dl	Decilitre
g	Gram
g	Gravity
IU	International Unit
kDa	Kilo Dalton
kg	Kilogram
kj	Kilojoules
L	Litre
M	Molar
mg	Milligram

min	Minute
ml	Millilitre
mm	Millimetre
mM	Millimolar
ng	Nanogram
nM	Nanomolar
pMol	Pikomolar
rpm	Revolutions per minute
w/d	Wet -to-dry weight ratio

II   CHEMICAL COMPONENTS

2DG	2-deoxy-D-[^{3}H] glucose
BDM	Butanedione monoxime
BSA	Bovine serum albumin
Ca^{2+}	Calcium
$CaCl_2$	Calcium chloride
CO_2	Carbon dioxide
$CuSO_4$	Copper sulfate
EDTA	Ethylenediaminetetraacetic acid
EGTA	Ethyleneglycoltetraacetic acid
H_2O	Water
HCl	Hydrochloric acid
KCl	Potassium chloride

KH_2PO_4	Potassium dihydrogen phosphate
$MgSO_4$	Magnesium sulphate
Na^+	Sodium
Na_2CO_3	Disodium carbonate
Na_2HPO_4	Sodium Phosphate
NaH_2PO_4	Sodium dihydrogen phosphate
NaK^+ tartrate	Sodium potassium tartrate
$NaOH$	Sodium hydroxide
Na_2SO_4	Sodium sulphate
$NaCl$	Sodium chloride
$NaHCO_3$	Sodium bicarbonate
NADH	Nicotinamide adenine dinucleotide
NADPHOX	Nicotinamide adenine dinucleotide phosphate oxidase
Na_3VO_4	Sodium orthovanadate
O_2	Oxygen
PMSF	Phenylmethyl sulfonyl fluoride
PVDF	Polyvinylidene fluoride
TBS	Tris-buffered saline
TTC	Triphenyltetrazolium chloride

OTHER

AKT   See PKB

ANOVA   Analysis of variance

APS   Adaptor protein

BMI   Body mass index

CAP   Cbl-associated protein

CbI   Casitas b-lineage lymphoma

CVD   Cardiovascular disease

DAG   Diacylglycerol

DIO   Diet-induced-obesity

ECL   Enhanced chemiluminescence

EDD   End-diastolic diameter

EF   Ejection fraction

ELISA   Enzyme-linked immunosorbent assay

ERK   Extracellular signal-regulated kinase

ESD   End-systolic diameter

FFA   Free fatty acid

FS   Fractional shortening

GH   Growth hormone

GLUT1/4	Glucose transporter 1/4
Grb2	Growth factor receptor-bound protein 2
GS	Glycogen synthase
GSK-3	Glycogen synthase kinase-3
HCD	High caloric diet
HDL	High-density lipoprotein
HOMA	Homeostasis model assessment
IGF	Insulin like growth factors
IL-6	Interleukin-6
IP	Intraperitoneal
IP3	Inositol trisphosphate
IR	Insulin receptor
IRSs	Insulin receptor substrates
LDL	Low-density lipoprotein
LV	Left ventricle
LVH	Left ventricular hypertrophy
MAP	Mitogen activated protein
MEK	See MAP
mSOS	Murine son of sevenless

n	Sample number
NHANES	National Health and Nutrition Examination Survey
NIH	National Institute of Health
NO	Nitric oxide
PAI-1	Plasminogen activating inhibitor-1
PDK1	Phosphoinositide-dependent protein kinase 1
PH	Pleckstrin homology
PI(3,4,5)P3	Phosphatidylinositol-3, 4-, 5-phosphate
PI3K	Phosphoinositide-3 kinase
PIP2	Phosphatidyl inositol (4,5) bisphosphate
PKB/AKT	Protein kinase B
PKC	Protein kinase C
Raf 1	Rapidly accelerated Fibrosarcoma
RAS	Renin-angiotensin system
SDS-PAGE	Sodium dodecyl sulfate–polyacrylamide gel electrophoresis
SEM	Standard error of the mean
Ser	Serine
SRC	Standard rat chow

Thr	Threonine
TNF-α	Tumor necrosis factor-α
Tyr	Tyrosine
VLDL	Very low-density lipoproteins
WHO	World Health Organization
α	Alpha
β	Beta

LIST OF FIGURES

LIST OF TABLES

PROBLEM STATEMENT

The worldwide escalation in the incidence of obesity and its strong association with insulin resistance, type 2 diabetes and the cardiovascular complications that accompany these disease states have elicited interest in the underlying mechanisms of these pathologies (Gregor MF and Hotamisligil GS, 2011; Galassi A *et al.,* 2006). Aberrant protein kinase signalling has been implicated in obesity associated insulin resistance, diabetes and the resulting cardiovascular phenotype seen in obese patients (Eldar-Finkelman H *et al.,* 2010). In insulin resistance, insulin is unable to fully activate protein kinase B also known as Akt (PKB/Akt). One of the downstream targets of this protein is glycogen synthase kinase-3 (GSK-3). Detrimental effects of unopposed activity of GSK-3, also in the heart, have recently been described (Henriksen EJ and Dokken BB, 2006). This may stand central to some of the adverse consequences of insulin resistance in the heart. The role of GSK-3 in the development of the cardiovascular complications of obesity and insulin resistance, is currently unknown.

MOTIVATION FOR RESEARCH

In our quest to understand the causes and aetiology of the development of cardiovascular pathology in obesity, we have focused on the insulin signalling pathway. Our laboratory uses a pre-diabetic model of diet induced obesity and insulin resistance. Preliminary data generated in our laboratory showed that there are abnormalities in the insulin signalling pathway (Huisamen *et al.,* 2011). One of the abnormalities observed in this pathway, is that cardiomyocytes from these pre-diabetic hearts are insensitive to insulin stimulation. Specifically, we found a down-regulation of PKB/Akt, which is known to mediate the metabolic effects of insulin such as glycogen synthesis and glucose uptake (Huisamen *et al.,* 2011).

This data corroborates the findings of Henriksen EJ and Dokken BB (2006). Additionally, it was found that this down-regulation of PKB/Akt is associated with GSK-3 protein up-regulation in skeletal muscle of both obese rodents and type 2 diabetic humans (Henriksen EJ and Dokken BB, 2006). This up-regulation of GSK-3 is thus linked with a decrease in whole body insulin sensitivity and attenuated glucose uptake by peripheral tissue (Michael A *et al.,* 2004). These abnormalities have lead to the hypothesis that since increased GSK-3 activity may also in turn, via serine phosphorylation of IRS-1, result in impaired insulin signalling, inhibition of GSK-3 should mirror the actions of insulin, thereby reducing the production of glucose by enhancing glucose storage to combat the hyperglycemia seen in the insulin resistant state and type 2 diabetes (Sutherland C, 2011).

GSK-3 is a serine/threonine protein kinase that was discovered in the early 1980s as an enzyme involved in regulation of glucose metabolism (Park KW *et al*., 2003). Since its discovery, its function has been extended to a multitude of cellular processes. GSK-3 is described as a unique protein kinase, because, unlike most protein kinases, it is active in resting cells and becomes deactivated when cells are stimulated by hormones such as insulin, endothelial growth factor and platelet growth factor (Lee J and Kim MS, 2007; Woodgett JR, 1994; Ciaraldi TP *et al.,* 2007). It regulates glucose metabolism in the insulin signalling pathway as follows (Lee J and Kim MS, 2007): Upon insulin stimulation the linear signalling cascade is activated starting with the insulin receptor (IR), insulin receptor substrates (IRSs), phosphoinositide-3 kinase (PI3K) and PKB/Akt, leading to the phosphorylation of GSK-3α/β at specific Serine-21/9 residues, thereby inactivating GSK-3's kinetic activity (Woodgett JR, 2001). This inactivation leads to a decrease in phosphorylation of glycogen synthase (GS), resulting in its activation, which promotes glycogen synthesis (Eldar-Finkelman H, 2002). GSK-3 regulates protein synthesis in a similar fashion, where phosphorylation of GSK-3α/β by PKB/Akt at specific Serine-21/9 residues also leads to its inactivation.

This subsequently leads to the activation of the translation initiation factor 2B (eIF2B), resulting in an increase in protein synthesis (Welsh GI and Proud CG, 1993; Welsh GI *et al.,* 1997). Chronic inhibition of GSK-3 thus poses a serious problem because it may result in an increase in protein synthesis, hence resulting in the development of myocardial hypertrophy. This hypothesis is further supported by the fact that inactive GSK-3 also influences the activity of transcription factors, such as nuclear factor of activated T cell-c3 (NFATc3) and GATA-4. Active GSK-3 represses the actions of NFATc3 and GATA-4; thus inactivation relieves this repression and as a result these transcription factors enter the nucleus where they initiate the transcription of genes implicated in the development of myocardial hypertrophy (Graef IA *et al.,* 1999; Morisco C *et al.,* 2001).

CHAPTER 1: LITERATURE REVIEW

1.1 The epidemiology of obesity

Obesity is a fast growing problem that is reaching epidemic proportions worldwide (James PT *et al.,* 2004). Obesity related death is the second largest environmental cause of death, accounting for more than 300 000 deaths per year in the United States (Mokdad AH *et al.,* 2001). Obesity in countries such as Brazil, China and Sub-Saharan Africa, including South Africa, is also increasing rapidly and exceeds levels reported in affluent countries (Kelly T *et al*., 2008). According to the World Health Organization, more than 1 billion adults worldwide are overweight, 300 million of whom are obese (World Health Organization, 2011). The World Health Organization has further projected that by 2015 there will be about 2.3 billion overweight adults, 700 million of whom will be obese. The National Health and Nutrition Examination Survey (NHANES) also reported that the prevalence of obesity in children and adolescents has tripled between 1980 and 2002 (Ogden CL *et al.,* 2006). In 2002, the obesity epidemic in South Africa was as high as 29% in men and 56% in women (Puoane T *et al.,* 2002). This increasing prevalence is projected to decrease the life expectancy of current and future generations because obesity is associated with various co-morbidities such as insulin resistance, type 2 diabetes mellitus, dyslipidaemia, hypertension, stroke and coronary artery disease (Olshansky SJ *et al.,* 2005; Björntorp P *et al*., 1988). More importantly, obesity has long been recognised as an independent risk factor for cardiovascular disease (CVD) (Hubert HB *et al.,* 1983).

Major scientific advances in our understanding of the molecular pathways leading to insulin resistance and type 2 diabetes have been made during the last 10–15 years. However, these disease states still pose significant limitations when it comes to treatment. Understanding the pathophysiology in obesity induced insulin resistance and type 2 diabetes mellitus might advance this quest for novel treatment options.

1.2   Definition of obesity

Obesity is defined as a medical condition in which excess body fat has accumulated to the extent that it may have an adverse effect on health (Lopaschuck GD, 2007). Rapidly changing life conditions, including the easy availability of energy-dense diets (increased fat and sugar intake), coupled with reduced physical activity, resulting mostly from the transfer to a Western lifestyle, are considered to be the most important factors in the development of obesity (Grundy MS, 2004; Hicks R, 2006). Genetic factors play a decisive role in a minority of cases, and in most cases only because of an inborn predisposition (Parizkova J *et al.,* 2007). The degree of obesity is most often evaluated using the body mass index (BMI). BMI is defined as weight in kilograms divided by height in meters squared (kg/m^2); this measurement correlates strongly with total body fat content in adults. Accordingly, a BMI value of 25 is the cut-off value most used to characterize normal weight. Values of 25–30 characterize an overweight individual, while 30–35 characterizes the 1st degree, 35–40 the 2nd degree, and 40–45 the 3rd degree of obesity (National Institute of Health (NIH) 1998; WHO 2000). Unfortunately, BMI fails to consider body fat distribution. There is a growing body of evidence which shows that visceral fat (often referred to as abdominal or central obesity), is more predictive of the metabolic and cardiovascular changes that occur in obesity.

Thus BMI in addition to waist circumference or waist-to-hip ratio measurements are currently being used to accurately determine the degree of obesity in humans (Dobbelsteyn CJ, 2001). In animals two types of models are currently used in obesity research: genetic and dietary models. The former allows researchers to study the underlying biology of obesity focusing on specific genes and pathways, while the latter is thought to represent the etiology of obesity in modern society (Tschöp M *et al.,* 2001). This high caloric diet-induced obesity model mimics human obesity in many aspects such as increased body weight and adiposity, increased circulating leptin and insulin levels, increased triglyceride levels and decreased insulin sensitivity (Li S *et al*., 2008).

1.3   Obesity and insulin resistance

As discussed in the previous section (1.2), obesity is regarded as a complex disease, ultimately caused by an imbalance between caloric intake and energy expenditure. It is commonly associated with alterations in metabolic function, where the development of the insulin resistant state is seen as the starting point of this derangement (Bogardus C *et al*., 1985). Further, obesity and insulin resistance has a major pathogenic role in the development of type 2 diabetes mellitus (Reaven GM, 1988; Morisco C, 2006). Insulin resistance is a pathological state in which target cells, namely the liver, skeletal muscle, adipose tissue and the heart, fail to respond to normal concentrations of insulin (Mlinar B *et al.,* 2007; Saltiel AR, 2001). Thus higher than normal concentrations of insulin are needed to maintain normoglycemia. Dysfunctional adipose tissue accounts for the major metabolic derangements seen in obese and insulin resistant individuals. Under normal conditions, adipose tissue acts as a store of surplus energy during increased food intake or reduced energy expenditure (Sethi JK and Vidal-Puig AJ, 2007).

In obesity associated insulin resistance, a prolonged caloric/energy imbalance results in increased lipolysis, where excessive storage of triglycerides, eventually leads to the release of large amounts of free fatty acids (FFA) (Hutley L and Prins JB, 2005). Additionally, adipocyte-derived peptides such as leptin, resistin, tumor necrosis factor-α (TNF-α), adiponectin, plasminogen activating inhibitor-1 (PAI-1), and interleukin-6 (IL-6) are also released (Vázquez-Vela ME, 2008). The excessive release of these FFA along with the adipocyte–derived peptides then incites lipotoxicity (Hutley L and Prins JB, 2005). The resulting lipotoxicity affects adipose as well as non-adipose tissue, resulting in excess fat being deposited in ectopic tissue such as liver, skeletal muscle, pancreas (figure 1) and the heart.

In the liver, FFA causes an increased production of glucose, triglycerides and secretion of very low-density lipoproteins (VLDL). The associated lipid/lipoprotein abnormalities include reductions in high-density lipoprotein (HDL) cholesterol and an increased density of low-density lipoproteins (LDL) (Eckel RH *et al.* 2005). The abnormalities associated with increased triglycerides include inhibition of lipogenesis, which prevents adequate clearance of serum triacylglycerol levels that contribute to hypertriglyceridemia. Additionally, increases in triglycerides cause lipotoxicity that results in insulin-receptor dysfunction. The consequent insulin-resistant state, arising from the receptor dysfunction, creates hyperglycemia with compensated hepatic gluconeogenesis. The latter increases hepatic glucose production, further accentuating the hyperglycemia caused by insulin resistance (Boden G *et al.,* 1994; Pan DA *et al.,* 1997).

In the muscle, FFA inhibit insulin mediated glucose uptake which results in reduced insulin sensitivity, contributing to the development of hyperglycemia (Eckel J and Reinauer H, 1990; Eckel RH *et al.,* 2005).

In the pancreas, increases in circulating FFA incite lipotoxicity and results in a decreased secretion of pancreatic β-cell insulin, which eventually results in β-cell exhaustion (Unger RH, 1995).

The pro-inflammatory cytokines also result in enhanced hepatic glucose production, the production of VLDL by the liver and insulin resistance in muscle (not shown in the diagram) (Eckel RH *et al.,* 2005).

In addition to the factors named above, obesity and insulin resistance also affect the peptide hormone leptin. This hormone is a non-glycosylated peptide hormone that is produced by adipocytes (Pittas AG *et al.,* 2004). In peripheral tissue, leptin prevents fat deposition in non adipose tissue, hence enhancing insulin sensitivity in muscle and fat, and also prevents lipotoxicity in pancreatic β-cells (Zhuang *et al.,* 2009). Leptin dysfunction is observed in obesity. This dysfunction is accompanied by a substantial increase in insulin secretion from the pancreas, resulting in a decrease in the biological effects of insulin, hence promoting the development of insulin resistance (not shown in the diagram) (Seufert J, 2004).

In the heart, exposure of the vasculature and muscle cells to high levels of FFA initiates multiple cellular processes, including impaired insulin signalling (Belfort R *et al.,* 2005), oxidative stress (Du X *et al.,* 2006), alterations in local rennin-angiotensin system (RAS) (Watanabe S *et al.,* 2005) and enhanced vascular smooth muscle cell adrenergic sensitivity (Stepniakowski KT *et al.,* 1995). All of these factors contribute to cardiac, vascular and metabolic insulin resistance (not shown in the diagram).
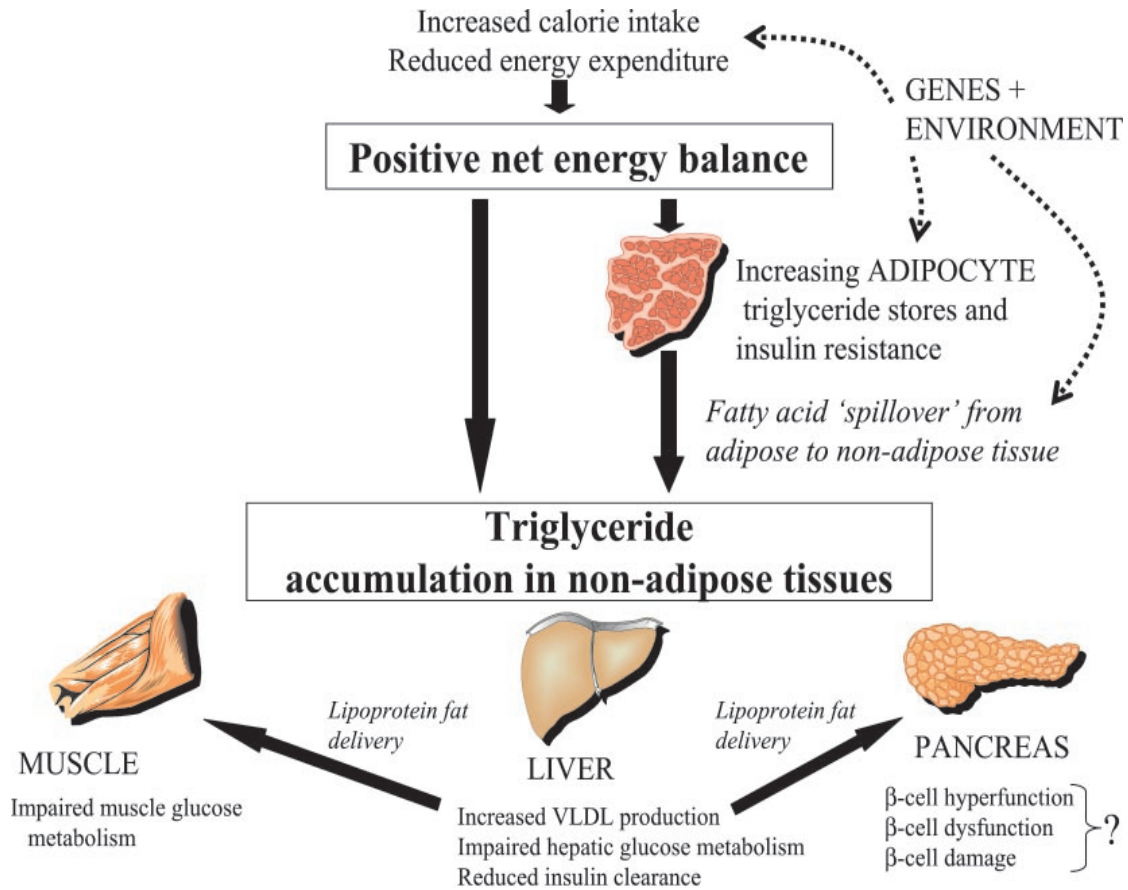
Figure 1: *A positive energy imbalance, as a result of increased caloric intake and reduced energy expenditure, causes accumulation of triglycerides in adipose tissue which leads to increased lipolysis. The latter causes an increase of FFA in the circulation and triglycerides accumulate in non-adipose tissue such as the liver, pancreas and muscle. This in turn results in many of the typical features characteristic of the insulin resistant state (Lewis GF et al., 2002).*

1.3.1 Actions of insulin

Insulin is a potent anabolic hormone that is secreted by the β-cells of the pancreatic islets of Langerhans. It exerts a broad spectrum of anabolic effects in multiple tissues and is essential for appropriate tissue development, growth and maintenance of whole-body glucose homeostasis (Wu X and Garvey WT, 2011). In the liver and skeletal muscle insulin regulates glucose homeostasis by augmenting glycogen formation, it reduces hepatic glucose output by inhibiting gluconeogenesis and glycogenolysis, and increases the rate of glucose uptake (Saltiel AR and Kahn R, 2001). Insulin also affects lipid metabolism as it augments the availability of glycerol and fatty acids for triglyceride synthesis, by increasing the uptake of glucose into adipose tissue and by inhibiting lipolysis (Wu X and Garvey WT, 2011). In the heart, insulin regulates metabolism by modulating glucose transport, glycolysis, glycogen synthesis, lipid metabolism and protein synthesis (Brownsey RW *et al.,* 1997). In addition it enhances cardiac contractility (Abel ED, 2004). Myocardial excitation is associated with the trans-membrane movement of the extracellular Ca^{2+} into cardiomyocytes through activated Ca^{2+} channels and reverse Na^{2+}/Ca^{2+} exchange. This influx of Ca^{2+} stimulates the additional release of Ca^{2+} from the sarcoplasmic reticulum via the ryanodine receptors, which results in myofilament activation and contraction. Studies in isolated human cardiomyocytes suggest that insulin enhances Ca^{2+} influx through activation of L-type Ca^{2+} channels and reverse-mode Na^{2+}/Ca^{2+} exchange, thereby enhancing contraction (Maier S *et al.,* 1999; von Lewinski D *et al.,* 2005). In the vasculature, insulin stimulates an increased production of nitric oxide (NO) from vascular endothelium, thereby enabling vasodilation (Zeng G and Quon MJ, 1996).

1.3.2   Molecular mechanisms of insulin signalling

1.3.2.1   Normal insulin signalling

Insulin action begins with the binding of insulin to a heterotrimeric receptor on the cell membrane of the target cells (liver, skeletal muscle, adipose tissue and the heart). Insulin receptors are membrane glycoproteins composed of two α- and two β-subunits (Kido Y *et al.,* 2001). Binding of insulin to the extracellular α-subunit results in a conformational change that bring the α-subunits closer together, and enables adenosine triphosphate (ATP) to bind to the intracellular domain of the β-subunit, leading to autophosphorylation of distinct tyrosine residues on the β-subunit (Jacobs S and Cuatrecasas P, 1981; Shoelson SE *et al.,* 1991; van Obberghen E *et al.,* 2001). Ligand-dependent stimulation of the β-subunit tyrosine kinase activity is critical for promulgation of the insulin signal (Wu X and Garvey WT, 2011). Six tyrosine (Tyr) residues in the β-subunit undergo phosphorylation and have been shown to serve different roles in insulin signalling (Shoelson SE *et al.,* 1991). Phosphorylation of Tyr^{972} has been shown to establish the recognition motif and docking sites, providing stability for substrate phosphorylation. Tyrosine phosphorylation sites at positions Tyr^{1158}, Tyr^{1162} and Tyr^{1163} are essential for mediating an increase in subunit tyrosine kinase activity, while phosphorylation sites Tyr^{1328} and Tyr^{1334} are involved in the mitogenic responses (Cheatham B and Kahn CR, 1995). Following insulin binding and receptor autophosphorylation, the insulin receptor phosphorylates intracellular protein substrates (figure 2). Eleven intracellular substrates have been identified, which are rapidly phosphorylated on the tyrosine residues by ligand-bound insulin receptor (Saltiel AR and Kahn R, 2001). The insulin receptor substrates (IRSs), immediate substrates for the insulin receptor tyrosine kinases, play an important role in the actions of insulin. IRSs propagate insulin signal transduction through docking, apposition, interaction and activation of downstream signalling molecules. This provides a point of divergence of the insulin transduction pathway (Khan AH and Pessin JE, 2002).

This divergence leads to the activation of the metabolic phosphoinositide-3 kinase (PI3K), Cbl-associated protein (CAP)/ Casitas b-lineage lymphoma (CbI)/ TC10 and mitogenic (rennin-angiotensin system (RAS)/Mitogen activated protein (MAP) kinase) pathway (Saltiel AR and Kahn R, 2001; Khan AH and Pessin JE, 2002). Binding of IRS1-4 to PI3K is critical in mediating the metabolic effects of insulin (Gual P *et al.,* 2005; White MF, 2002). Upon phosphorylation of the p85 subunit of PI3K it associates with the p110 subunit to produce phosphatidylinositol-3,4,5-phosphate PI(3,4,5)P3 through phosphorylation on the 3 position of the integral membrane protein, phosphatidyl inositol 4,5 bisphosphate (PIP_2). This leads to the recruitment and activation of phosphoinositide-dependent protein kinase 1 (PDK1) which is responsible for the downstream activation of atypical protein kinase C (PKC) ζ on Threonine 410 (Thr^{410}) and PKB/Akt on Thr^{308}, thereby enhancing the activity of these kinases (Wu X and Garvey WT*,* 2011).

PKB/Akt is a serine/threonine protein kinase with a molecular weight of 57 kDa (Hajduch E *et al.,* 2001). This kinase is a critical signalling molecule in all eukaryotic cells and has diverse functions in human physiology and diseases (Manning BD and Cantley LC, 2007). There are three PKB/Akt isoforms, i.e. PKB/Akt1, PKB/Akt2 and PKB/Akt3 (α, β and γ) present in higher eukaryotes, and each has an amino terminal pleckstrin homology (PH) domain, a kinase domain and a carboxyl terminal regulatory domain (Hajduch E *et al.,* 2001). PKB/Akt is well established as an effector of the PI3K signalling pathway in all cells (Fruman DA and Cantley LC, 2002), and is regulated by phosphorylation. In the PI3K pathway PIP_2 and PIP_3 bind to the PH domain of PKB/Akt, therefore altering its conformation, leading to its phosphorylation and activation (Hajduch E *et al.*, 2001). This phosphorylation takes place at Thr^{308} of the kinase domain and Serine 473 (Ser^{473}) of the C-terminal domain (Coffer PJ *et al.,* 1998).

Upon activation, PKB/Akt phosphorylates and controls the activities of several downstream substrates. In glucose metabolism PKB/Akt is involved in translocation of glucose transporters (mainly GLUT 4) to the plasma membrane, thereby promoting glucose uptake by the cells (Khan AH and Pessin JE, 2002). Once plasma glucose is available in excess, PKB/Akt phosphorylates GSK-3, which normally phosphorylates and inhibits glycogen synthase (GS), a rate-limiting enzyme of glycogenesis. Inhibition of GSK-3 by PKB/Akt thus favours glycogen synthesis and storage in muscles, liver, adipose tissues and the heart (Hajduch E *et al.,* 2001).

In parallel with the PI3K pathway the CAP/Cbl/TC10 pathway also participates in glucose uptake stimulation (Watson RT and Pessin JE, 2001). This pathway diverges at the level of the insulin receptor kinase, which mediates tyrosine phosphorylation of the Cbl proto-oncogene through a process that does not involve IRSs. In this pathway, prior to the phosphorylation step of Cbl, the adaptor protein (APS) is recruited to the insulin receptor β-subunit. This results in Cbl binding to APS, permitting the phosphorylation of Cbl. The Cbl associated protein (CAP) is also recruited with Cbl, resulting in a cascade which reinforces glucose uptake stimulation, by inducing GLUT-4 translocation, which is also stimulated by the PI3K pathway (Baumann CA *et al*., 2002).

Another component of signal divergence comes from engagement of the RAS/MAP kinase signalling pathway (figure 2), which is critical in cell growth and mitogenesis. In this pathway the insulin receptor mediates the activation of the RAS/MAP kinase pathway through the activation of substrate docking molecules such as SHC, Growth factor receptor-bound protein 2 (Grb2) (a small cytosolic adaptor protein), murine Son of Sevenless (mSOS) (GDP/GTP exchange factor) and Ras. Ras activation triggers the activation of Rapidly accelerated fibrosarcoma (Raf-1) kinase. Raf-1 kinase then initiates a cascade leading to sequential phosphorylation and activation of kinase MEK (MAPK/ERK kinase), which in turn phosphorylates extracellular regulated kinases (ERK1 and ERK2) on their threonine and tyrosine residues. These activated ERKs phosphorylate multiple targets that mediate the mitogenic actions of the Ras/MAP kinase pathway and the growth promoting effects of insulin (Boulton TG *et al.,* 1991). Changes in this pathway were not addressed in this study.
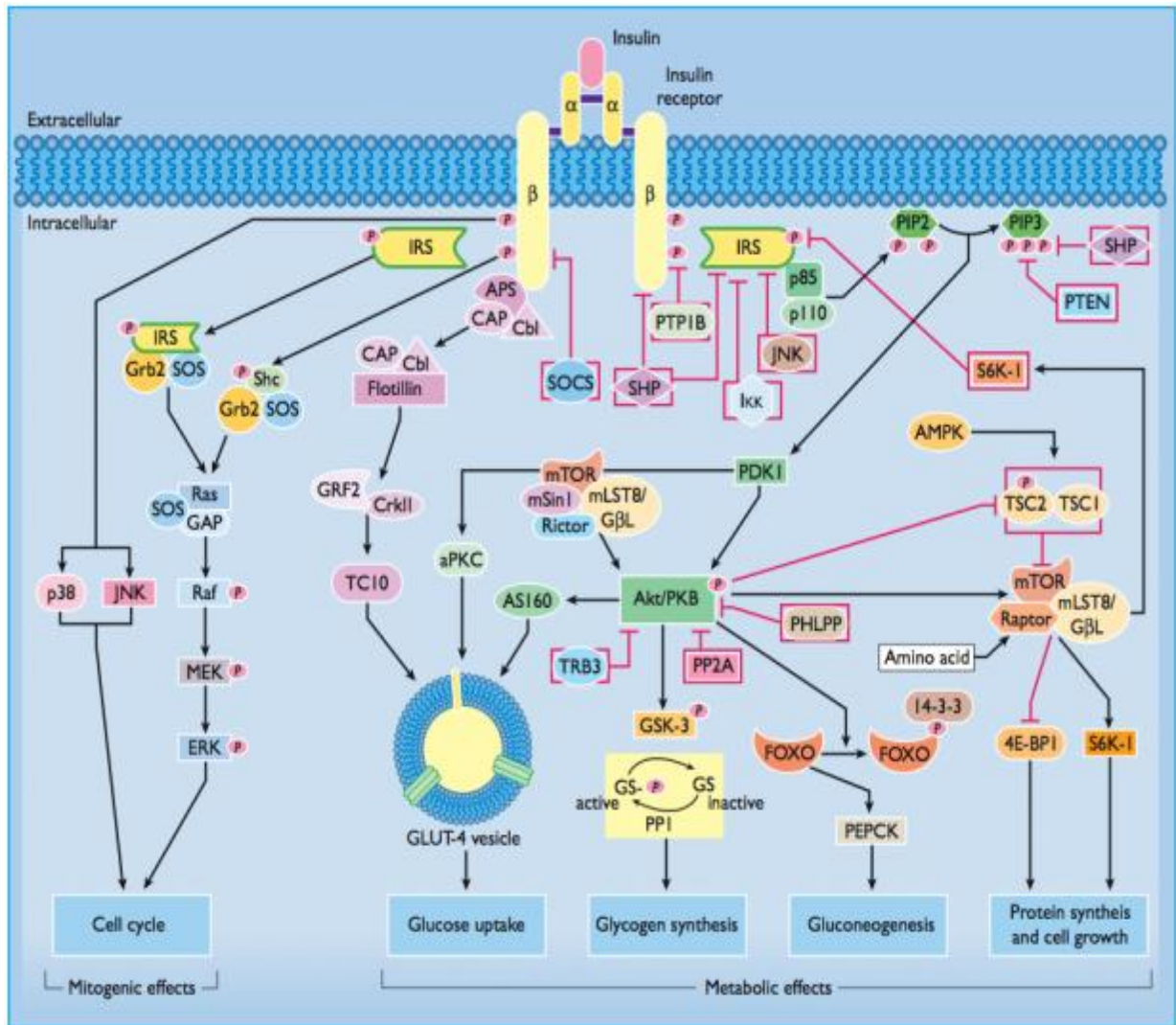
Figure 2: *Principal components of the insulin signalling pathway showing the metabolic and mitogenic effects of insulin. The arrows represent an activation process, blocked arrows represent an inhibition process. Adapted from Wu X and Garvey WT (2011).*

1.3.2.2 Impairment of insulin signalling resulting in insulin resistance

Defects in the actions of insulin occur at several levels in the insulin signalling pathway. At the insulin receptor level, the number of cell-surface receptors, in target tissue such as the liver, skeletal muscle and the heart, are down-regulated by chronic exposure to high concentrations of insulin, *in vivo* (Muniyappa *et al.,* 2007). This affects insulin-stimulated glucose uptake and activation of glycogen synthase (GS) (Brunning JC *et al.,* 1998; Okamoto H *et al.,* 2004). In a knockout mouse model with a decrease in cell-surface insulin receptors in skeletal muscle, the animals were shown to have features of the metabolic syndrome, including an increase in fat mass, triglycerides and serum FFA, but retained normal basal glucose transport (Wojtaszwewski JF *et al.,* 1999). This phenotype was analogous to that seen in patients with insulin resistance, where defects in the insulin receptors also resulted in the development of severe insulin resistance and glucose intolerance. In endothelial cells, a decrease in the IRs causes a decrease in the production of NO, which affects vasodilation (Muniyappa R *et al.,* 2007). This shows that the functional activity of the insulin receptors is critical for effective insulin action. Regarding the insulin receptor substrate, it was found that deletion of IRS1 produced insulin resistance in mice (Deborah J *et al.,* 2001). In another experiment, it was shown that mice lacking IRS2 develop severe diabetes at 8-15 weeks of age; this was attributed to the reduction in β-cell mass and reduced secretion of insulin, hence insulin no longer served a compensatory role (Hirashima Y *et al.,* 2003). IRSs propagate the insulin signal transduction and activate downstream signalling molecules. Theoretically, defects at receptor level influences many downstream signalling molecules in the insulin signalling pathway, resulting in the pathogenesis of many diseases.

1.4   General aspects of myocardial hypertrophy

Wang X and colleagues (2003) defined cardiac hypertrophy as an adaptive response of the heart to hemodynamic overload during which terminally differentiated cardiomyocytes increase in size without undergoing cell division. This hypertrophic response can broadly be classified as either physiological or pathological cardiac hypertrophy (figure 3) (Nadal-Ginard B *et al.,* 2003; Bernardo BC, 2010). The former occurs during growth, or it can be induced by endurance exercise and it can also be observed during pregnancy. Pathological cardiac hypertrophy, on the other hand, is a response to stress signals that arise from a variety of cardiovascular disorders, including pressure and volume overload due to valvular dysfunction, arterial hypertension, ischemic heart disease or intrinsic contractile abnormalities resulting from sarcomere protein mutations. Pathological and physiological hypertrophy can also be sub classified as concentric or eccentric hypertrophy (figure 4) (Grossman W *et al.,* 1975; Pluim BM *et al.*, 2000; Agrawal R *et al.,* 2010; Bernardo BC, 2010), where the former results in an increase in the number of parallel contractile elements which leads to an increase in wall thickness which lowers wall stress. This phenomenon generally occurs as a result of pressure overload, for example in hypertensive patients. Eccentric hypertrophy, on the other hand, results in an increase in chamber size and end-diastolic volume and enhances stroke volume. This phenomenon is observed when the heart is subjected to volume overload, for example owing to valve defects. The concomitant change in chamber cavity size and geometry induce detrimental effects in the long-term when cardiac output fails to meet the increased demand (Jacob R and Gulch RW, 1998). The defining features of hypertrophy are an increase in cardiomyocyte size, enhanced protein synthesis, an overt increased risk of ventricular dysfunction and a higher organisation of the sarcomere.
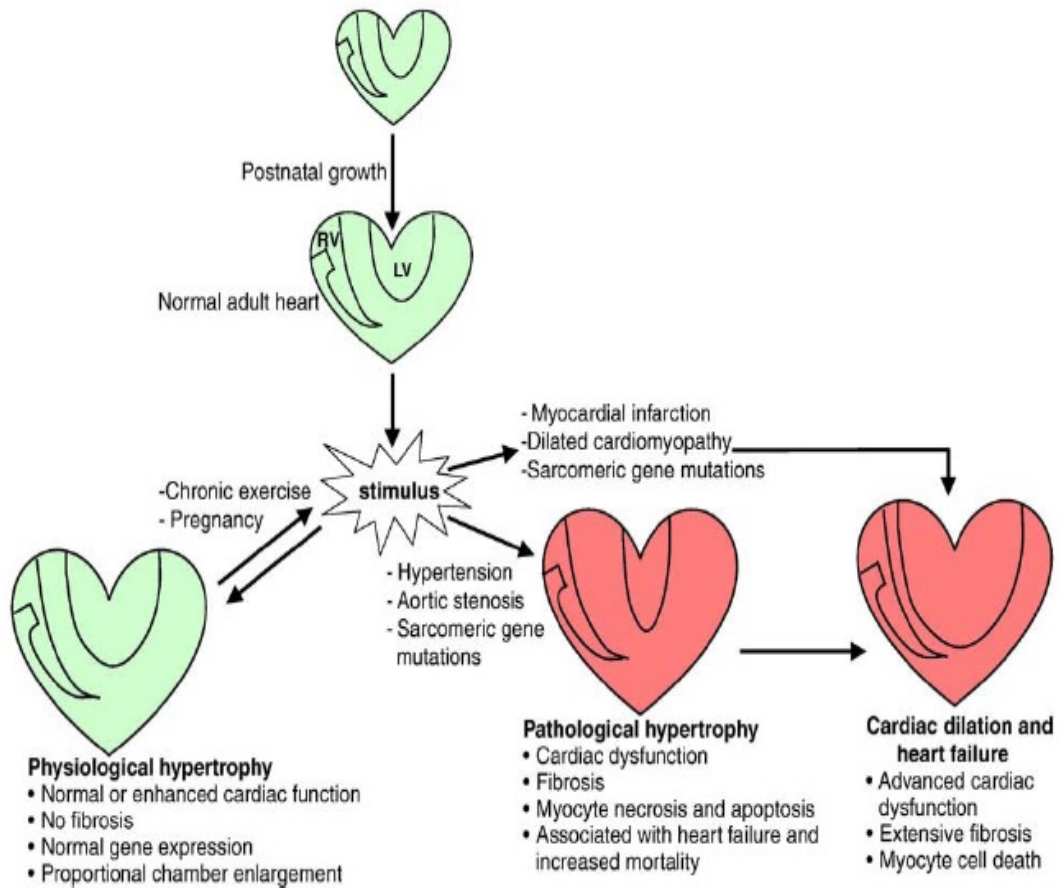
Figure 3: *Cardiac hypertrophy can be classified as physiological or pathological. The former is reversible and is characterized by normal cardiac morphology and function. In contrast, hypertrophy that occurs in settings of disease (pathological hypertrophy) is detrimental for cardiac structure and function and can lead to heart failure (Bernardo et al., 2010).*

15
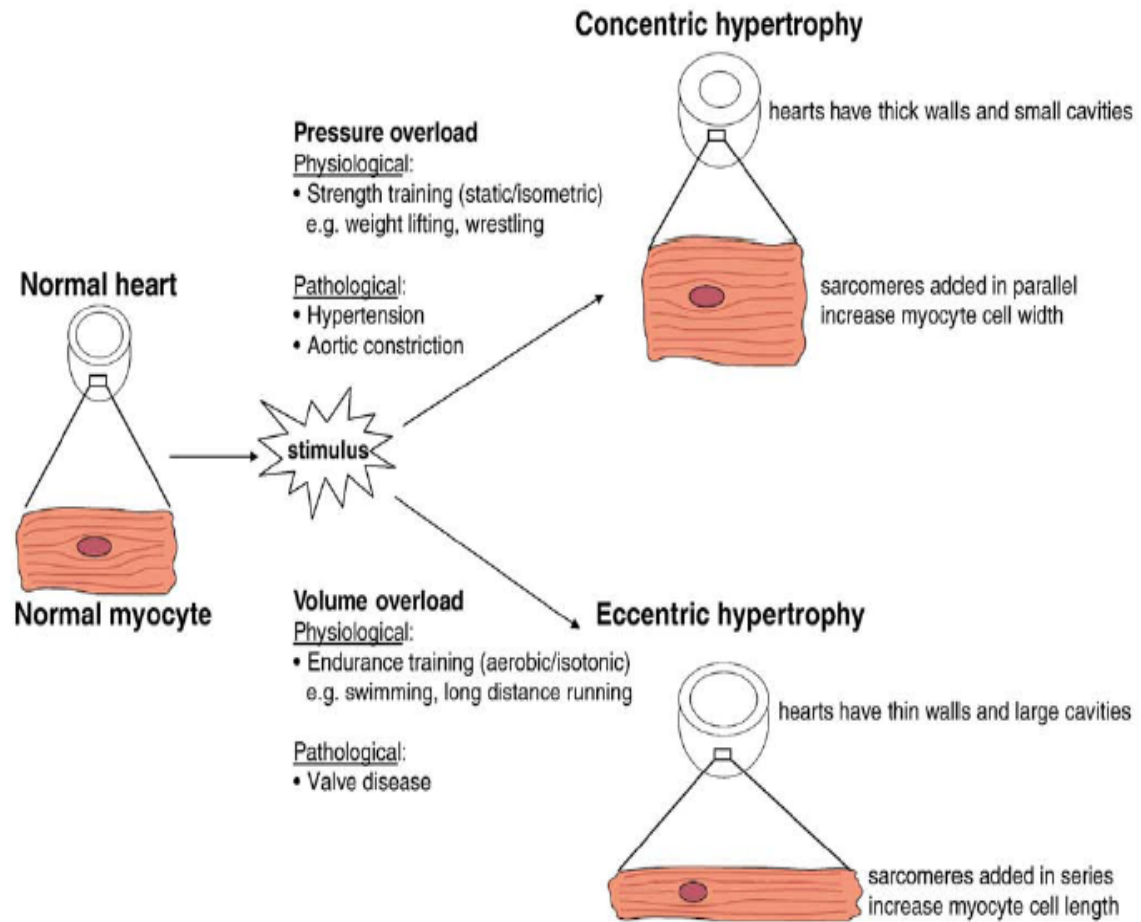
Figure 4: *Different stimuli induce different forms of cardiac hypertrophy. Pressure overload causes thickening of the left ventricle wall due to the addition of sarcomeres in parallel and results in concentric hypertrophy. Volume overload induces an increase in muscle mass via the addition of sarcomeres in series and results in eccentric hypertrophy (Bernardo et al., 2010).*

1.4.1 Overview of the signalling cascade/proteins implicated in mediating physiological and pathological hypertrophy

Physiological hypertrophy is mediated by growth factors such as insulin like growth factors (IGF) and growth hormone (Reviewed by Bernardo *et al.,* 2010). These growth factors interact with their tyrosine kinase associated receptors, which cause receptor dimerisation, autophosphorylation and activation of PI3K. As described previously, this kinase transforms PIP2 into PIP3, which recruits a second kinase PKB/Akt to the plasma membrane and causes its phosphorylation. This phosphorylated PKB/Akt can by itself induce the expression of hypertrophy-associated genes. Downstream of PKB/Akt, inhibition of GSK-3 can further promote this hypertrophic response by promoting protein synthesis or by activating the transcription of genes which mediate the hypertrophic response. Pathological hypertrophy, on the other hand, is caused by activation of the neurohormonal pathway that involves angiotensin II, endothelin I or catecholamines. They all produce pathological hypertrophy through the activation of the Gαq coupled signalling pathway, which subsequently activates phospholipase Cβ. This phospholipase hydrolyses PIP2 to Diacylglycerol (DAG) and Inositol trisphosphate (IP3). IP3 results in the release of Ca^{2+} from intracellular stores and also activates the phosphatase calcineurin. Calcineurin regulates the alterations in gene expression that are associated with pathological hypertrophy by dephosphorylating the transcription factor nuclear factor of T cell (NFAT) (Molkentin JD *et al.,* 1998). This dephosphorylation of NFAT causes its nuclear translocation and modulates gene expression. By contrast, DAG activates members of the PKC family, which can also contribute to the altered regulation of gene expression observed in cardiac hypertrophy (figure 5).
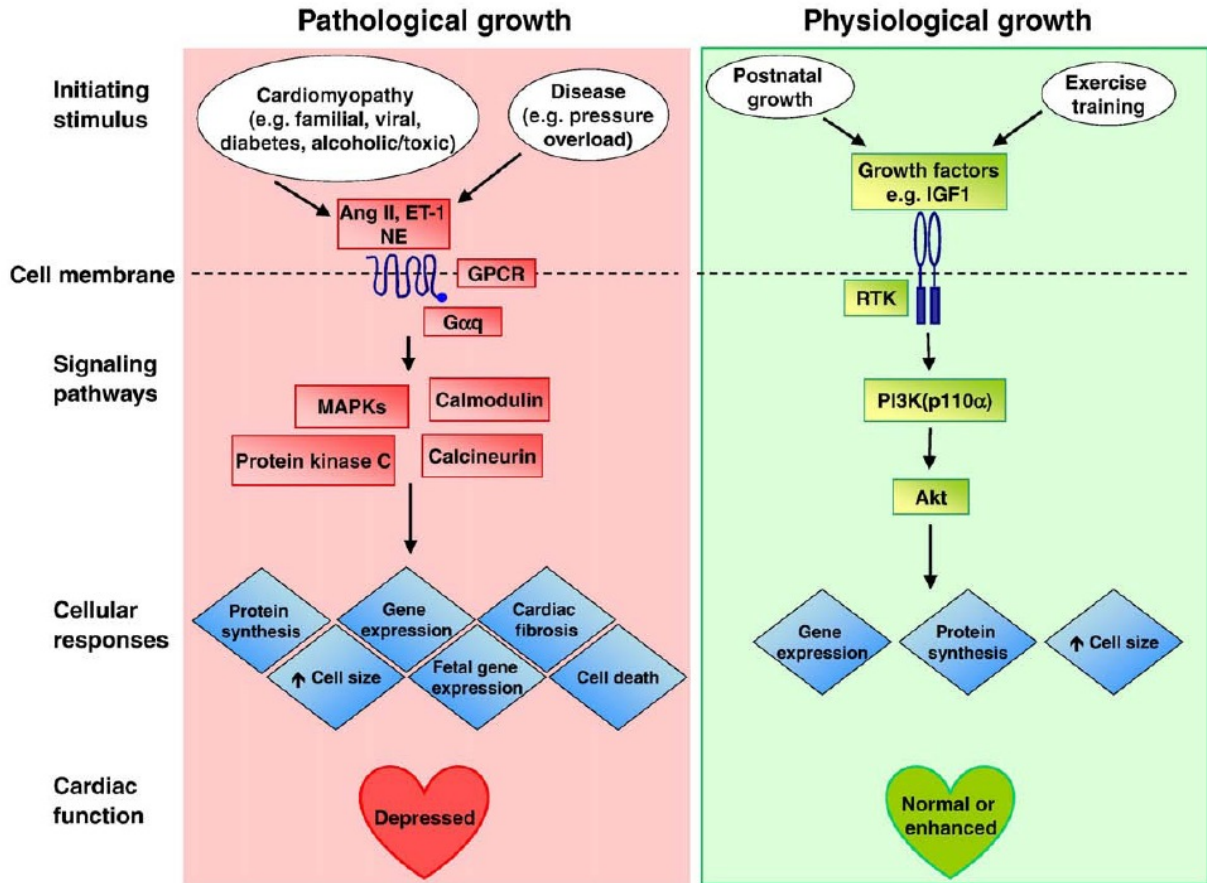
Figure 5: *A schematic overview of the signalling pathways of pathological and physiological hypertrophy. Outlined are the key initiating stimuli, signalling pathways, cellular responses and cardiac function consequences of each pathway (Bernardo et al., 2010).*

1.5   Obesity and the development of myocardial hypertrophy

Heart failure is defined as "a complex clinical syndrome that can result from a structural or functional cardiac disorder that impairs the ability of the ventricle to fill with or eject blood. The cardinal manifestations of heart failure are dyspnea and fatigue, which may limit exercise tolerance; and fluid retention, which may lead to pulmonary congestion and peripheral edema" (ACC/AHA, 2005). This syndrome is divided into 4 stages, A, B, C and D, as defined by American College of Cardiology/American Heart Association (ACC/AHA, 2005). In stage A, patients show no symptoms of heart failure, no structural alteration, but are at risk of developing heart failure because of comorbidities such as coronary artery disease, hypertension or diabetes mellitus. In stage B, patients still do not show symptoms of heart failure, but have developed structural abnormalities, such as left ventricular hypertrophy, ventricular dilation, valvular disease or previous myocardial infarction. In stage C, patients have symptomatic heart failure and are in therapy. Finally, in stage D, patients have end-stage heart failure and are receiving maximal medical therapy (ACC/AHA, 2005; Klein L *et al.,* 2003). Heart failure arises from a variety of aetiologies, including obesity. This association between obesity and heart failure has been under-recognized in the past, however, an increasing number of epidemiologic studies now report this association (Duflou J *et al*., 1995; Dwyer EM *et al*., 2000). Clinical studies have also confirmed the association of adiposity with left ventricular dysfunction, independent of hypertension, coronary artery disease and other heart disease (Hubert HB *et al*., 1983; Kenchaiah S *et al.,* 2002). Most types of heart failure are preceded by cardiac hypertrophy. In obesity the increase in extracellular volume, which consists of the intravascular space and interstitial fluid space, is identified as one of the ways in which obesity can result in the development of myocardial hypertrophy.

This expansion of total blood volume leads to increased left ventricular filling, which in turn leads to chamber dilation and increased cardiac output (Licata G *et al.,* 1991; Alexander JK; 1985). The majority of the literature suggests that an increase in stroke volume accounts for the increase in cardiac output in obese individuals (Messerli FH *et al.,* 1982). To compensate for these factors, adaptive myocardial hypertrophy together with left ventricular dilation occurs, resulting in eccentric hypertrophy. Adaptive myocardial hypertrophy is initially a compensatory mechanism, aimed at maintaining cardiac output. However, with time, this left ventricular dilation increases wall stress, which stimulates left ventricular myocardial growth and leads to an elevation in left ventricular mass, indicating a decompensated myocardial hypertrophic state (Opie LH, 1991). It is within this setting that the development of heart failure arises.

In addition to structural changes, obesity also results in changes in cardiac function. Many studies have evaluated left ventricular (LV) systolic function in obesity. The findings from these studies vary, where some groups report normal or improved ejection fraction (EF) and fractional shortening (FS), implying that these individuals have improved systolic function. Other studies have, however, reported depressed ejection fraction (EF) and fractional shortening (FS) values (Abel ED *et al.,* 2008). This difference in findings could be due to the prevalence of comorbidities, such as hypertension, diabetes and vascular diseases, which can independently contribute to the development of LV dysfunction. Also, the difference in techniques used by the different groups can account for the heterogeneity in the findings. The use of more sensitive equipment, such as Tissue Doppler Imaging, which in addition to EF and FS, measures sensitive parameters, such as end-systolic and -diastolic diameter, end-systolic and -diastolic volumes, relative wall thickness, mean velocity circumferential shortening, pre-ejection period and ejection period, gives a clearer picture of the effects of obesity on LV systolic function.

Studies using these sensitive methods have revealed that, despite normal EF values in obese individuals, myocardial function remains reduced. Furthermore, they also observed a reduction in myocardial contractility (Garavaglia GE *et al.,* 1988). The studies that have evaluated LV diastolic function in obesity have also given variable results. Using Tissue Doppler Imaging, two groups have reported evidence of reduced early diastolic tissue velocity and diastolic strain rate in obese individuals compared to normal weight subjects (Wong CY *et al*., 2004). Decreases in these parameters are associated with a decrease in the rate of LV relaxation (Pascual M *et al.,* 2003).

1.6   General overview of the GSK-3 protein

Glycogen synthase kinase-3 (GSK-3) was identified in the early 1980s as an enzyme involved in the control of glycogen metabolism (Woodgett JR and Cohen P, 1984). In recent years GSK-3 has been reported to participate in a multitude of cellular processes, ranging from cell membrane-to-nucleus signalling, gene transcription, protein translation and cytoskeletal organisation to cell cycle progression and survival, to name a few (Meijer L *et al.,* 2004). GSK-3 is a serine/threonine kinase that is ubiquitously expressed (Park KW *et al*., 2003). In humans there are two GSK-3 isoforms, GSK-3α with a molecular weight of ~51 kDa and GSK-3β with a molecular weight of ~47 kDa, that account for all GSK-3 activity (Woodgett JR, 1990). In addition, the GSK-3β mRNA undergoes alternative splicing between exon 8 and 9 that produces two different protein products, namely GKS-3β1 and GSK-3β2 (Mukai F *et al.,* 2010; Sutherland C, 2011). The protein isoforms of GSK-3 are encoded by two distinct genes located on chromosomes 19q13.1-2 and 3q13.3-q21 (Woodgett JR, 1990). These isoforms exhibit a high degree of sequence similarity in their catalytic domains, however, outside of this kinetic domain, their sequence differ substantially and little is known about their isoform-specific functions (Ciaraldi TP *et al.,* 2007).

Therefore, despite the fact that these isoforms are structurally similar, their expression patterns, substrate preferences and cellular functions are not identical (Woodgett JR, 2001). Genetic ablation of one or both of the GSK-3 isoforms has provided clues as to cellular processes governed by their activity. In genetic knockout studies performed by Hoeflich KP and colleagues (2000) it was found that mice embryos carrying homozygous deletions of exon 2 of the GSK-3β isoform suffer from massive liver degeneration caused by extensive hepatocyte apoptosis, leading to death at around embryonic day 16. This lead to the conclusion that GSK-3β function is not compensated for by GSK-3α. In another study, MacAulay K and colleagues (2005) found that mice lacking GSK-3α remained viable and exhibited a small improvement in insulin sensitivity and glucose tolerance.

1.6.1   Regulation of the GSK-3 protein

As stated previously, GSK-3 is involved in many cellular processes, thus regulation of its activity is critical to ensure that signalling pathways are appropriately coordinated. To achieve this, GSK-3 is subject to many levels of regulation. These include regulation by phosphorylation, cellular localisation and protein-protein interactions.

1.6.1.1   Regulation by phosphorylation

GSK-3 is described as a unique protein kinase, because unlike most protein kinases, it is active in resting cells and becomes deactivated when cells are stimulated by hormones such as insulin, endothelial growth factor and platelet growth factor (Woodgett JR, 1994; Ciaraldi TP *et al.,* 2007). The most well defined mechanism of GSK-3 regulation is the phosphorylation of the N terminal at Serine 9 (Ser^9) in GSK-3β and Serine 21 (Ser^{21}) in the GSK-3α isoform (Markou T *et al.,* 2008).

The following substrate proteins can phosphorylate GSK-3 on serine residues, thus having an inhibitory effect on its activity: PKB/Akt (PI3K pathway), some isoforms of PKC, protein kinase A (PKA), p90^{RSK} and p70S6 kinase (Murphy E and Steenbergen C, 2005). GSK-3 is also inhibited by cardiac hypertrophic stimuli induced by the activation of endothelin-1 and Fas, in response to pressure overload (Haq S *et al.,* 2000). In addition, the actions of GSK-3 are regulated by the phosphorylation state of its substrates. This is due to the fact that most GSK-3 substrates, but not all, must be pre-phosphorylated or primed in order for GSK-3 to phosphorylate them. GSK-3 has been shown to phosphorylate non-primed substrates, but this results in less efficient phosphorylation. In contrast to inactivation via serine phosphorylation, GSK-3 can be phosphorylated on tyrosine residues, resulting in its activation, i.e. Tyr^{279} of GSK-3α and Tyr^{216} of the GSK-3β isoform (Murphy E and Steenbergen C, 2005). This means that GSK-3 tyrosine phosphorylation results in facilitative autophosphorylation, while serine phosphorylation is regulatory. The kinase responsible for tyrosine phosphorylation of GSK-3 protein is poorly understood.

1.6.1.2 *Regulation by cellular localisation*

Intracellular localization of GSK-3 isoforms controls its access to its substrates. GSK-3 is predominantly localised in the cytosol, however, it can also be present in the nucleus and mitochondria. The level of GSK-3 in any compartment is not static but changes dynamically in response to intracellular cues. For example, during the G1 phase of the cell cycle, GSK-3β is located predominantly in the cytoplasm, but during the S phase, a significant fraction enters the nucleus, promoting its ability to phosphorylate cyclin D1 in the nucleus (Diehl JA *et al.,* 1998; Jope RS and Johnson GVW, 2004).

1.6.1.3 Regulation by protein-protein interactions

GSK-3 activity can also be regulated by protein-protein interactions, an example being in the canonical Wnt signalling pathway (Jope RS and Johnson GVW, 2004). In this pathway the absence of a Wnt signal causes β-catenin to assemble in a cytosolic multi-protein complex composed of APC (tumour suppressor protein), GSK3 and the scaffolding protein axin. A sequential phosphorylation of β-catenin by casein kinase I and by GSK 3 at Ser/Thr residues targets β-catenin for ubiquitination and proteasomal degradation. In the presence of Wnt, β-catenin phosphorylation and degradation is inhibited, resulting in β-catenin being available for transcriptional regulation. This pathway serves as a classic example of how GSK-3 in complex with other proteins regulates cellular function (figure 6).
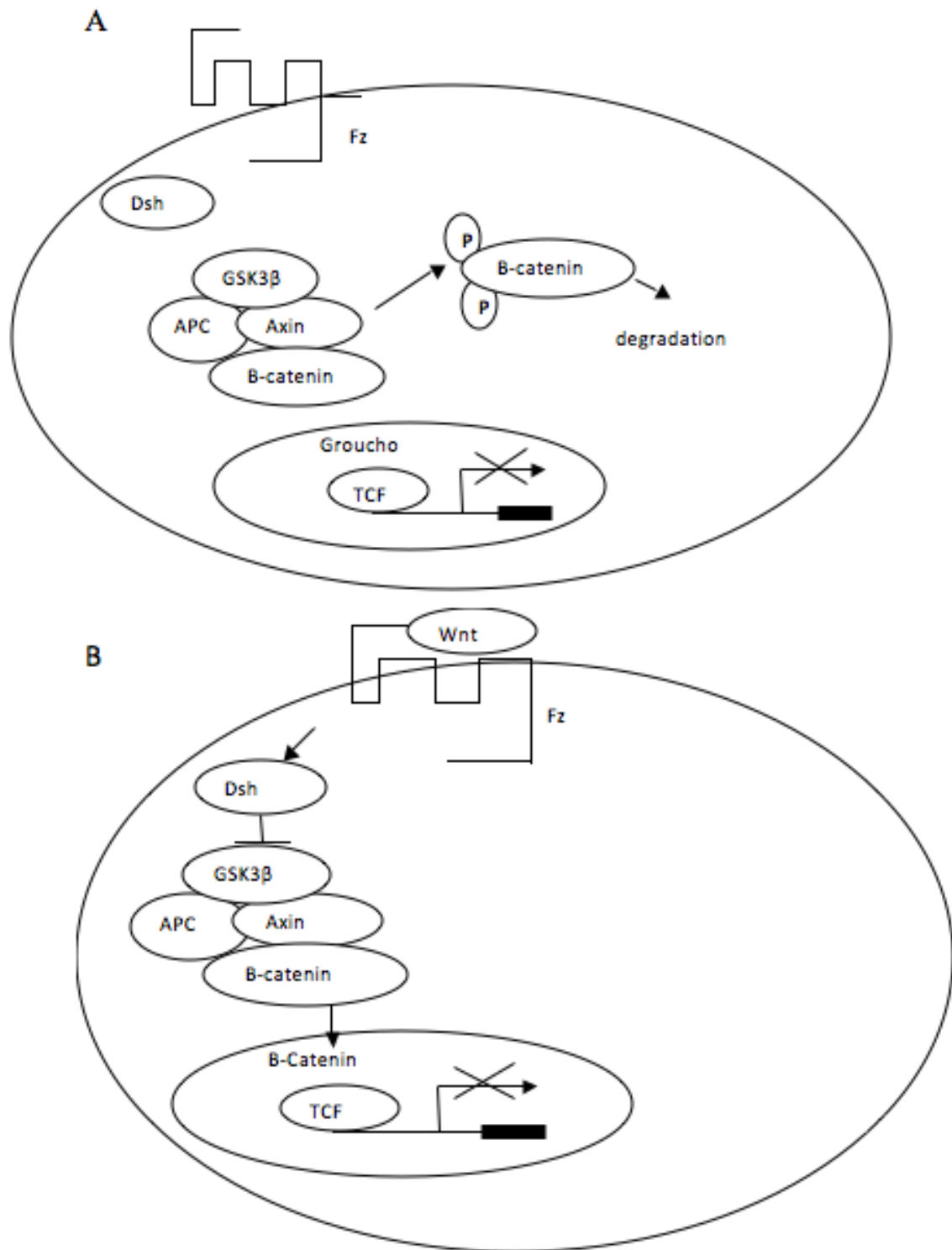
Figure 6: *An overview of the Wnt signalling pathway: In this pathway, signals are transmitted from the extracellular signalling protein Wnt to the transcriptional regulator β catenin, which controls the expression of numerous target genes, including the gene for cyclin D1 and the transcription factor Myc. β-catenin may exist in a membrane bound form in complex with the cell adhesion molecule E-cadherin or in a cytosolic form. In the absence of a Wnt signal (Figure A) β -catenin is assembled in a cytosolic multi protein complex composed of APC (tumour suppressor protein), GSK3 and the scaffolding protein axin. A sequential phosphorylation of β-catenin by casein kinase I and by GSK 3 at Ser/Thr residues marks β-catenin for ubiquitination and proteasomal degradation. In the presence of Wnt (Figure B), β -catenin phosphorylation and degradation is inhibited, and β -catenin is available for transcriptional regulation (Rayasam GV et al., 2009).*

1.6.2   Substrates of the GSK-3 protein

There are a number of proteins that have been identified as GSK-3 substrates. These proteins are implicated in a multitude of cellular processes. Of particular importance to our study are the following substrate proteins: GS, implicated in the insulin signalling pathway, and; NFAT and GATA-4, implicated in the pathogenesis of myocardial hypertrophy.

1.6.3   The role of GSK-3 protein in the development of insulin resistance and type 2 diabetes mellitus

Whole–body blood glucose homeostasis is a continuous process that is controlled by the efficient absorption of glucose and storage of excess glucose as glycogen. Glycogen synthase (GS) is a key enzyme which mediates the conversion of glucose to glycogen. In unstimulated cells GS is inactive. Insulin activates GS by inactivating GSK-3 (Cross *DA et al., 1995*; Rayasam GV *et al.,* 2009). This inactivation leads to a decrease in phosphorylation of GS, resulting in its activation, which promotes glycogen synthesis.

Abnormal GSK-3 activity has been implicated in the pathogenesis of insulin resistance and type 2 diabetes mellitus. Increased expression and activity of GSK-3 has been reported in the skeletal muscle of type 2 diabetes mellitus patients (Henriksen EJ and Dokken BB, 2006). This increase was associated with reduced muscle glycogen deposition. An increase in GSK-3 activity was also found in animal models. Eldar-Finkelman H *et al.* (1999) found that GSK-3 kinetic activity was higher in the fat cells of a C57/BL6 mouse strain fed a high caloric diet. These findings lead to the hypothesis that increased GSK-3 kinetic activity might result in impaired insulin signalling, which is implicated in the pathogenesis of the insulin resistant state and the development of type 2 diabetes. GSK-3 can also phosphorylate IRS-1 on a serine residue, thereby down-regulating glucose uptake (Eldar-Finkelman H and Krebs EG, 1997). This phosphorylation of IRS-1 by GSK-3 impairs insulin action (Eldar-Finkelman H and Krebs EG, 1997). Therefore, inhibition of GSK-3 should mirror the actions of insulin, by reducing glucose production and enhancing glucose storage to combat the hyperglycemia seen in the insulin resistant state and type 2 diabetes (Sutherland C, 2011). Many pharmaceutical companies have thus embarked on a quest to generate potent selective inhibitors of GSK-3 as potential antidiabetic agents which lower blood glucose.

1.6.4 The role of GSK-3 protein in the development of myocardial hypertrophy

1.6.4.1 *NFAT proteins and GATA-4 transcription factors*

NFAT proteins are a family of Rel homology domain containing transcription factors composed of five members: NFAT1 (also known as NFATp or NFATc2), NFAT2 (also known as NFATc or NFATc1), NFAT-3 (also known as NFATc4), NFAT4 (also known as NFATx or NFATc3) and NFAT5 (Hogan PG *et al.,* 2003).

The regulatory domain of NFAT mediates its activation, and calcium signalling mediates the effects of NFAT proteins. Upon calcium stimulation, hyper-phosphorylated NFAT proteins are dephosphorylated by calcineurin. This dephosphorylated NFAT then translocates to the nucleus, where it can complex with activated MEF2, and modulate gene transcription. In cardiac muscle, MEF2 is likely to cooperate with NFAT in the development of cardiac hypertrophy (Ramirez MT *et al.,* 1997; Molkentin JD *et al.,* 1998; Passier R *et al.,* 2000). This was demonstrated in a study where NFATc deficient mice were generated for direct evaluation of NFAT function. In this study they found that NFATc3 was partially responsible for calcineurin induced hypertrophy, as demonstrated by an attenuated hypertrophic response to pressure-overload in NFATc3 deficient mice (Wilkins BJ *et al.,* 2002). Besides calcineurin, nuclear translocation of NFAT is influenced by a number of parallel signalling pathways in the regulation of the hypertrophic response. GSK-3 is a downstream effector of the PI3K-PKB/Akt pathway and is essential for physiological hypertrophy. GSK-3 phosphorylates NFAT proteins, inhibiting both their nuclear localization and DNA-binding activity (Graef IA *et al.,* 1999). Overexpression of constitutively active GSK-3 mutants attenuated the hypertrophic response in cultured cardiac myocytes and induced NFAT translocation (Morisco C *et al.,* 2000; Haq S *et al.,* 2000). Transgenic expression of the same mutant inhibited hypertrophic growth in response to isoproterenol stimulation and pressure overload. These data suggest that other signalling pathways, particularly insulin signalling as found in the insulin resistant state, can also influence NFAT activity, which is implicated in the development of myocardial hypertrophy. Besides kinase regulation, the transcriptional activity of NFAT is also regulated by interaction with other transcription factors such as GATA-4, co-activators such as Ras and co-repressors such as MEK1 (Ichida M and Finkel T, 2001).

GATA proteins serve as binding partners for NFAT. GATA transcription factors are required for binding to the specific consensus DNA sequence (A/T)GATA(A/G) (Patient RK and McGhee JD, 2002). The GATA family consists of six proteins, GATA 1-6. GATA 1, 2 and 3 are important regulators of hematopoietic stem cells and their derivatives, whereas GATA-4, 5, and 6 are expressed in various mesoderm and endoderm-derived tissues, including the heart (Molkentin JD, 2000). GATA-4 plays an essential role in activating the myocardial hypertrophic gene program. This was demonstrated in a study where they found that overexpression of GATA-4 induced a greater than 2-fold increase in cardiac myocyte size in cultured cardiomyocytes (Pikkarainen S *et al.,* 2004; Molkentin JD, 2000). In a mouse model this hypertrophy further led to contractile dysfunction at 8 months of age. These results thus suggest that GATA-4 is a sufficient transcriptional regulator for the development of cardiac hypertrophy. GATA-4 activity is regulated by several signalling molecules including Erk, p38 MAPK and GSK3. GSK3 negatively regulates GATA-4 transcriptional activity through N-terminal phosphorylation. This phosphorylation subsequently promotes nuclear export of GATA-4. In transgenic mouse hearts expressing an activated mutant of PKB/Akt, it was found that GSK3 is hyperphosphorylated and inhibited (Condorelli G *et al.,* 2002). This inhibition of GSK-3 subsequently resulted in nuclear accumulation of GATA-4. This data shows that nuclear shuffling of GATA-4 represents an important mechanism whereby GSK3 regulates cardiac hypertrophy.

1.6.5   Inhibition of the GSK-3 protein

Aberrant protein kinase signalling has been implicated in obesity associated insulin resistance, diabetes and the resulting cardiovascular phenotype seen in obese patients. Protein kinases have thus become important targets for the development of therapeutic agents. Glycogen synthase kinase-3 is one such kinase which has received particular attention.

This has led to the development of a new generation of GSK-3 inhibitors with specific clinical implications, especially in the potential of these inhibitors to treat diseases such as type 2 diabetes, muscle hypertrophy, Alzheimer's disease, certain types of cancer, bipolar- and mood disorders, to name a few, that currently have significant limitations in therapeutic treatment. Lithium was the first GSK-3 inhibitor to be discovered and has been widely used to test the role of this enzyme in many disease states (Klein PS and Melton DA, 1996). However, it is non-specific and this has led to the development of potent, more specific inhibitors of GSK-3. There are three distinct regions of GSK-3 that are targeted by inhibitors to suppress its activity, namely the Metal ion (Mg+2) binding site, the substrate interaction domain and the ATP binding pocket (van Wauwe J and Haefner B, 2003). Most of the GSK-3 inhibitors that are available are ATP competitive inhibitors. As discussed in the preceding literature review, dysregulation of GSK-3 may affect the state of insulin resistance as well as the development of myocardial hypertrophy. In addition, it was found that GSK-3 is overexpressed in the muscle of type 2 diabetic patients. In this study we therefore researched the effects of a GSK-3 inhibitor supplied by Novartis namely an aminopyrimidine class, CHIR118637 (CT20026), GSK-3 inhibitor developed by Chiron. This class of inhibitors are also ATP competitive inhibitors. They have been shown to be very specific and inhibit the kinetic activity of both GSK-3 α and β isoform.

1.7 Hypothesis

Chronic inhibition of GSK-3 will (i) induce myocardial hypertrophy in control animals or (ii) exacerbate the development of existing hypertrophy in a pre-diabetic model of diet induced obesity and insulin resistance.

1.8 Objectives

1. Assess the extent of the development of myocardial hypertrophy in a rat model of diet induced obesity and insulin resistance.

2. Assess the expression levels of GSK-3 protein in the heart of the pre-diabetic animals in comparison to controls.

3. Assess the effect of inhibition of GSK-3 protein on the development of myocardial hypertrophy in both control and pre-diabetic animals

CHAPTER 2: MATERIALS AND METHODS

2.1   Animals

An experimental design was employed in this study where age-matched male Wistar rats were used. At four weeks after birth, the rats were weaned and placed on a standard rat chow diet. The animals were housed at the University of Stellenbosch Central Research Facility and had free access to food and water, with temperature and humidity kept constant at 22ºC and 40%, respectively. Furthermore, a 12 hour artificial day/night cycle was maintained. Throughout the study, the revised South African National Standard for the care and use of laboratory animals for scientific purposes was followed (SABS, SANS 10386, 2008). The study was assessed and approved by the Committee for Ethical Animal Research of the Faculty of Health Sciences, University of Stellenbosch. Ethics approval number is: 10GK_HUI01.

2.2   Grouping, feeding and treatment

When the animals had reached the desired weight (180±20g), they were randomly assigned to two groups and were placed on separate diets for 20 weeks. Control animals (n=34) received the standard rat chow (SRC), consisting of 60% carbohydrates, 30% protein and 10% fat, while the diet animals (n=34) received the high caloric diet (HCD), which resembles a Western-type diet, consisting of 65% carbohydrates, 19% protein and 16% fat (Pickavance LC *et al*., 1999) (table 1). The high caloric diet was prepared to contain 33% SRC, 33% sweetened full cream condensed milk (Clover [R]), 7% sucrose and 27% water (Pickavance LC *et al*., 1999) (table 2). Animals on the high caloric diet had a higher intake of calories per day compared to their age-matched control counterparts; 570±23kJ and 371±18kJ (table 1).

Table 1: *Dietary composition and energy consumption of control and diet induced obesity (DIO) rats (Du Toit EF et al., 2005; Pickavance LC et al., 1999).*

	Control	Diet Induced Obesity (DIO)
Carbohydrates	60%	65%
Protein	30%	19%
Fat	10%	16%
Energy consumption	371±8 kJ/day	570±23 kJ/day

Table 2: *Dietary composition of high caloric diet (Pickavance LC et al., 1999).*

High caloric diet composition	
Standard rat chow (SRC)	33%
Sweetened full cream condensed milk (Clover ®)	33%
Sucrose	7%
Distilled water	27%

Obesity in this model is induced by means of hyperphagia, and not by means of changes in the dietary composition of the food (Pickavance LC *et al.,* 1999). Hyperphagia-induced obesity in rats has been characterized in our laboratory and shown to be physiologically relevant and comparable to the human equivalent of metabolic syndrome as a result of obesity (Du Toit EF *et al.*, 2005). It was observed that, after 16 weeks of this diet, the animals developed signs of myocardial hypertrophy (Du Toit EF *et al.*, 2008). In order to ensure that hypertrophy was well pronounced in our model of diet induced obesity (DIO), a feeding period of 20 weeks was chosen, as opposed to the 16 weeks previously employed in our laboratory.

For a period of 8 weeks, beginning in week 13, half of the animals in both groups (control group: n=17 and diet group: n=17) received Glycogen Synthase Kinase (GSK)-3 inhibitor CHIR118637 (CT20026) treatment (supplied by Novartis). Chirone (CHIR118637) inhibitors are ATP competitive inhibitors, have been shown to be specific and target both GSK-3α and β isoforms (Cline GW *et al*., 2002; Meijer L *et al*., 2004). The GSK-3 inhibitor was administered to the rats individually, in the form of gelatine/ jelly cubes of equal size and volume (1 ml), to ensure absolute compliance and dose control. The dose of GSK-3 inhibitor was calculated based on the normal daily dosage prescribed by the manufacturer of 30 mg/kg/day.

2.3   Overview of experimental procedures

At the end of the 20 week time period, three series of experiments were conducted (figure 8). (i) The animals were fasted overnight and were subjected to echocardiography (n=6) (see pg. 36) to determine *in vivo* myocardial function and morphology. Afterwards, the animals were sacrificed by intra-peritoneal injection of sodium pentobarbital at a dose of 160mg/kg followed by exsanguination. The animals were continually monitored until total loss of consciousness was observed, as indicated by a total lack of response after a foot pinch. The body weight of sedated animals was recorded and blood collected via a once-off tail prick for measurement of plasma glucose concentration using a glucometer (GlucoPlusTM, Montreal, Canada). The hearts were removed, weighed, snap frozen and stored in liquid nitrogen for subsequent biochemical analysis to determine the expression of GSK-3, PKB/Akt, NFAT-3 and GATA-4. Further incisions were made exposing the fat masses in the viscera. The peritoneal and retroperitoneal fat were removed and weighed as a measurement of adiposity and to estimate the degree of obesity. The tibia was removed and its length determined.

Blood was collected from the abdominal cavity and subjected to centrifugation (micro-centrifuged at 1000 g at 4°C for 15 min); where after the serum aliquots were stored at −80 °C, to be used for metabolic analysis at a later stage. The serum insulin and blood glucose values that were obtained were used to calculate the Homeostatic model assessment of insulin resistance (HOMA-IR) (Matthews DR *et al*., 1985). Finally the lungs were removed and their wet weight was recorded. (ii) The animals were sacrificed and cardiomyocytes were prepared. The ability of the cells to accumulate radiolabelled deoxy-glucose after stimulation with insulin was determined. (iii) The animals were sacrificed, cardiomyocytes were prepared and used for fluorescence microscopy where the localization of key proteins implicated in the hypertrophy signalling cascade was monitored. Cell size was also determined using light microscopy.
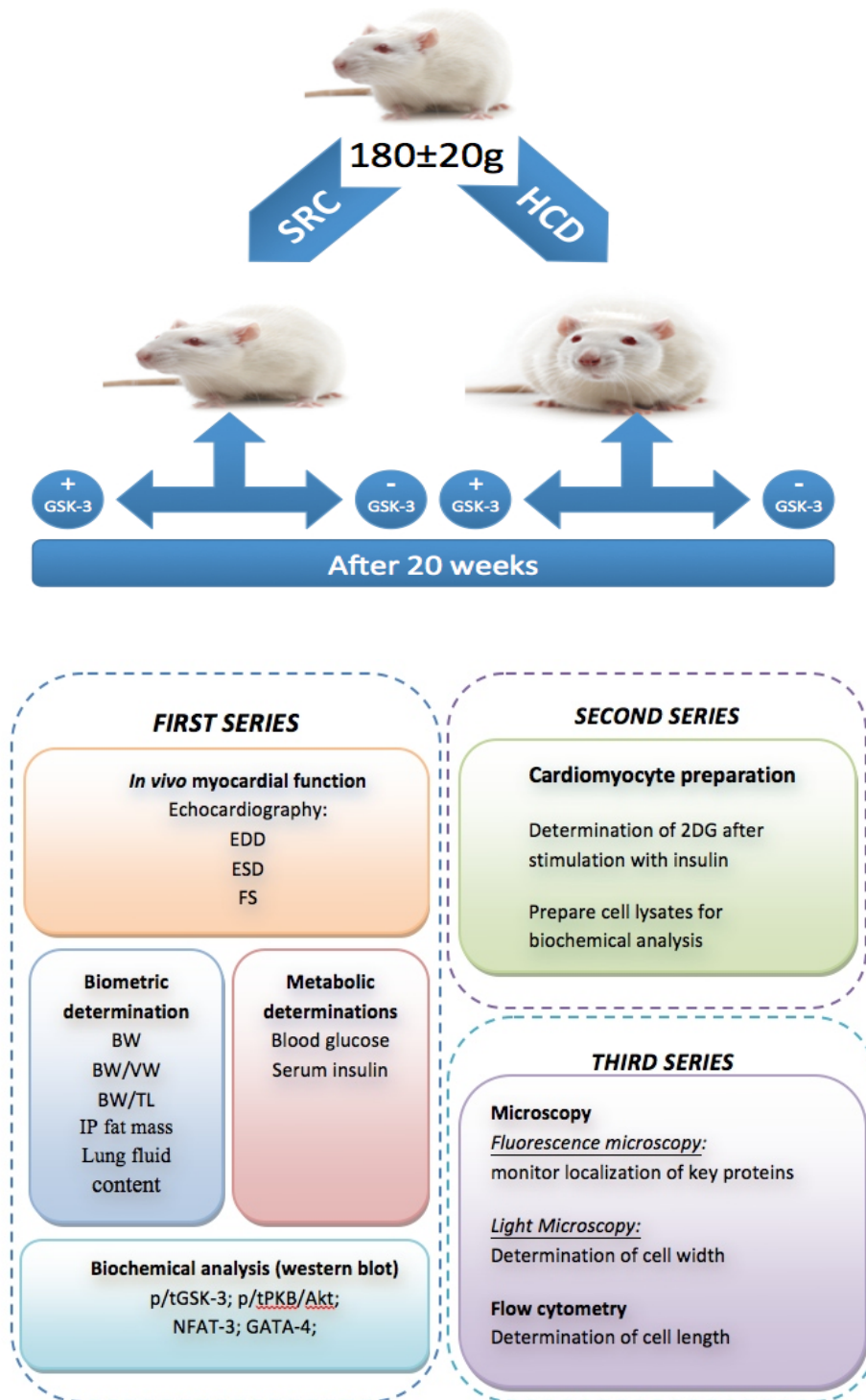
***Figure* 7**: *Overview of experimental procedures. Standard rat chow (SRC), high caloric diet (HCD), End diastolic diameter (EDD), End systolic diameter (ESD), body weight (BW), ventricular weight (VW), tibia length (TL), Intraperitoneal (IP), phospho/total (p/t), Glycogen synthase kinase (GSK-3), Protein kinase B (PKB/Akt), Glycogen synthase (GS), Nuclear Factor of Activated T Cells (NFAT-3) and 2-Deoxy-D-[³H] Glucose (2DG).*

2.3.1   Biometric determinations

2.3.1.1   *Determination body weight, ventricular weight and visceral fat content*

The body weight, ventricular weight, peritoneal and retroperitoneal fat were recorded as described in the experimental overview above.

2.3.2   Metabolic determinations

2.3.2.1   *Blood glucose*

Fasted plasma glucose concentration was measured using a glucometer (GlucoPlusTM, Montreal, Canada) as described in the experimental overview above.

2.3.2.2   *Serum insulin determination: Radioimmunoassay (RIA)*

The Coat-A-Count® (Diagnostic Products Corporation, LA, USA) assay is a solid-phase radioimmunoassay (RIA), where radioactive ^{125}I-labeled insulin is used. The insulin in the blood sample competes with radiolabelled insulin for binding sites on the insulin-specific antibody. This antibody is immobilized to the wall of the polypropylene tubes. Decanting the supernatant from the tubes terminates the competition and isolates the antibody bound fraction of the radiolabeled insulin. By counting the tubes in the gamma-counter, the presence of insulin in the blood sample can be measured against a standard curve. All samples were done in duplicate. Prior to the commencement of the assay, all the components of the assay were brought to room temperature, as instructed by the manufacturers. Uncoated 12 x 74 mm polypropylene tubes were labelled for total count (T) and non-specific binding (NSB) respectively.

Insulin-antibody coated tubes were labelled for standards (figure 9) and serum sample. 200 μL of the zero calibrator A was pipetted into the NSB and A tubes. 200 μL of the remaining calibrators and serum samples were pipetted in duplicate into the tubes prepared (table 3). 1.0 ml of ^{125}I insulin (table 3) was added to each tube and subsequently vortexed. Samples were incubated for 18 to 24 hours at room temperature and decanted thoroughly. This was done by placing each tube (except the total count tube) in a foam decanting rack and allowing the tubes to drain for 2 to 3 minutes. Following this, each tube was blotted on absorbent paper and to remove the excess moisture a cotton bud was used while avoiding touching the antibody coated part of the tube. Removal of excess fluid enhances the precision of the assay. The radioactivity of each tube was then measured in a gamma counter (Cobra II Auto Gamma, A. D. P, South Africa) for 1 min per tube and the sample antibody binding affinities, calculated from the insulin standard curve, which was generated by the gamma counter (figure 10).

Table 3: *Tabular representation of the calibrators and World Health Organization International Reference Preparation (IRP) of Insulin used (code 66/304).*

Calibrator	Approximate μIU/ml 1st IRP[code: 66/304]
A	0
B	5
C	15
D	50
E	100
F	200
G	350
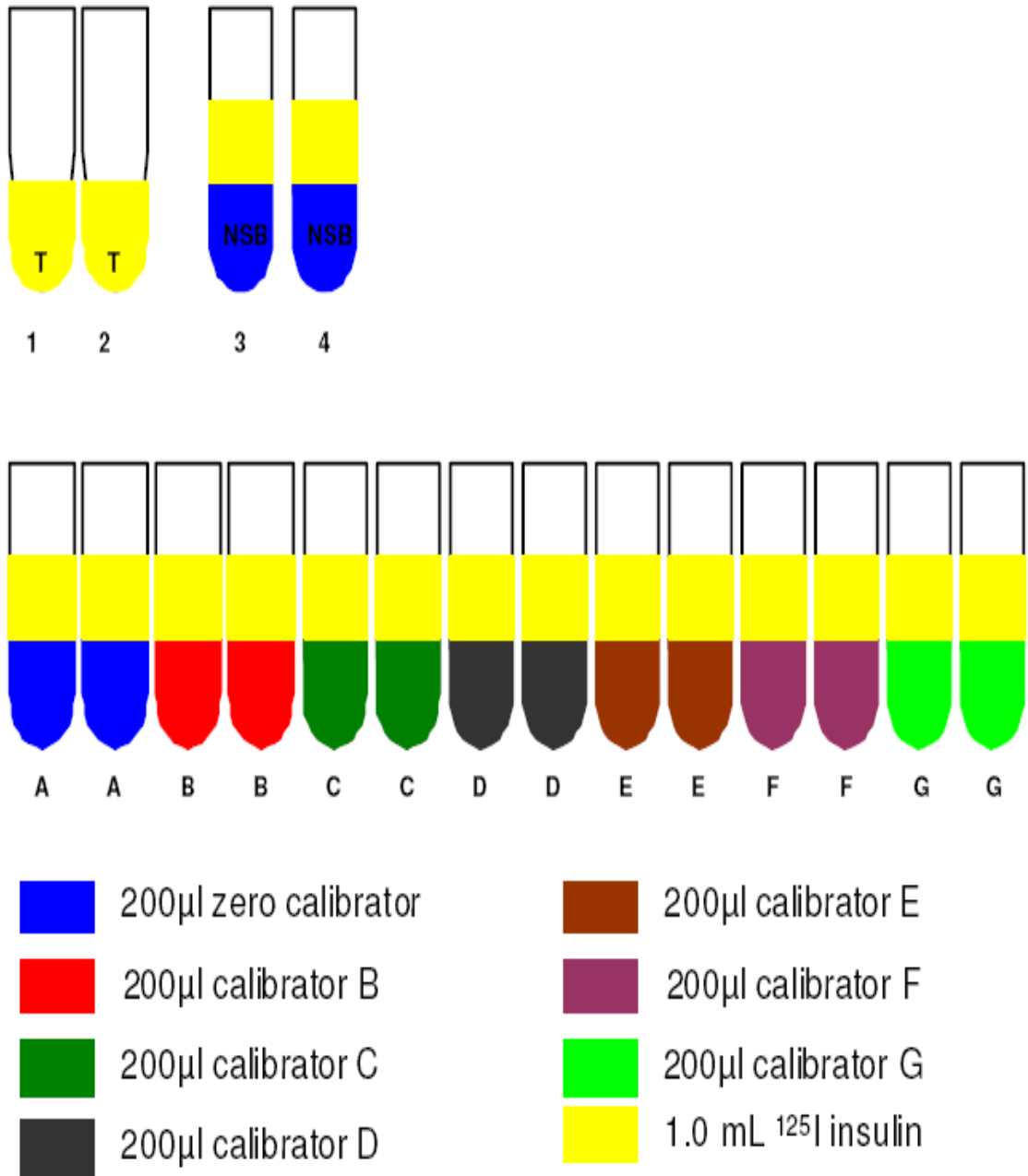
Figure 8: *Schematic representation of tube preparation.*
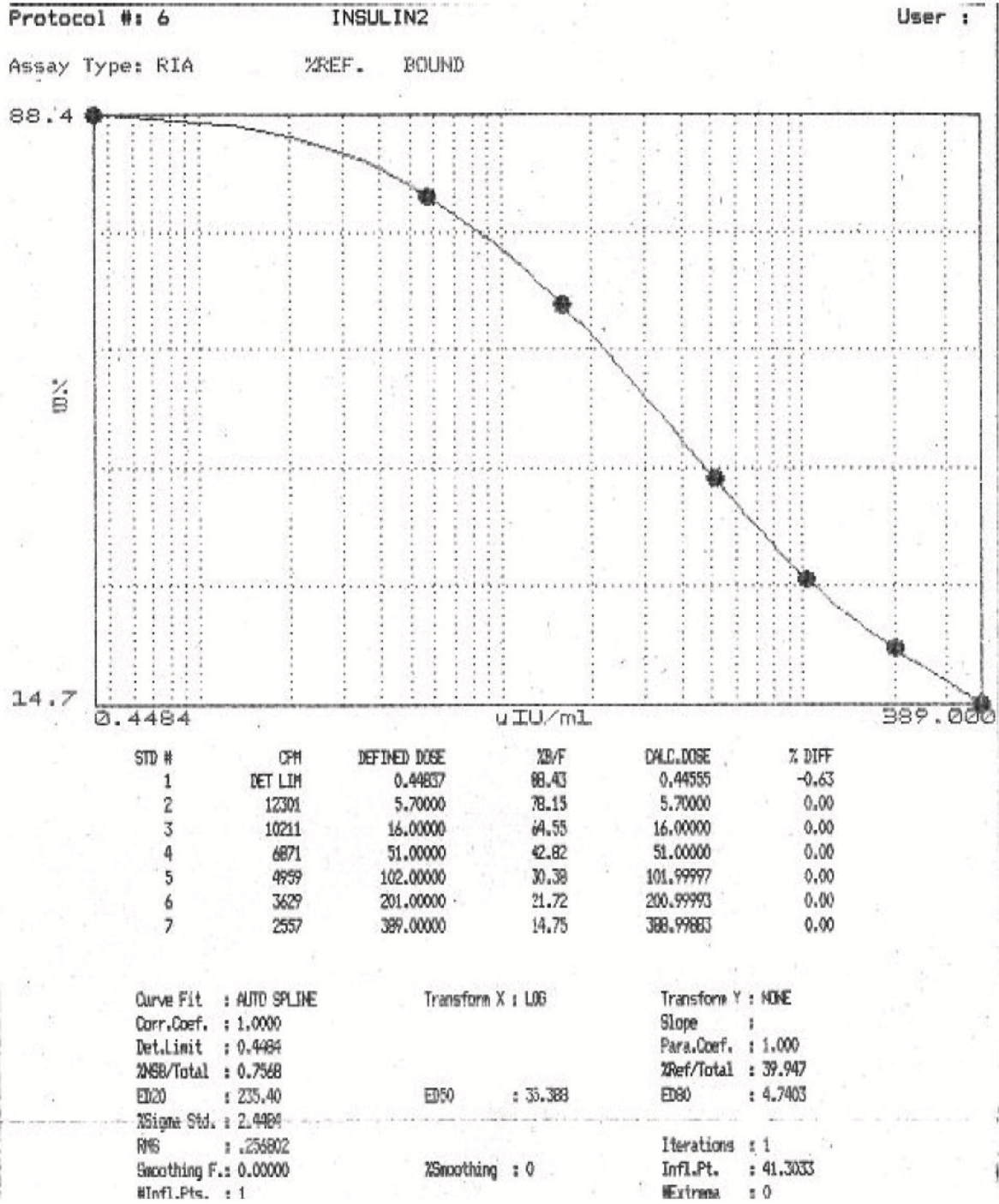
Figure 9: *Standard curve generated by the gamma-counter*

2.3.2.3   *HOMA-IR index*

HOMA-IR was used to estimate the degree of insulin resistance (Bonora E *et al*., 2002). A low HOMA-IR value indicates high insulin sensitivity and a high HOMA-IR indicates low insulin sensitivity/insulin resistance (Bonora E *et al.*, 2002).

Calculation of Homeostatic model assessment of insulin resistance (HOMA-IR)

HOMA-IR = fasting plasma glucose level (mmol/l) x fasting serum insulin level (µIU/ml) ÷ 22.5 (Matthews DR *et al*., 1985).

2.3.3   Preparation of cardiomyocytes

Adult ventricular cardiomyocytes were prepared from a separate group of animals after a diet period of 20 weeks (experimental series two). The cardiomyocytes were isolated from untreated control, untreated DIO, treated control +GSK-3 inhibitor and treated DIO + GSK-3 inhibitor animals. We employed the isolation method previously described by Fischer Y and colleagues (1991), which was subsequently modified in our laboratory (Huisamen B *et al.*, 2001). Hearts were excised from fully anaesthetized animals, and placed in ice-cold Krebs-Henseleit buffer. After isolation, hearts were cannulated via the aorta and retrogradely perfused, at a temperature of 37˚C, with a calcium free HEPES buffer "Solution A" containing: 6mM KCl, 1mM Na_2HPO_4, 0.2mM NaH_2PO_4, 1.4mM $MgSO_4$, 128mM NaCl, 10mM HEPES, 5.5mM D-glucose and 2mM pyruvate, pH 7.4, for five minutes to rinse out the blood. The perfusate was continually gassed with 100% O_2. Thereafter the heart was perfused, in a re-circulating fashion, in 50ml HEPES digestion buffer (100ml "Solution B" containing: "Solution A" + 0.7% fatty acid free BSA + 1mg/ml collagenase + 18mM 2,3 butanedione monoxime (BDM)) for 15 min. 50µl of $CaCl_2$ (100mM stock solution) was administered at 20 and again at 25 minutes of total perfusion time, respectively. Successful digestion was confirmed when perfusate flowed continuously.

After digestion, hearts were removed from the perfusion apparatus and the ventricles carefully removed from atria. The ventricular tissue was then gently torn apart and incubated in a post-digestion buffer (50ml "Solution C" containing: 50% of "Solution A" + 50% of "Solution B" + 1% BSA + 1% fatty acid free BSA + 0.2mM $CaCl_2$) for 15 min at 37°C in a shaking water-bath (180 strokes/min). A step-wise administration of calcium for a period of 5 minutes followed until a final concentration of 1.25mM was reached (4 x 100μl and 1 x 125μl of 100mM stock solution $CaCl_2$). Thereafter, the tissue was filtered through a nylon mesh (200 x 200μm) and samples were gently subjected to centrifugation at (100 rpm for 3 min). The cell pellet was re-suspended in Solution D ("Solution D" containing: "Solution A" + 2% fatty acid free BSA + 1.25mM $CaCl_2$) and the cells were allowed to settle for 5 min under gravity through the 2% BSA solution into a loose cell pellet. Only live, cardiomyocytes will settle. The supernatant, containing dead or dying cells, was aspirated and the cell pellet obtained was re-suspended in Solution D and left to stabilize on a slow rotator at room temperature for two hours. After the 2 hours had lapsed, the cells were allowed to settle under gravity and the supernatant gently removed. The cells were then washed twice with Solution E ["Solution E" containing: "Solution A" (minus D-glucose and pyruvate) + 2.0% fatty acid free BSA + 1.25mM $CaCl_2$) and allowed to settle under gravity, where after the supernatant was removed and the cell pellet used for 2-deoxy-D-[^{3}H] glucose (2DG) uptake experiments as discussed below.

The HEPES, pyruvate and BDM were all obtained from Sigma-Aldrich (St Louis, MO), the D-glucose was obtained from Merck (Pty) Ltd - South Africa, the Collagenase Type II was purchased from Worthington Biochemical Corporation (Lakewood, NJ) and the BSA was obtained from Roche (Cape Town).

2.3.4   Determination of 2-Deoxy-D-[³H] Glucose (2DG) uptake by cardiomyocytes

The ability of the cardiomyocytes to accumulate 2DG was measured as described previously by (Fischer Y *et al.*, 1991; Donthi RV *et al.*, 2000 and Huisamen B *et al.*, 2001). The cardiomyocyte cell pellet (see above) was suspended in 8ml of Solution E. 500µl of the cell suspension containing approximately 0.5µg protein was assayed in a total volume of 750µl. An assay in the presence of phloretin (final concentration of 400µM) was included to measure non-carrier mediated glucose uptake. The cells were then left to equilibrate for 15 min in a shaking water bath (180 strokes/minute) at 37 °C. Cells were then stimulated with or without 1nM, 10nM or 100nM insulin for 30 minutes. The samples were prepared in duplicate. The samples were then incubated with 1.5µCi/ml 2DG (PerkinElmer, Boston) in a final concentration of 1.8µM deoxy-glucose for 30 min, to allow for glucose uptake. In order to stop carrier-mediated (GLUT1 and GLUT4) glucose uptake 50µl (final concentration of 400µM) phloretin was added to each sample. Following a 2 min microfuge at 1000 g, this 2DG containing supernatant was aspirated and cells were washed twice with a basic HEPES buffer that contained: 6mM KCl, 1mM Na_2HPO_4, 0.2mM NaH_2PO_4, 1.4mM $MgSO_4$, 128mM NaCl and 10mM HEPES. The cell pellet was then dissolved in 0.5ml of 1 N NaOH at 70 °C in a water bath for 30 to 40 min; where after 0.5ml of dH_2O was added. Of this, 2 x 50µl of the sample was used for the determination of the protein content using the method of Lowry. In order to determine cell-associated radioactivity, the rest of the cell lysate was mixed with 2ml of scintillation fluid and kept overnight in the dark before counting in a scintillation counter (Beckman). 2DG uptake was presented as pmol 2DG/mg protein/30 min.

2.3.5   Protein determination Lowry method

As discussed, 2 x 50μl of the sample dissolved in 0.5N NaOH, was utilized to determine the protein content using the Lowry method (Lowry OH *et al.*, 1951). For this method three BSA protein standards of known concentration [0.238 mg/ml; 0.476 mg/ml and 0.952 mg/ml] were used and 0.5N NaOH was used as the blank. The reaction buffer, which contained 2% Na_2CO_3, 1% $CuSO_4.5H_2O$ and 2% NaK+ tartrate, was freshly prepared prior to experimentation. The assay was done in duplicate and 50μl of blank, standards and samples were used to perform the protein assay. 1ml of the reaction medium was added to the blank, standards and samples at 10 second intervals, rapidly vortexed and allowed to stand at room temperature for 10 min. Afterwards 0.1ml Folin-Ciocalteu's phenol reagent (1:2 dilution with distilled water) was added at the same 10 second intervals, vortexed and allowed to stand for 30 min. This resulted in a colour development of which the absorbance was read spectrophotometrically at 750nm against the blank. The standard curve was used to determine the protein concentrations of the samples.

2.3.6   Indices of cardiac hypertrophy

2.3.6.1   Ventricular weight to body weight ratio

At the time of sacrifice, the hearts were rapidly removed and placed in a 4˚C Krebs-Henseleit solution to arrest the heart. Both atria were rapidly removed along with the excess non-cardiac tissue, leaving only the ventricles. The ventricles were blotted on an absorbent paper towel, weighed, freeze clamped and stored in liquid nitrogen for biochemical analysis. Hypertrophy is indicated by an increase in ventricular weight normalised for body weight (ventricular weight/body weight). This method has been used in other publications as a measure of hypertrophy (Skoumal R *et al*., 2004; Asai T *et al*., 2005).

2.3.6.2   *Ventricular weight to tibia length ratio*

During the sacrifice, the right hind limb was amputated. This was done close to the hip joint in order not to damage the tibia. The tibia was then cleaned, removing all the muscle tissue and the length was measured in cm with a calliper. The heart weight was then expressed as a ratio to the tibia length. This approach was found to be a more accurate index of cardiac hypertrophy than the heart weight-to-body weight ratio in conditions where there are fluctuations in body weight (Yin FC *et al*., 1982; Brede M *et al*., 2003; and Saupe KW *et al*., 2003).

2.3.7   Lung sampling and determination of the lung fluid content

After the animals were sacrificed, representative tissue samples were taken from both lungs and the wet weight was recorded. The samples were then weighed again after 4-5 days of drying at 70°C. The wet -to-dry weight ratio was calculated as follows:

w/d= (weight $_{wet}$ −weight $_{dry}$)/weight $_{wet}$ x 100 (Klinzing S *et al.,* 2000).

Accumulation of fluid in the lungs is used as an indicator of heart failure.

2.3.8   *In vivo* myocardial function

2.3.8.1   *Echocardiography*

After 20 weeks on the feeding program, echocardiography was performed to determine cardiac geometry and function. A 5% isoflurane/oxygen mix was used for the induction of anaesthesia. The rats were placed on a Deltaphase operating board in a left lateral decubitus position. Anaesthesia was maintained with a mixture of 1.5% isoflurane/oxygen. The images were acquired with a Siemens Acuson Sequoia 512 Ultrasound system and a 15L8 transducer (Siemens, Berlin, Germany) and were analysed at the time of acquisition. This was a blinded study, and all studies were performed and interpreted by the same operator. Short-axis 2-dimensional and M-mode measurements of the LV diameters were taken at the level of the papillary muscle and all measurements were averaged over 3 consecutive cardiac cycles.
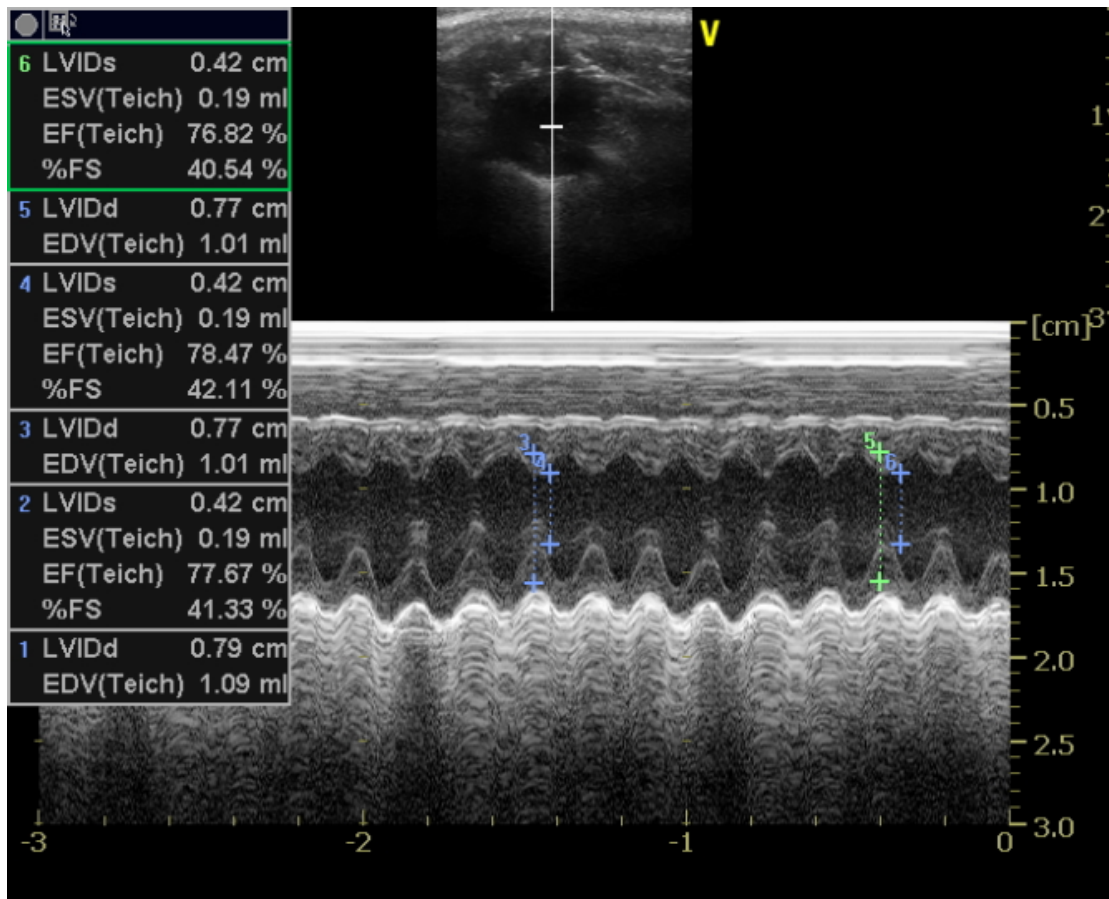
Figure 10 *A typical echocardiogram indicating the left ventricular dimensions of the rat heart that were ued to determine in vivo myocardial function*

Investigated parameters

For morphological characterisation of the hearts, the following echocardiographic parameters were compared between the different groups.

(Left ventricular) End-diastolic diameter (EDD)

(Left ventricular) End-systolic diameter (ESD)

From these parameters, the LV fractional shortening (in %) was calculated as follows:

%FS={(EDD – ESD) / EDD} x 100

After echocardiography, the rats were placed in a cage and allowed to recuperate.

2.3.9   Biochemical analysis

2.3.9.1   *Western Blotting:*

Freeze clamped hearts were used to determine the expression of key proteins in the insulin signalling pathway and pathways linked to hypertrophy.

2.3.9.2   *Protein extraction of different tissue fractions*

Cardiac tissue was fractionated into a nuclear, cytosolic and membrane fraction (figure 11). The proteins of interest were extracted from the cardiac tissue by means of two lysis buffers (lysis buffer with or without Triton X-100) the first buffer contained the following: 20mM Tris-HCl (pH 7.5), 1mM EGTA, 1mM EDTA, 1mM NaCl, 1mM β -glycerophosphate, 2.5mM tetra-sodium-pyrophosphate, 1mM sodium orthovanadate (Na_3VO_4), 1% Triton X-100, 10μg/ml leupeptin, 10μg/ml aprotinin and 50μg/ml phenylmethyl sulfonyl fluoride (PMSF), while the second buffer did not contain any Triton X-100. Frozen heart tissue ($\pm$ 360mg) was pulverized and homogenized, using a Polytron PT-10 homogenizer (2 x 4 sec, setting 4) in 0.8ml cold lysis buffer without Triton X-100. The homogenate was left to stand on ice for 15 minutes allowing digestive processes to take place. After 15 minutes, the homogenate was transferred to Sorvall SS34 rotor centrifuge tubes and samples were subjected to centrifugation at 1000 g (2500 rpm) for 10 min at 4°C, where after the supernatant (containing cytosolic and membrane fraction) was collected in a separate set of Beckmann® TL 50 rotor centrifuge tubes. The pellet containing the nuclear fraction was kept. The supernatant (containing the cytosolic and membrane fraction) was then centrifuged, using the ultra-centrifuge (Beckmann®, TL 50 rotor centrifuge), at 33 000 rpm for 1 hour. The supernatant obtained by this centrifugation contained the cytosolic fraction while the pellet contained the membrane fraction. A Bradford (Bradford MM, 1976) protein assay was performed on the supernatant to determine the protein content in the samples.

To the membrane fraction 200μl of lysis buffer with Triton X-100 was added and a Potter Elvehjem Teflon homogeniser used to digest the pellet. 2 x 50μl of the lysate was precipitated in 0.5N NaOH, in order to determine the protein content using the Lowry method (Lowry OH *et al.*, 1951). Using the pellet from the first centrifugation, 600μl of lysis buffer with Triton X-100 was added to the pellet and the contents were transferred to a Potter Elvehjem Teflon homogeniser, homogenised five times, transferred to centrifuge tubes, and left on ice for 30 min. Thereafter, the samples were centrifuged at 15 000 g (13 000 rpm) for 30 min, using the Sorvall SS34 rotor. The supernatant contained the nuclear fraction and the pellet was discarded. A Bradford protein assay was also performed on this fraction to determine the protein content in our samples.

Homogenization in buffer without Triton
Centrifugation @ 1000 g, 10min

Supernatant (cytosolic + membrane fractions)
Centrifugation @ 33 000g, 1hour

Pellet (nuclear fraction)
Homogenize in buffer + Triton
Centrifugation @ 15 000, 30min

Supernatant (cytosolic fraction)
Bradford for protein

Pellet (membrane fraction)
Homogenize in buffer + Triton
Lowry for protein

Supernatant (nuclear fraction)
Bradford for protein

Pellet discarded

Figure 11: Schematic representation of fractionation procedure.

The Bradford solution contained: 0.6mM Coomassie Brilliant Blue G-250, 95% ethanol and 85% (w/v) phosphoric acid. Colour development (absorbance) was read spectrophotometrically at 595nm against a blank and sample values were determined from a standard curve generated from bovine serum albumin (BSA) of known concentrations. This sensitive method is suitable for measuring microgram quantities of proteins. Samples for Western blotting were diluted in Laemmli sample buffer (4% SDS, 20% glycerol, 10% 2-mercaptothanol, 0.0004% bromphenol blue and 0.125M Tris-HCl) to contain equal amounts of protein per volume unit (Laemmli UK, 1970). The samples were then boiled for 5 minutes and aliquots stored at -80°C.

2.3.9.3   Protein separation

All stored aliquots were boiled for 5 min and samples were subjected to centrifugation at 15000rpm for 5 min. 50μg protein was loaded in a stacking polyacrylamide gel and the proteins separated according to their molecular weights by a sodium dodecyl sulfate–polyacrylamide gel electrophoresis (SDS-PAGE) in running buffer. The running buffer contained: 50mM Tris, 384mM glycine and 1% SDS. A standard Bio-RAD Mini-Protein III system was used. A protein ladder, obtained from Fermentas Life Sciences, was used as marker to identify the molecular weights of the proteins of interest. The proteins separated within the SDS-gel were then transferred to polyvinylidene fluoride (PVDF) membranes (ImmobilonTM P, Millipore) with an applied electrical current of 200V, 200mA for 1 hour, in a tank filled with transfer buffer. The transfer buffer consisted of 25mM Tris, 192mM glycine and 20% methanol. At the end of the transfer period, the membranes were immersed in fresh methanol and left to air dry. This was done so that the membranes could be stained with 5% Ponçeau Red in acetic acid (reversible protein stain), for visualization of proteins and to confirm whether adequate transfer did occur.

Once the Ponçeau Red was rinsed off, the non-specific binding sites on the membranes were blocked by gently incubating the membrane in 5% fat-free milk, made up in a TBS-Tween solution (Tris-buffered saline (TBS) plus 0.1% Tween 20), for between 1 and 2 hours, at room temperature on a shaker. At the end of the blocking period, the membranes were thoroughly washed in the TBS-Tween solution. These membranes were then probed with primary antibodies directed against: NFAT-3 (Cell Signaling Technology; 1:400), Gata-4 (Santa Cruz Biotechnology Inc; 1:400), total and phospho-PKB/Akt (Ser473) (Cell Signaling Technology; 1:1000) and total and phospho GSK-3 (β-47kDa and α-51kDa) (Cell Signaling Technology; 1:1000) and left to incubate overnight at 4°C (membranes were probed for phospho protein and stripped to determine total protein expression levels).

2.3.9.4   *Immunodetection of protein*

After the overnight primary antibody incubation, the membranes were thoroughly washed in TBS/Tween and incubated in a Horseradish-peroxidase conjugated secondary antibody (from donkey), (Amersham Life Science, Sandton, Johannesburg), for 1 hour at room temperature on a shaker. This conjugated antibody binds to the already bound primary antibody. To remove the excess secondary antibody, the membranes were washed extensively in TBS/Tween and kept moist. Proteins were visualized by covering the membrane with enhanced chemiluminescence (ECL) detection reagent (Amersham Life Science, Sandton, Johannesburg) for 1 minute and then exposing it to an autoradiography film (Hyperfilm ECL, RPN 2103). The Horseradishperoxidase reacts with the detection reagent in a luminescence reaction and the resulting light emission is captured on the radiography film. Band intensities were then densitometrically quantified using UN-SCAN-IT (version 5.1, Silkscience) image analysis software.

For analysis, all the data was normalised to the untreated condition. In all instances the membranes were stripped, by incubating for 5 min in 0.2M NaOH and re-blotted with antibody against β-tubulin (Cell Signaling Technology; 1:1000) to verify the uniformity of protein loading and the transfer efficiency across the test samples, in instances where there was unequal loading these values were not used.

2.3.10 Immunofluorescence for the detection of NFATc-3 and GATA-4 localization.

Immunofluorescence is a technique allowing the visualization of a specific protein or antigen in cells or tissue sections by binding a specific antibody chemically conjugated with a fluorescent dye such as fluorescein isothiocyanate (FITC). There are two major types of immunofluorescence staining methods: 1) direct immunofluorescence staining in which the primary antibody is labelled with fluorescence dye, and 2) indirect immunofluorescence staining in which a secondary antibody labelled with fluorochrome is used to recognize a primary antibody (Rosendal S and Black FT, 1972).

In our experiment the indirect immunofluorescence method was used to visualise NFATc3 and GATA-4 distribution and localisation in cardiomyocytes in our model of diet induced obesity and insulin resistance. For this technique, cardiomyocytes were prepared as described previously. After the resting period the cells were plated in laminin coated 6 well plates. A concentration of $10.0mg/cm^2$ was used and the plates were left for a period of 2-3 hours (Bird SD *et al*., 2003). The laminin facilitates cardiomyocyte attachment. After this time had elapsed, Solution E was removed (see p 42) and the monolayer of cells was washed twice with sterile PBS (0.1M). A 1:1 ratio of the fixative methanol/acetone (1ml/coverslip) was added, and incubated at 4ºC for 10 minutes. The fixative was subsequently removed and cells were air dried for 20 minutes at room temperature. Cells were rinsed with PBS and the coverslips were then transferred onto temporary microscope slides. 100µl 5% donkey serum was added for 20 minutes at room temperature.

After draining the serum, 100µl primary antibody was added. In this particular case, the following primary antibodies were used NFATc3 (Santa Cruz Biotechnology Inc) (source: goat polyclonal antibody, 1:50 dilution) and GATA-4 (Santa Cruz Biotechnology Inc) (source: rabbit polyclonal antibody, 1:200 dilution) (Tokudome T *et al.,* 2005) while PBS was added to the controls. This was incubated overnight at 4ºC. The primary antibody solution was removed and the cells were once again rinsed carefully with PBS. The cells were then incubated with 100µl of a Donkey anti-goat FITC (green) (Santa Cruz Biotechnology Inc) and Donkey anti-rabbit Texas Red (Santa Cruz Biotechnology Inc) conjugated secondary antibody solution (1:200 dilution) (Tokudome T *et al.,* 2005), where the former was directed against NFATc3 and the latter against GATA-4, for 30 minutes at room temperature. In addition, 100µl Hoechst 33342 (1:200) dye was added for a further 10 minutes. The cells were finally washed 3 times with PBS and mounted on permanent microscope slides. The serum, primary and secondary antibodies and Hoechst dye were made up with sterile PBS. Image acquisition was performed on an Olympus Cell® system attached to an IX 81 Inverted fluorescence microscope equipped with a F-view-II cooled CCD camera (Soft Imaging Systems). Using a Xenon-Arc burner (Olympus Biosystems GMBH) as light source, images were acquired using the 360nm, 472nm or 572nm excitation filter. Emission was collected using a UBG triple-bandpass emission filter cube (Chroma). Images were acquired through z-stacks, using an Olympus Plan Apo N60x/1.4 Oil objective. Four random areas within each image were taken to depict the localization of NFATc3 and GATA-4. The scale used was 0.002nm for high magnification and 0.2nm for lower magnification.

2.3.11 Light microscopy for cell size determination

For cell width determination the images were acquired using the same Olympus Cell® system. An inverted light microscope equipped with a F-view-II cooled CCD camera (Soft Imaging Systems) was used on the fixed cells that were prepared for the immunofluorescence experiment described above. Approximately 60-80% of the cells on the cover slips were rod-shaped cardiac myocytes. Between 40-50 cells were selected from each group (n=2-3), using 3 different planes. Using the program, Act2U (Ver. 1.70 Nikon Corporation, Japan), the width of each cell was measured diagonally from a visible nucleus.

2.4 Statistical analysis

All data were presented as mean ± standard error of the mean (SEM), unless otherwise stated. When comparisons between two groups were made, the two-tailed unpaired Student t-test was used. For multiple group comparisons 2 way-ANOVA followed by a Bonferroni post-hoc test was used. *p < 0.05* was considered as statistically significant. All statistical analysis of data was performed using GraphPad Prism 5®.

CHAPTER 3: RESULTS

3.1 Biometric and metabolic data of 20 week untreated and treated control, untreated and treated DIO animals

Table 4: *Biometric and metabolic data of 20 week untreated and treated control, untreated and treated DIO animals. All values are expressed as mean ±SEM. n=5-6; p<0.05;*p<0.005; ‡p<0.0005; $^{¥}$p<0.01; $^{+}$p<0.001*

	Control		DIO	
	Untreated	Treated	Untreated	Treated
Body weight (g)	402±11	447±11 [#]	529±26 [*]	529±18
Ventricular weight (g)	0.983±0.030	1.075±0.022 [#]	1.158±0.029 [*]	1.127±0.045
Intraperitoneal fat (g)	16.6±1.7	18.8±1.9	35.5±3.7 [+]	36.2±3.2
Glucose (mmole/L)	5.52±0.34	5.43±0.32	6.68±0.37 [#]	5.82±0.42
Serum insulin (pmoe/L)	17.12±0.80	28.18±3.36 [¥]	32.91±2.8 [‡]	22.93±1.62 [#]
HOMA	4.20±0.31	6.64±1.04 [¥]	7.54±1.63 [+]	7.08±1.64

After 20 weeks on the respective diets, (i) the DIO rats were significantly heavier than their age-matched control counterparts (529±26 g vs. 402±11 g; *p<0.005). This obese state was also associated with a significant increase in (ii) the ventricular weight (1.158±0.029 g vs. 0.983±0.030 g; *p<0.005), (iii) intraperitoneal fat mass (35.5±3.7 g vs. 16.6±1.7 g; $^{+}$p<0.001), (iv) fasted blood glucose (6.68±0.37 mmol/L vs. 5.52±0.34 mmol/L; $^{#}$p<0.05), and (v) serum insulin levels (32.91±2.8 pmol/L vs. 17.12±0.80 pmol/L; ‡p<0.0005). (vi) The mean HOMA index of the DIO animals was also significantly greater when compared to the controls (7.54±1.63 vs. 4.20±0.31; $^{+}$p<0.001). This data suggests that the DIO animals developed insulin resistance during this 20 week high caloric feeding programme.

The GSK-3 inhibitor treatment (i) increased the body weight significantly in the controls (treated control 447±11 g vs. untreated control 402±11 g; [#]p<0.05), however it had no significant effect on the body weight of the DIO animals (treated DIO 529±18 g vs. untreated DIO 529±26 g). (ii) The ventricular weight was significantly higher in the treated controls vs. their untreated control counterparts (treated control 1.075±0.022 g vs. untreated control 0.983±0.030 g; [#]p<0.05). This increase in ventricular weight was, however, not evident in the treated DIO animals vs. the untreated DIO counterparts (treated DIO 1.127±0.045 g vs. untreated DIO 1.158±0.029 g). (iii) The GSK-3 inhibitor treatment did not influence the intraperitoneal fat mass in the controls (untreated control 16.6±1.7 g vs. treated control 18.8±1.9 g), nor the DIO animals (untreated DIO 35.5±3.7 g vs. treated DIO 36.2±3.2 g). (iv) The GSK-3 inhibitor treatment had no significant effect on fasted blood glucose levels both in the controls (treated control 5.43±0.32 mmol/L vs. untreated control 5.52±0.34 mmol/L) and DIO animals (treated DIO 5.82±0.43 mmol/L vs. untreated DIO 6.68±0.36 mmol/L). (v) The GSK-3 inhibitor treatment increased fasted serum insulin levels significantly in the controls (treated control 28.18±3.36 pmol/L vs. untreated control 17.12±0.80 pmol/L; [¥]p<0.01) and decreased the fasted serum insulin levels of the DIO animals significantly (treated DIO 22.93±1.62 pmol/L vs. untreated DIO 32.91±2.77 pmol/L; [#]p<0.05). (vi) The mean HOMA index in the treated controls was significantly larger than in the untreated controls (treated control 6.64±1.04 vs. untreated control 4.20±0.31; [¥]p<0.01). In the treated DIO animals the GSK-3 inhibitor treatment had no significant effect on the mean HOMA index (treated DIO 7.08±1.64 vs. untreated DIO 7.54±1.63).

3.2 Cardiomyocyte preparation and glucose uptake

3.2.1 Basal glucose uptake by cardiomyocytes

At basal levels, the diet had no significant effect on glucose uptake in cardiomyocytes prepared from the control and DIO animals (control 15.08±1.26 pmol/mg protein/30min vs. DIO11.43±1.01 pmol/mg protein/30min). The GSK-3 inhibitor treatment also had no significant effect in the control animals (treated control 19.83±4.02 pmol/mg protein/30min vs. untreated control 15.08±1.26 pmol/mg protein/30min) and DIO animals (treated DIO 17.72±3.13 pmol/mg protein/30min vs. untreated DIO 11.43±1.01 pmol/mg protein/30min).
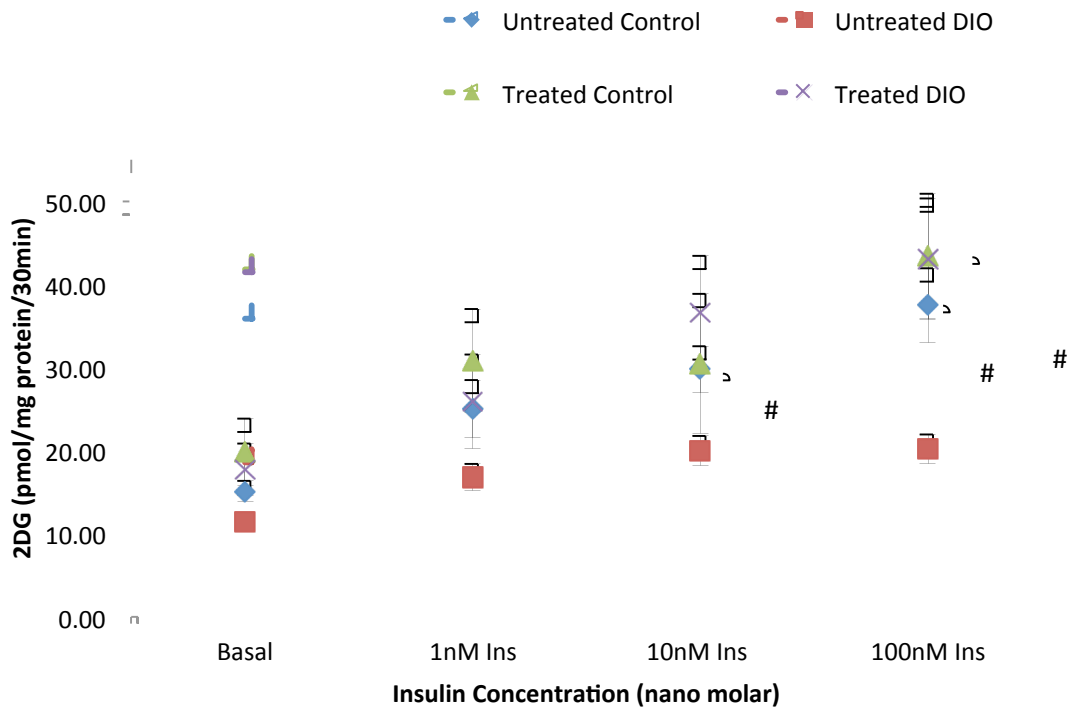
Figure 12: *Insulin-stimulated 2-deoxy-[³H]-glucose accumulation by isolated cardiomyocytes prepared from untreated and treated control and DIO animals. A concentration range from 1nM to 100nM insulin was used. All values are expressed as mean ±SEM. n=5; #p<0.05.*

3.2.2 Glucose uptake by cells after insulin stimulation at different concentrations

3.2.2.1 *Stimulation with 1nM insulin*

When the cardiomyocytes were stimulated with insulin at concentrations of 1nM, there was a decrease in the insulin sensitivity of the cardiomyocytes prepared from DIO animals (DIO 16.81±1.61 pmol/mg protein/30min vs. control 25.06±3.46 pmol/mg protein/30min) noticeable, however, this decrease was not significant. The GSK-3 inhibitor treatment had no significant effect on glucose uptake in the control animals (treated control 30.79±6.26 pmol/mg protein/30min vs. untreated control 25.06±3.46 pmol/mg protein/30min) and DIO animals (treated DIO 25.89±5.67 pmol/mg protein/30min vs. untreated DIO 16.81±1.61 pmol/mg protein/30min).

3.2.2.2 *Stimulation with 10nM insulin*

When the cardiomyocytes were stimulated with insulin at concentrations of 10nM, the cells prepared from DIO animals had a significantly impaired response to insulin compared to the control animals (DIO 20.00±1.76 pmol/mg protein/30min vs. control 29.80±2.76 pmol/mg protein/30min; [#]$p<0.05$). The GSK-3 inhibitor treatment had no significant effect on glucose uptake in the control animals (treated control 30.45±8.41 pmol/mg protein/30min vs. untreated control 29.80±2.76 pmol/mg protein/30min). In the DIO animals the GSK-3 inhibitor treatment increased glucose uptake (treated DIO 36.61±6.84 pmol/mg protein/30min vs. untreated DIO 20.00±1.76 pmol/mg protein/30min), however, this increase was not significant. Despite the fact that the increases in insulin stimulated glucose uptake was not significant in either of the treatment groups when compared to cells from untreated animals, a 2-way ANOVA showed a significant overall effect of the treatment ($p<0.05$).

3.2.2.3 *Stimulation with 100nM insulin*

When the cardiomyocytes were stimulated with insulin at concentrations of 100nM, the cells prepared from DIO animals had a significantly impaired response to insulin compared to the control animals (DIO 20.19±1.78 pmol/mg protein/30min vs. control 37.48±4.46 pmol/mg protein/30min; [#]$p<0.05$). The GSK-3 inhibitor treatment had no significant effect on glucose uptake in the control animals (treated control 43.41±7.52 pmol/mg protein/30min vs. untreated control 37.48±4.46 pmol/mg protein/30min). In the treated DIO animals there was a significant increase in glucose uptake (treated DIO 43.07±7.27 pmol/mg protein/30min vs. untreated DIO 20.19±1.78 pmol/mg protein/30min; [#]$p<0.05$) after stimulation with 100nM of insulin. At this concentration a 2-way ANOVA showed a significant overall effect of the treatment ($p<0.05$) on insulin stimulated glucose uptake.

3.3 Indices of myocardial hypertrophy

3.3.1 VW/BW ratio
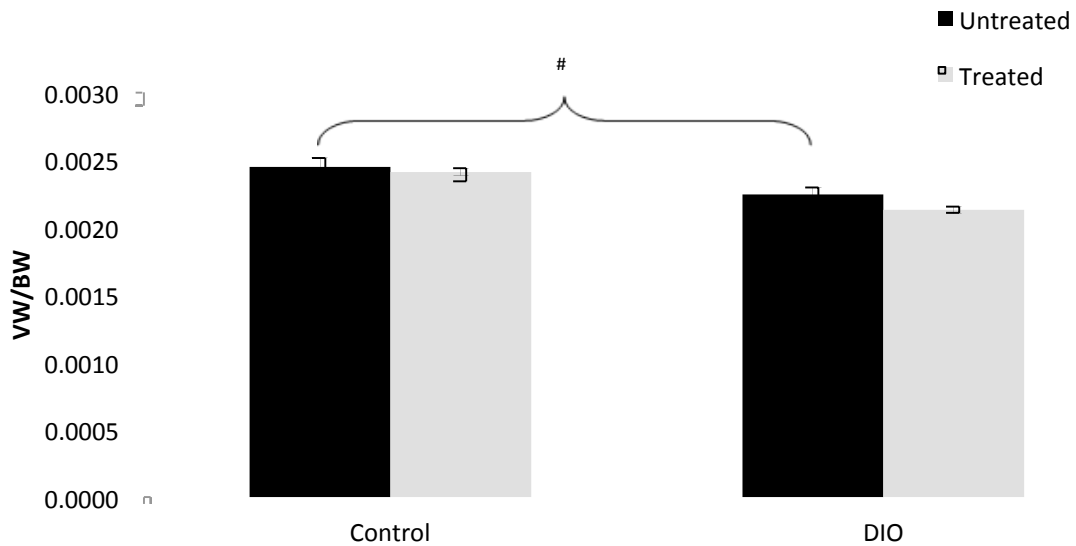
Figure 13: *VW/BW ratio of 20 week untreated and treated control and treated DIO animals. All values are expressed as mean ±SEM. VW-ventricular weight, BW-body weight n=6; [#]p<0.05*

There was a significant difference in the VW/BW ratio between the control vs. DIO rats ($2.45 \times 10^{-3} \pm 6.67 \times 10^{-5}$ vs. $2.21 \times 10^{-3} \pm 5.40 \times 10^{-5}$; [#]p<0.05). The GSK-3 inhibitor treatment had no significant effect on the VW/BW ratio in the controls (treated control $2.41 \times 10^{-3} \pm 2.94 \times 10^{-5}$ vs. untreated control $2.45 \times 10^{-3} \pm 6.67 \times 10^{-5}$) and in the DIO animals (treated DIO $2.13 \times 10^{3} \pm 2.30 \times 10^{-5}$ vs. untreated DIO $2.21 \times 10^{-3} \pm 5.40 \times 10^{-5}$).

3.3.2   VW/TL ratio
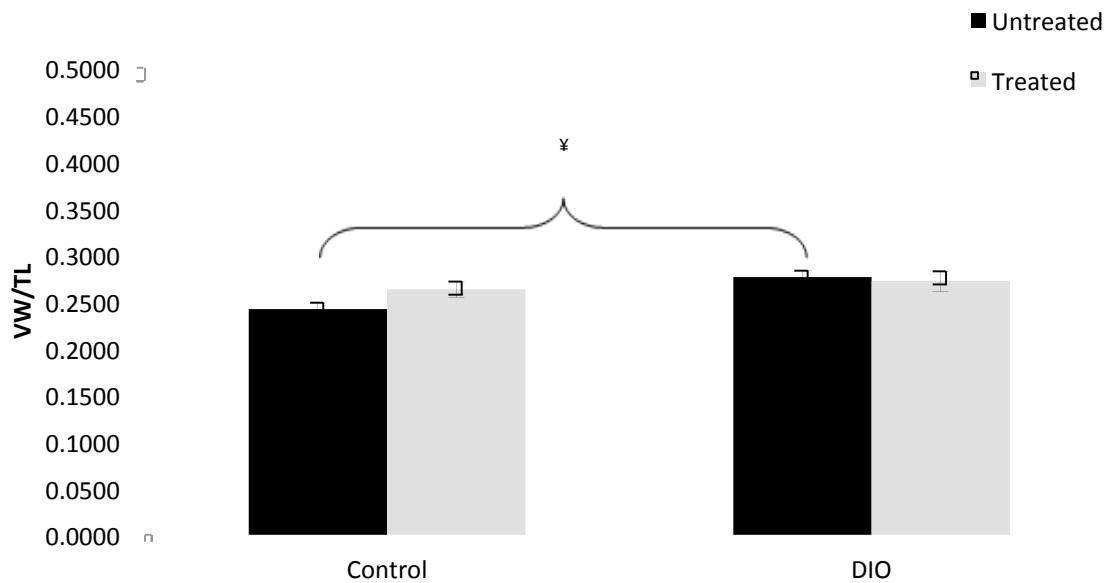
Figure 14: *VW/TL ratio of 20 week untreated and treated control and treated DIO animals. All values are expressed as mean ±SEM. VW-ventricular weight, TL-Tibia length n=6; ¥p<0.01*

There was a significant difference in the VW/TL ratio between the control vs. DIO rats (0.242 ± 0.007 vs. 0.276 ± 0.007; $^{¥}p<0.01$). This finding indicates that after 20 weeks on the diet, the hearts from the DIO rats had developed myocardial hypertrophy. The GSK-3 inhibitor treatment had no significant effect on the VW/TL ratio in the controls (treated control 0.263 ± 0.009 vs. untreated control 0.242 ± 0.007), nor in the DIO animals (treated DIO 0.272 ± 0.010 vs. untreated DIO 0.276 ± 0.007).

3.4   Lung fluid content
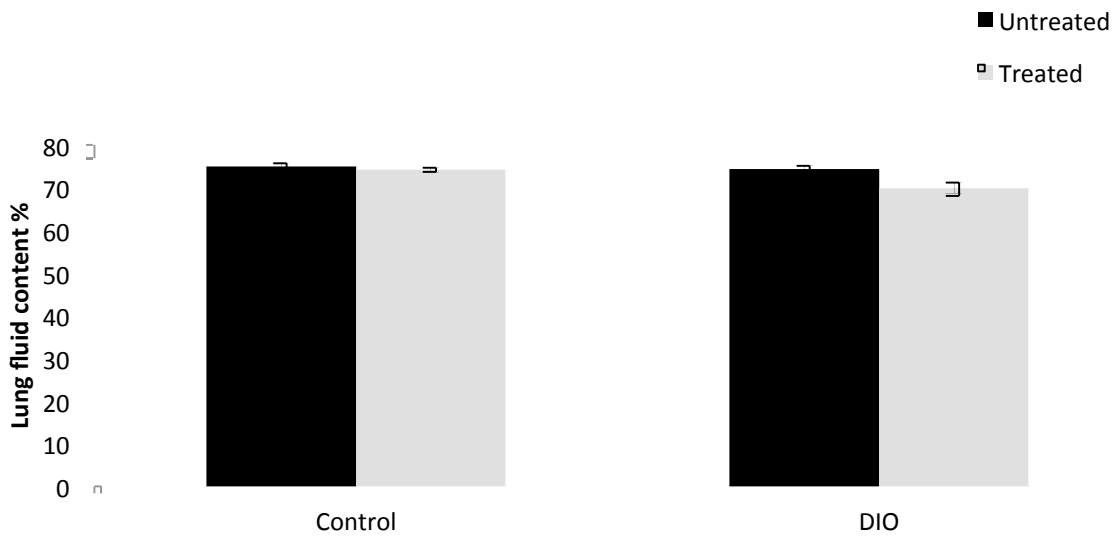
Figure 15: *Lung fluid content of 20 week untreated and treated control and treated DIO animals. All values are expressed as mean ±SEM. n=6*

There were no significant differences in the lung fluid content of 20 week control vs. DIO rats (74.96±0.75 % vs. 74.40±0.72 %). The GSK-3 inhibitor treatment also had no significant effect on lung fluid content in the controls (treated control 75.54±0.53 % vs. untreated control 74.96±0.75 %), nor DIO animals (treated DIO 73.17±1.27 % vs. untreated DIO 74.40±0.72 %).

3.5   *In vivo* myocardial function

3.5.1   Echocardiography

Table 5: *Echocardiography data of 20 week untreated and treated control, untreated and treated DIO animals. All values are expressed as mean ±SEM. % Fractional shortening (FS), End systolic diameter (ESD), End diastolic diameter (EDD). n=6;# p<0.05*

	Control		DIO		
	Untreated	Treated	Untreated	Treated	N
ESD (mm)	3.89±0.16	4.06±0.14	4.26±0.13	4.35±0.15	6
EDD (mm)	8.15±0.10	8.63±0.007[#]	8.48±0.11[#]	8.72±0.15	6
%FS	52.28±1.55	53.06±1.28	49.81±1.24	49.97±1.33	6

There were no significant differences in ESD in control vs. DIO rats (3.89±0.16 mm vs. 4.26±0.13 mm), however, there was a significant difference in EDD in the control vs. DIO animals (8.15±0.10 mm vs. 8.48±0.11 mm; [#]p<0.05). The GSK-3 inhibitor treatment had no significant effect on ESD in the controls (untreated control 3.89±0.16 mm vs. treated control 4.06±0.14 mm) or in the DIO animals (treated DIO 4.35±0.15 mm vs. untreated DIO 4.26±0.13 mm). EDD was significantly increased in the treated controls (treated control 8.63±0.07 mm vs. untreated control 8.15±0.10 mm; [#]p<0.05), however, there were no significant differences in EDD in the treated DIO animals (treated DIO 8.72±0.15 mm vs. untreated DIO 8.48±0.11 mm). There was a decrease in %FS in the control vs. DIO animals (52.28±1.55 % vs. 49.81±1.24 %), however, this decrease was not significant. This data indicates that the diet had no pronounced adverse effects on myocardial function *in vivo* in the DIO animals. The GSK-3 inhibitor treatment had no significant effect on %FS in the controls (untreated control 52.28±1.55 % vs. treated control 53.06±1.28 %), nor in the DIO animals (treated DIO 49.97±1.33 % vs. untreated DIO 49.81±1.24 %).

3.6 Biochemical Analysis:

3.6.1 Insulin signalling pathway

3.6.1.1 PKB/Akt

Figure 16: *Phospho and Total PKB/Akt expression levels of hearts from control vs. DIO rats.*

No cross comparisons were made between blots. All values expressed as mean ± SEM. n=6;

¥p<0.01

The total PKB/Akt expression levels were significantly higher in the DIO animals (DIO 124.0±7.1 % vs. control 100±4.9 %; $^{¥}$p<0.01). The phospho-PKB/Akt (Ser^{473}) was significantly decreased in the DIO animals (DIO 86.2±3.9 % vs. control 100±3.1 %; $^{¥}$p<0.01).

Figure 17: *Phospho/total PKB/Akt expression levels of hearts from control vs. DIO animals. All values expressed as mean ± SEM. n=6; $^{+}$p<0.001*

The ratio of phosphorylated vs. total PKB/Akt was significantly reduced in hearts from the DIO animals (DIO 58.3±3.6 % vs. control 83.5±5.3 %; $^{+}$p<0.001) compared to their control counterparts, thus less total PKB/Akt was phosphorylated in this group.

Figure 18: *Phospho and Total PKB/Akt expression levels of hearts from untreated vs. treated control. No cross comparisons were made between blots. All values expressed as mean ± SEM. n=6; [ε]p<0.0001*

There were no significant differences in total PKB/Akt expression levels in hearts from the untreated vs. treated control animals (untreated control 100.0±1.2 % vs. treated control 94.6±2.5 %). The phospho-PKB/Akt (Ser[473]) was significantly decreased in hearts from the treated control animals (treated control 53.4±4.7 % vs. untreated control 100±1.7 %; [ε]p<0.0001).

Figure 19: *Phospho/total PKB/Akt expression levels of hearts from untreated vs. treated control animals. All values expressed as mean ± SEM. n=6; $^{+}$p<0.001*

The ratio of phosphorylated vs. total PKB/Akt was significantly reduced in the treated control animals (treated control 38.7±3.9 % vs. untreated control 72.4±7.4 %; $^{+}$p<0.001) compared to their untreated control counterparts, thus less total PKB/Akt was phosphorylated in this group.
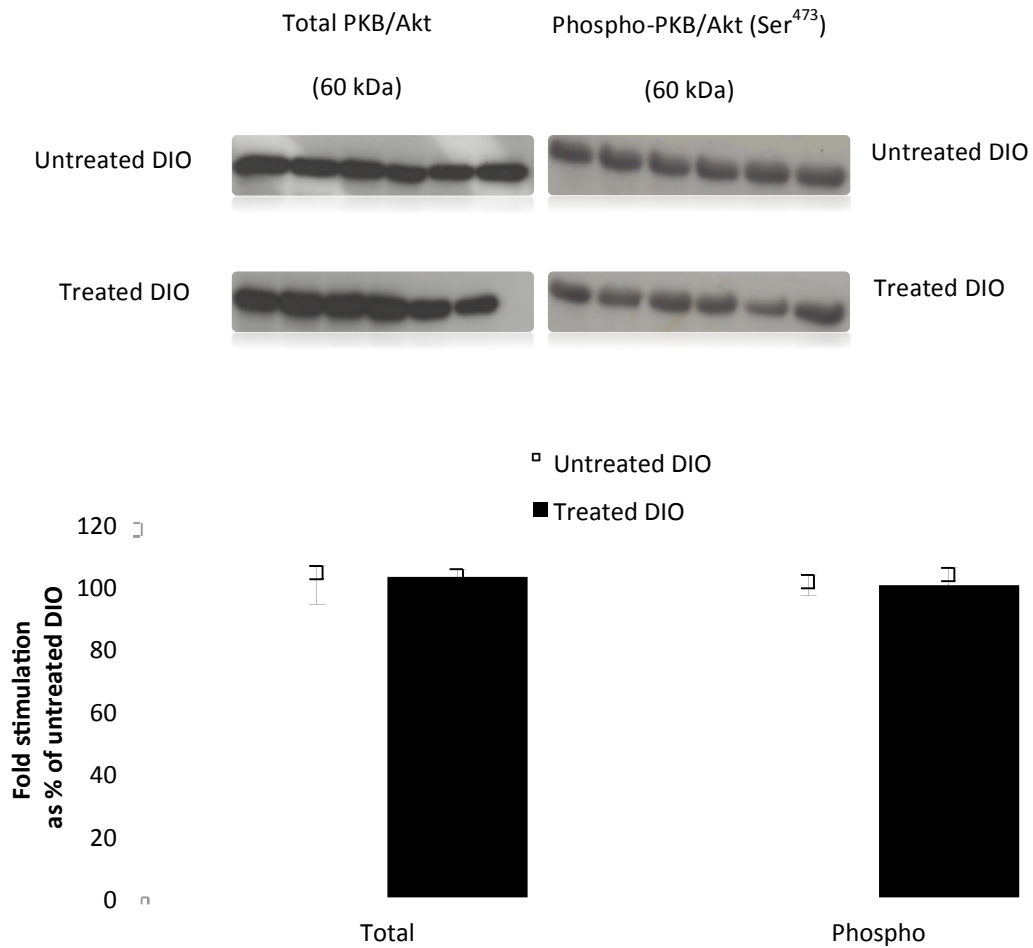
Figure 20: *Phospho and Total PKB/Akt expression levels of hearts from untreated vs. treated DIO animals. No cross comparisons were made between blots. All values expressed as mean ± SEM. n=6*

There were no significant differences in total (untreated DIO 100.0±6.2 % vs. treated DIO 102.6±2.6 %) and phospho-PKB/Akt (Ser[473]) (untreated DIO 100.0±3.3 % vs. treated DIO 100±5.5 %) expression levels in hearts from the untreated DIO vs. treated DIO.
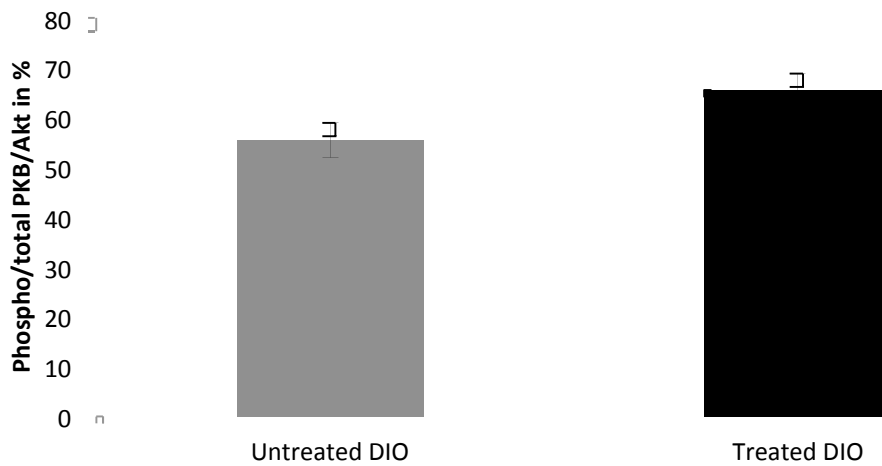
Figure 21: *Phospho/total PKB/Akt expression levels of hearts from untreated vs. treated DIO animals. All values expressed as mean ± SEM. n=6*

There were no significant differences in the ratio of phosphorylated vs. total PKB/Akt in the hearts from untreated DIO vs. treated DIO animals (untreated 52.9±3.5 % vs. treated DIO 50.9±3.3 %).
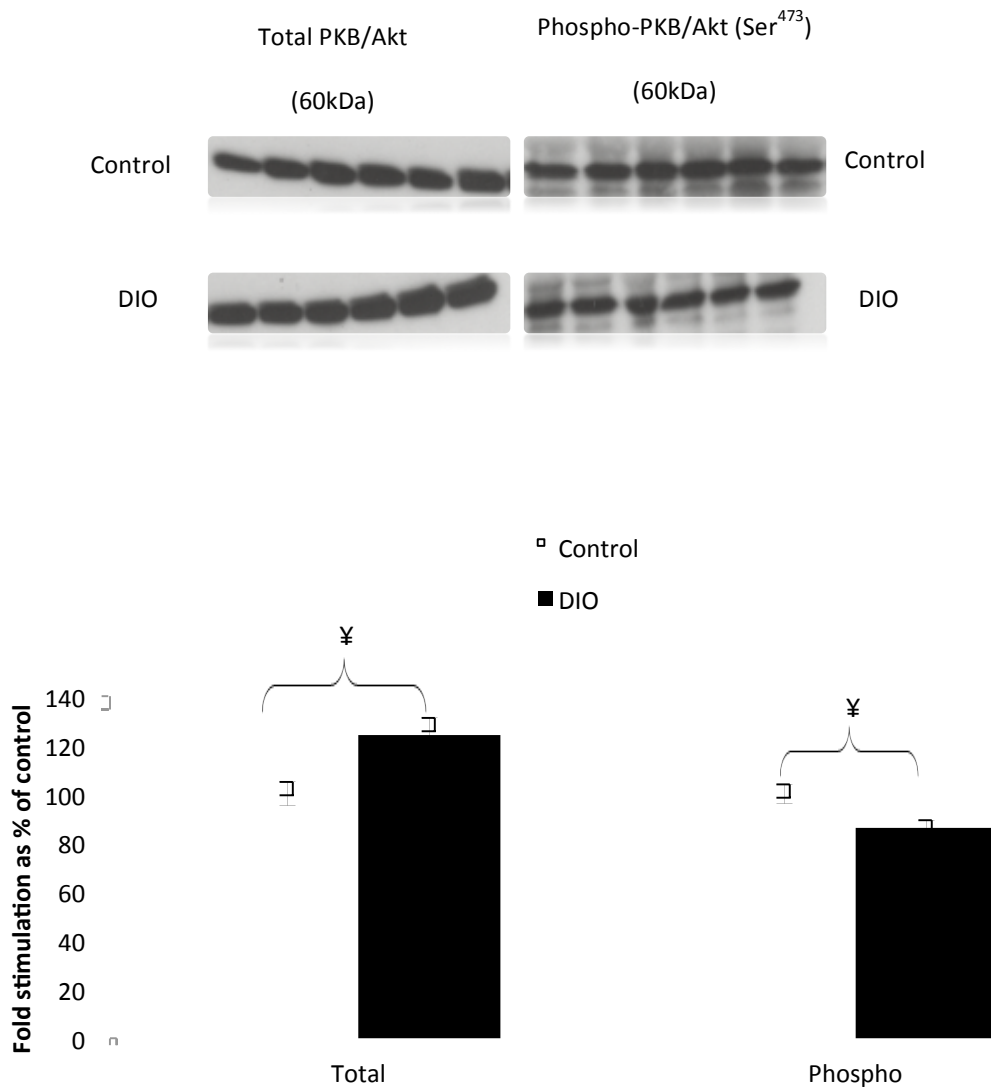
3.6.1.2 GSK-3β
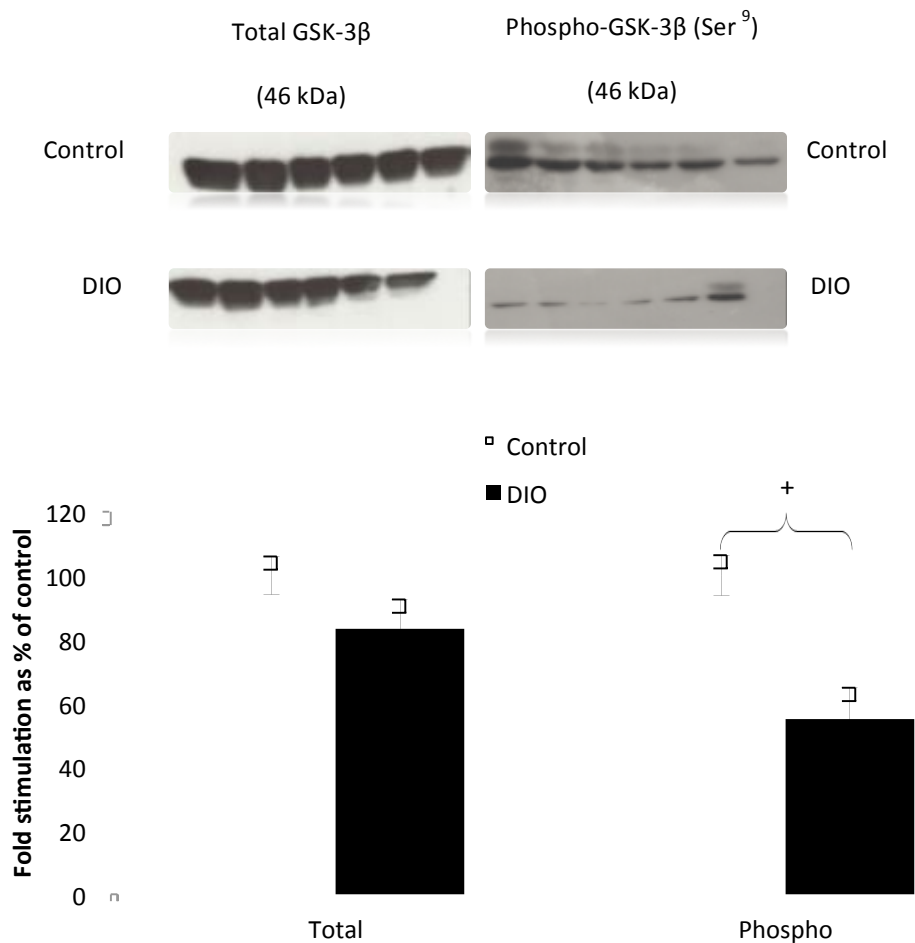
Figure 22: *Phospho and Total GSK-3β expression levels of hearts from control vs. DIO animals. No cross comparisons were made between blots. All values expressed as mean ± SEM. n=6; $^{+}p<0.001$*

There were no significant differences in total GSK-3β expression levels in hearts from control vs. DIO animals (control 100±6.2 % vs. DIO 83.2±9.3 %). The phospho-GSK-3β (Ser[9]) was significantly decreased in the DIO animals (DIO 54.9±9.9 % vs. control 100±6.4 %; $^{+}p<0.001$).
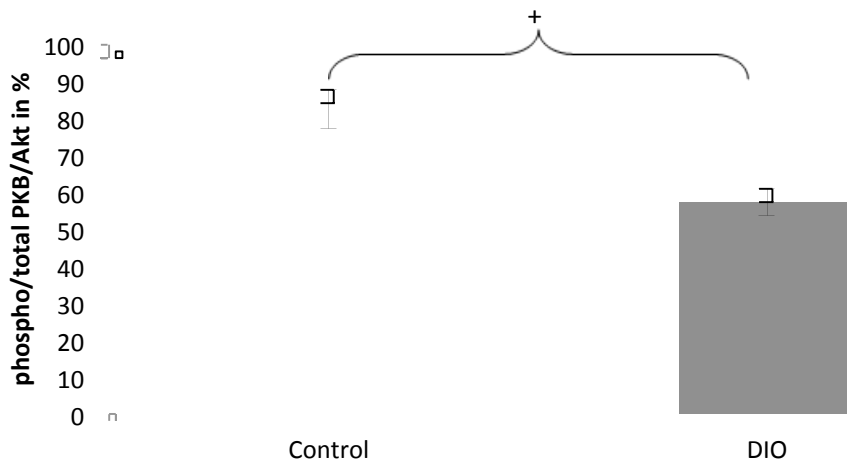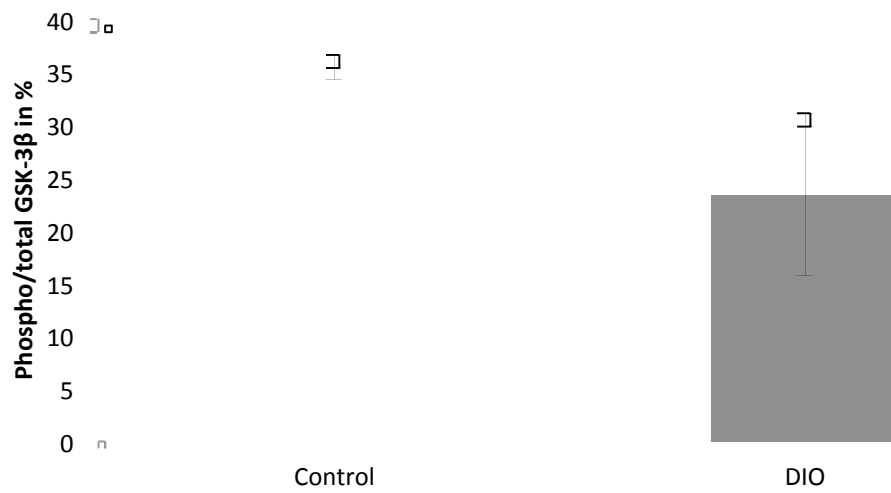
Figure 23: *Phospho/total GSK-3β expression levels of hearts from control vs. DIO animals. All values expressed as mean ± SEM. n=6*

There were no significant differences in the ratio of phosphorylated vs. total GSK-3β between hearts from control vs. DIO animals (control 35.4±1.2 % vs. DIO 26.6±7.7 %).
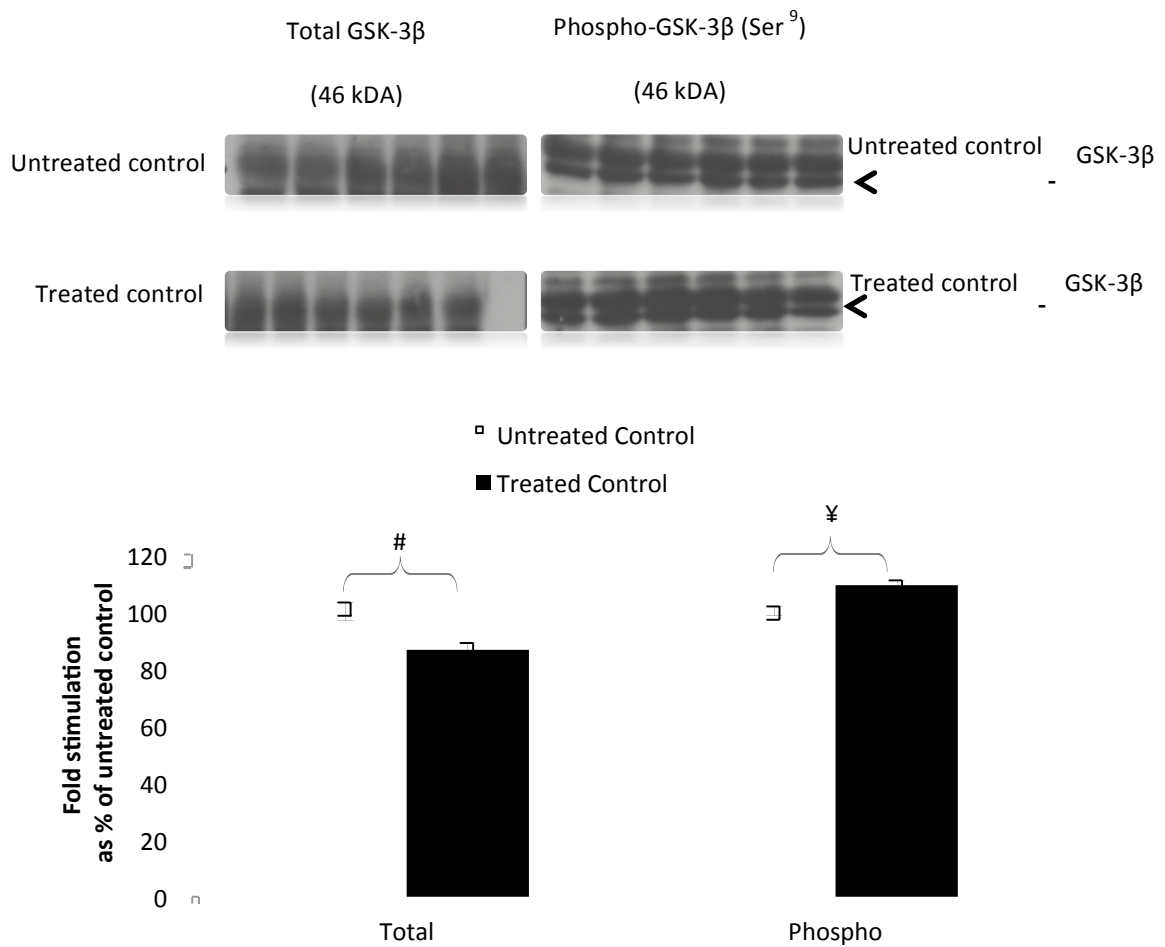
Figure 24: *Phospho and Total GSK-3β expression levels of hearts from untreated vs. treated control animals. No cross comparisons were made between blots. All values expressed as mean ± SEM. n=6; [#]p<0.05; [¥]p<0.001*

Total GSK-3β expression levels were significantly decreased in the hearts from treated control vs. untreated control counterparts (treated control 86.6±2.3 % vs. untreated control 100±3.1 %; [#]p<0.05), where as the phospho-GSK-3β (Ser[9]) was significantly increased in the hearts from treated control animals (treated control 109.2±1.6 % vs. untreated control 100±1.7 %; [¥]p<0.001).
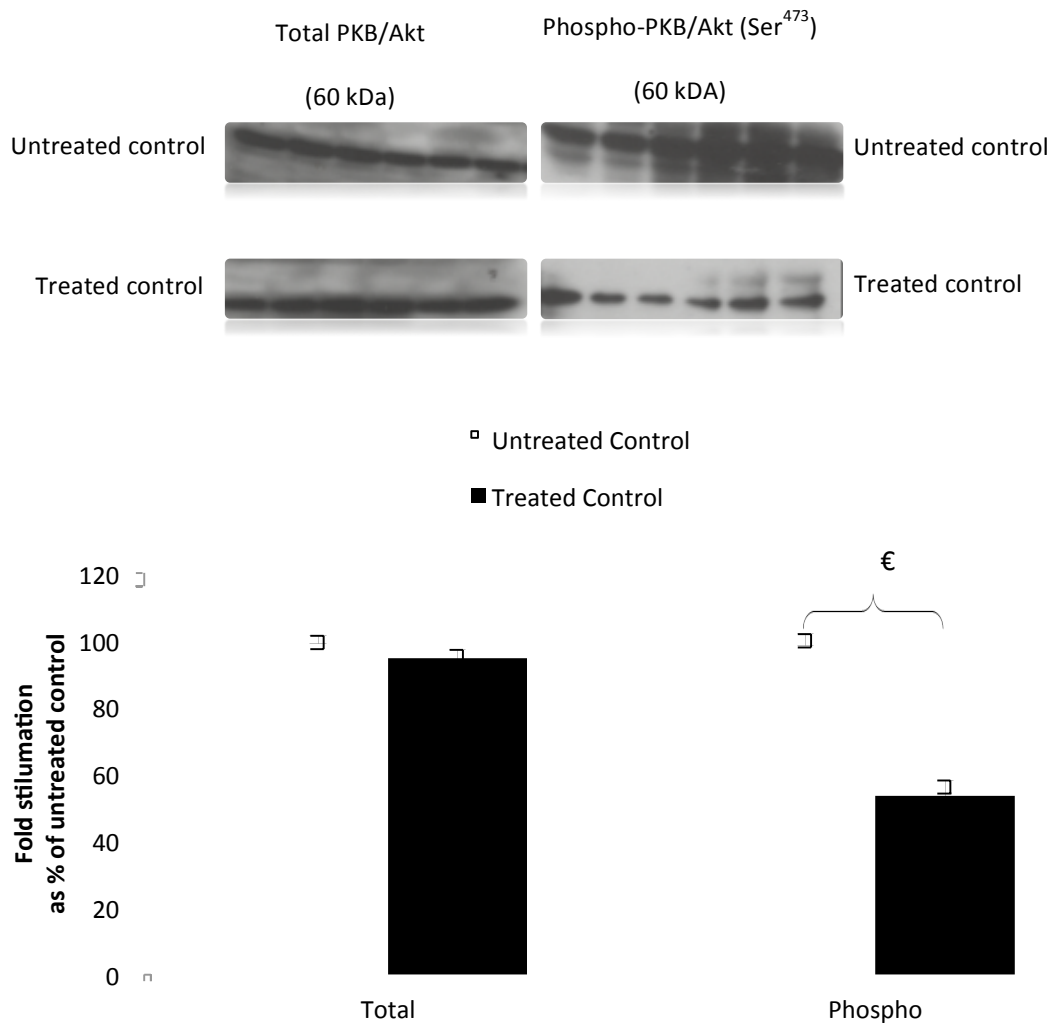
72
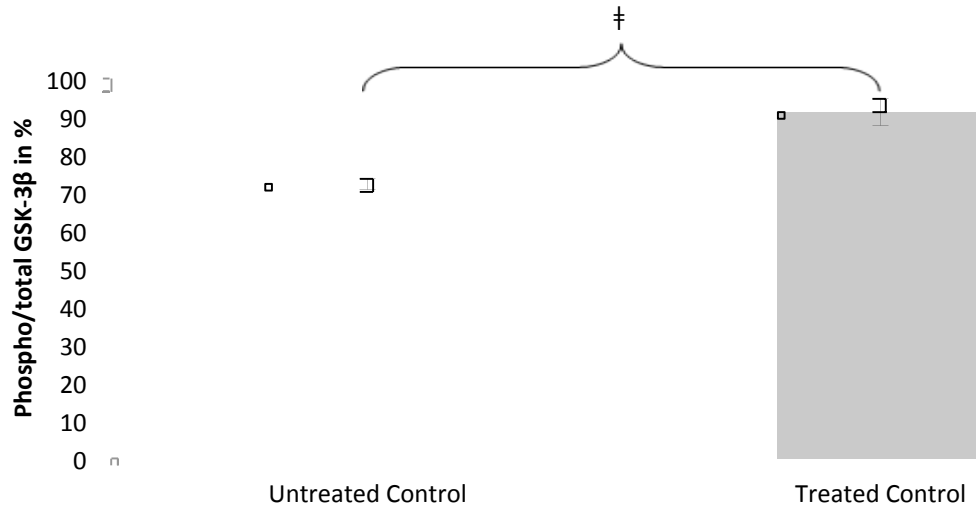
Figure 25: *Phospho/total GSK-3β expression levels of hearts from untreated vs. treated control animals. No cross comparisons were made between blots. All values expressed as mean ± SEM. n=6; ‡p<0.0005*

The ratio of phosphorylated vs. total GSK-3β was significantly increased in hearts from the treated control animals (treated con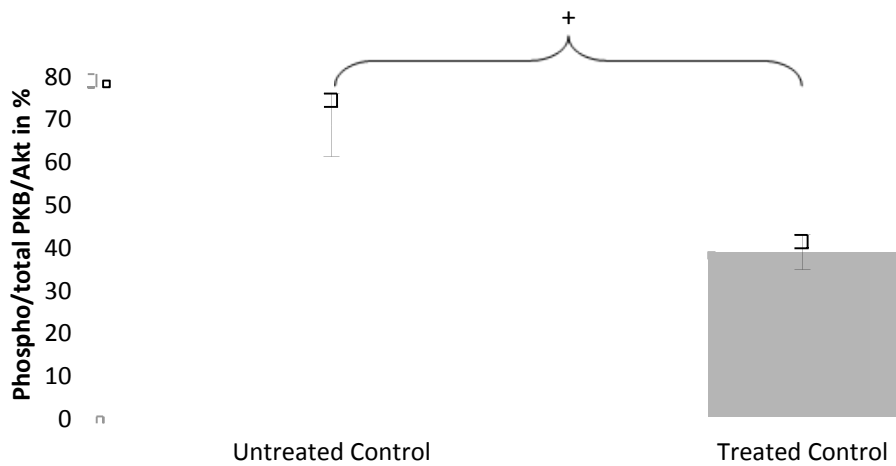trol 91.6±3.5 % vs. untreated control 72.5±1.4 %; ‡p<0.0005) compared to their untreated counterparts, thus more GSK-3β was phosphorylated in this group.
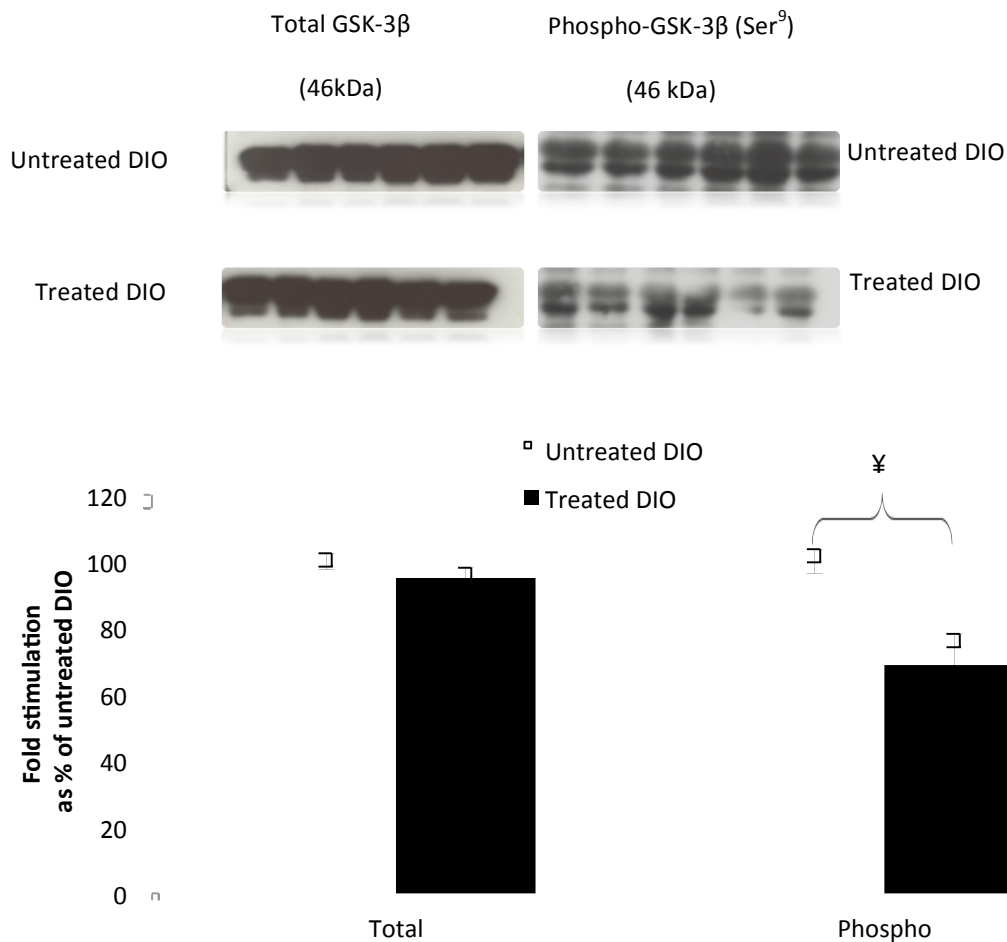
Figure 26: *Phospho and Total GSK-3β expression levels of hearts from untreated vs. treated DIO animals. No cross comparisons were made between groups. All values expressed as mean ± SEM. n=6; $^{¥}p<0.01$*

There were no significant differences in total GSK-3β expression levels in the hearts from untreated DIO vs. treated DIO animals (untreated DIO 100.0±2.4 % vs. treated DIO 94.9±3.2 %). Phospho-GSK-3β (Ser^9) expression levels were significantly decreased in hearts from the treated DIO animals when compared to their untreated counterparts (treated DIO 68.7±9.4 % vs. untreated DIO 100±3.7 %; $^{¥}p<0.01$).
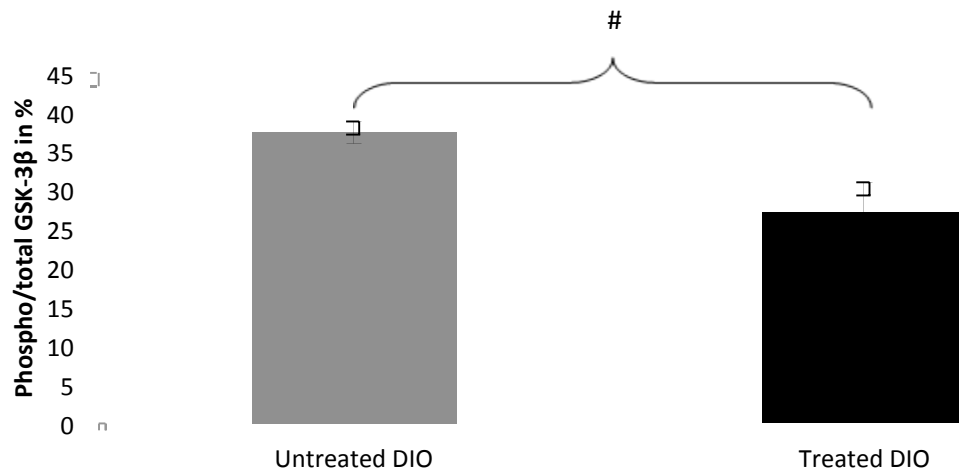
Figure 27: *Phospho/total GSK-3β expression levels of hearts from untreated vs. treated DIO animals. All values expressed as mean ± SEM; [#]p<0.05; n=3*

There was a significant differences in the ratio of phosphorylated vs. total GSK-3β in the hearts from untreated DIO vs. treated DIO animals (untreated 37.5±1.4 % vs. treated DIO 27.2±3.9 %; [#]p<0.05), thus less GSK-3β was phosphorylated in hearts from the treated DIO group.

3.6.2 Key proteins in pathways that mediate myocardial hypertrophy

3.6.2.1 NFAT-3 expression levels
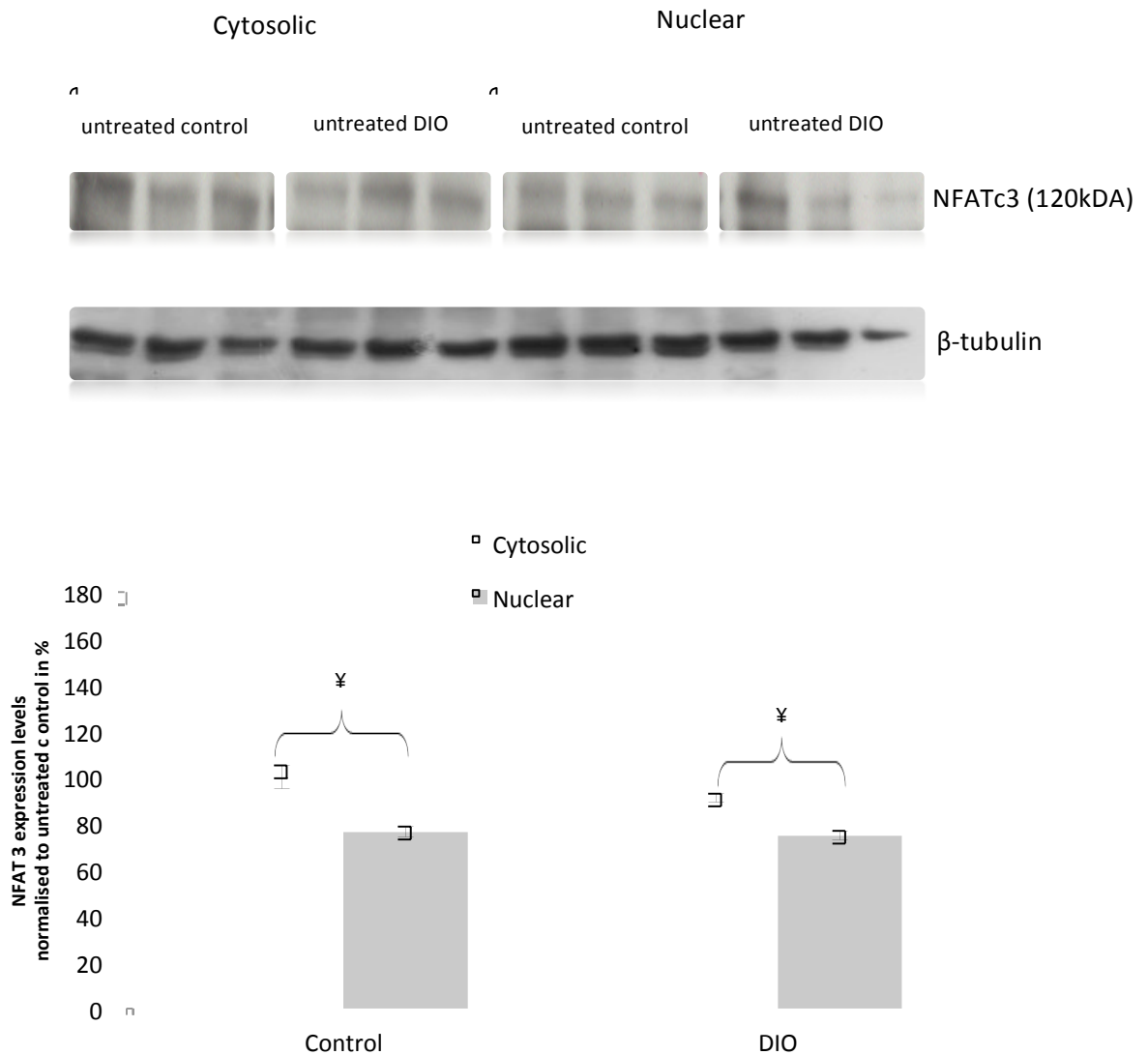
Figure 28: *NFAT-3 expression levels in the cytosolic and nuclear fraction of hearts from control vs. DIO animals. All values expressed as mean ± SEM; ¥p<0.01; n=7-9*

The total NFAT-3 expression levels were significantly higher in the cytosolic fraction than in the nuclear fraction in the hearts from control (cytosolic control 100±5.1 % vs. nuclear control 76.7±2.3 %; ¥p<0.01) and DIO animals (cytosolic DIO 91.1±1.9 % vs. nuclear DIO 74.8±2.1 %; ¥p<0.01).
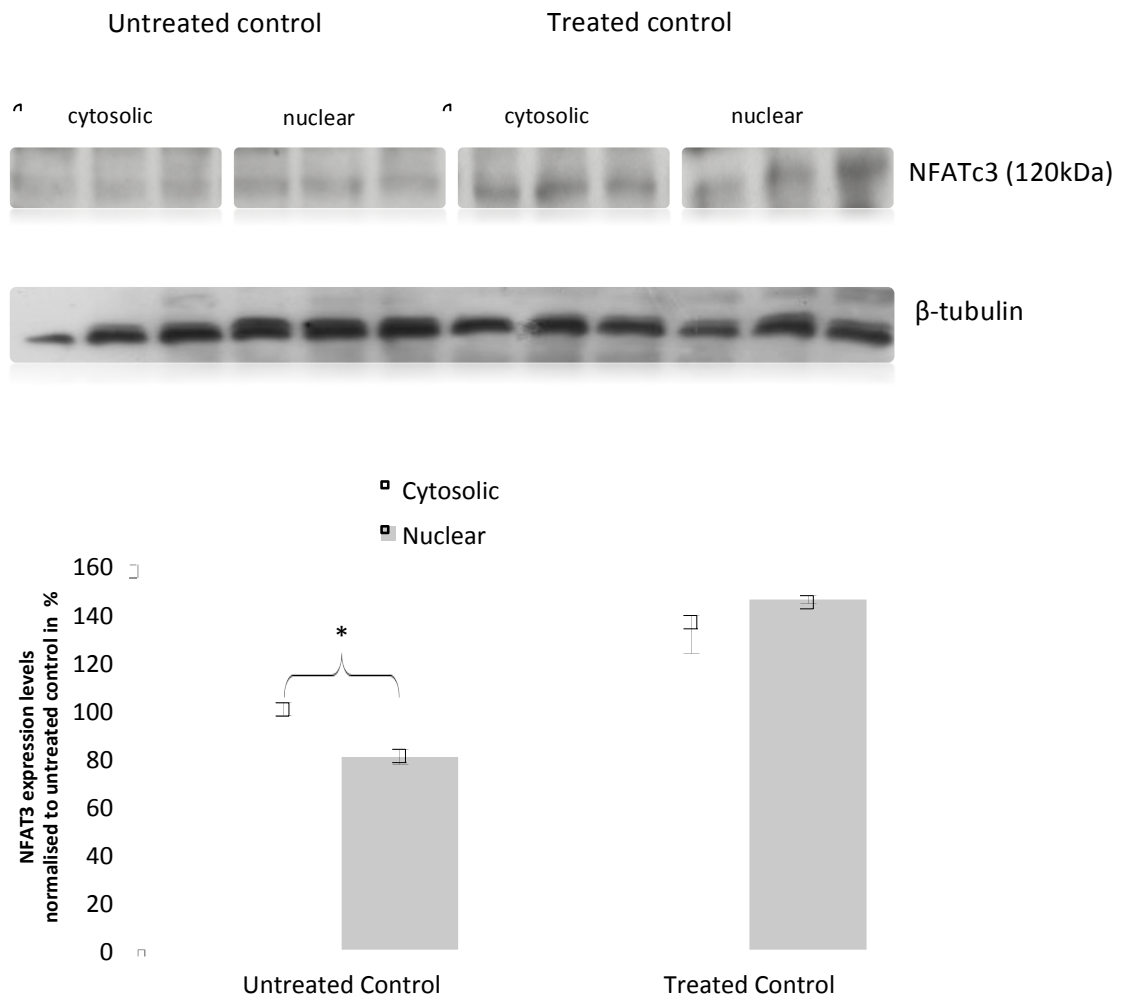
Figure 29: *NFAT 3 expression levels in the cytosolic and nuclear fraction of hearts from untreated vs. treated control animals. All values expressed as mean ± SEM; *p<0.05; n=7-9*

The total NFAT-3 expression levels were significantly higher in the cytosolic fraction than in the nuclear fraction in hearts from the untreated control animals (untreated cytosolic control 100±2.6 % vs. untreated nuclear control 80.1±3.2 %; *p<0.05). In hearts from the treated control animals total NFAT-3 expression levels were decreased in the cytosolic fraction and increased in the nuclear fraction (treated cytosolic control 131.0±7.9 % vs. treated nuclear control 145.6±1.6 %), however, this nuclear import was not significant.
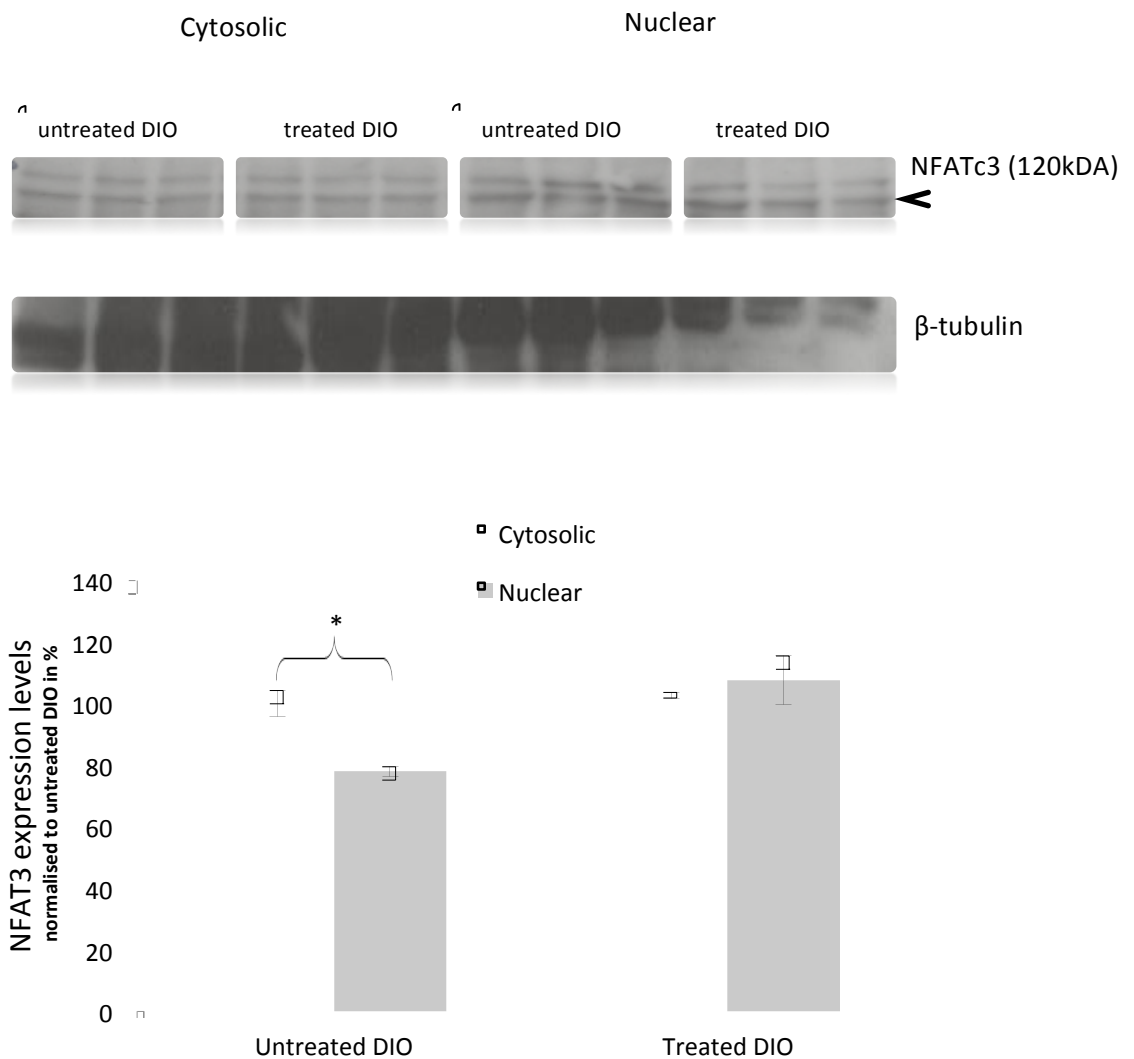
Figure 30: *NFAT 3 expression levels in the cytosolic and nuclear fraction of hearts from untreated vs. treated DIO animals. All values expressed as mean ± SEM; *p<0.05; n=7-9*

The total NFAT-3 expression levels were significantly higher in the cytosolic fraction than in the nuclear fraction in the hearts of untreated DIO animals (untreated cytosolic DIO 100±4.3 % vs. untreated nuclear DIO 78.0±1.5 %; *p<0.05). In hearts from the treated DIO animals total NFAT-3 expression levels were decreased in the cytosolic fraction and increased in the nuclear fraction (treated cytosolic DIO 102.7±1.0 % vs. treated nuclear DIO 107.6±7.9 %), however, this nuclear import was also not significant.

3.6.2.2   GATA -4 expression levels
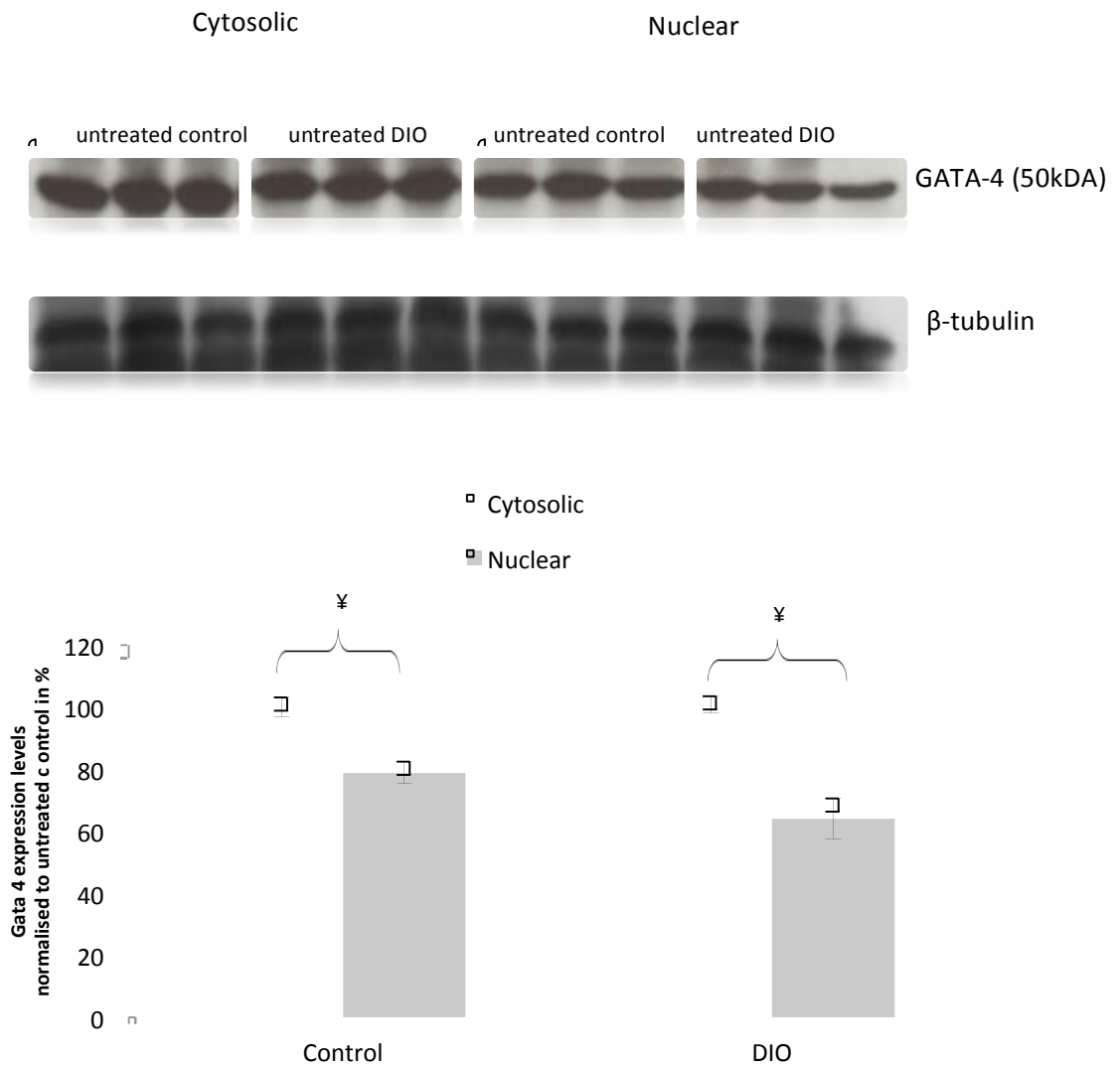
Figure 31: *GATA-4 expression levels in the cytosolic and nuclear fraction of hearts from control vs. DIO animals. All values expressed as mean ± SEM; n=7-9*

The total GATA-4 expression levels were significantly lower in the nuclear fraction than in the cytosolic fraction in hearts from the control (cytosolic control 100±3.1 % vs. nuclear control 78.8±3.6 %; [¥]p<0.01) and DIO animals (cytosolic DIO 100.8±2.7 % vs. nuclear DIO 63.9±6.6 %; [¥]p<0.01) with no differences between the levels in control and DIO rat hearts.
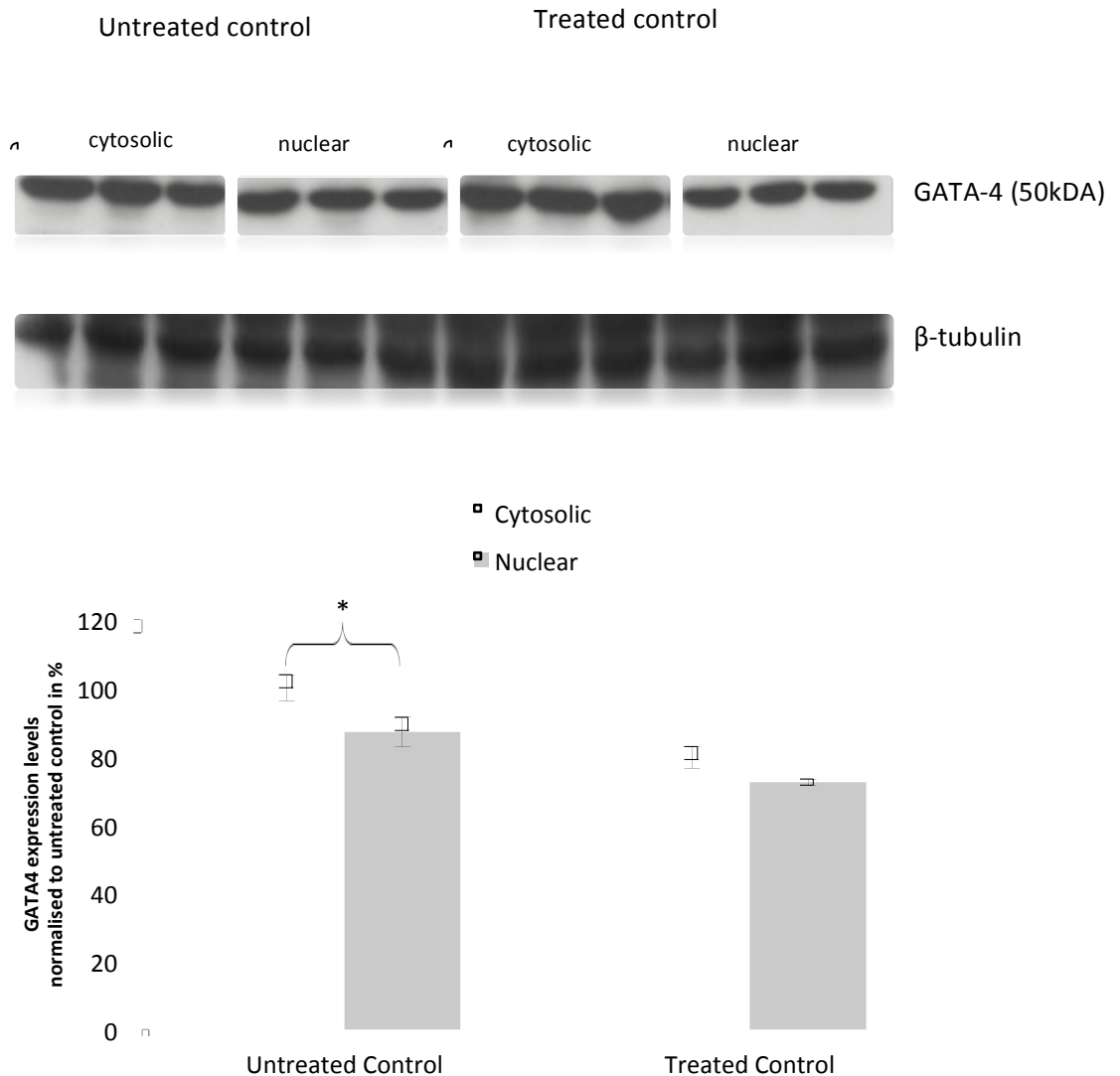
Figure 32: *GATA-4 expression levels in the cytosolic and nuclear fraction in hearts of untreated vs. treated control animals. All values expressed as mean ± SEM; *p<0.05; n=7-9*

The total GATA-4 expression levels were significantly higher in the cytosolic fraction than in the nuclear fraction in the hearts from untreated control animals (untreated cytosolic control 100±3.9 % vs. untreated nuclear control 87.1±4.3 %; *p<0.05). In hearts from the treated control animals total GATA-4 expression levels were increased in the cytosolic fraction and decreased in the nuclear fraction (treated cytosolic control 79.6±3.3 % vs. treated nuclear control 72.4±1.0 %), however, this nuclear import was also not significant.
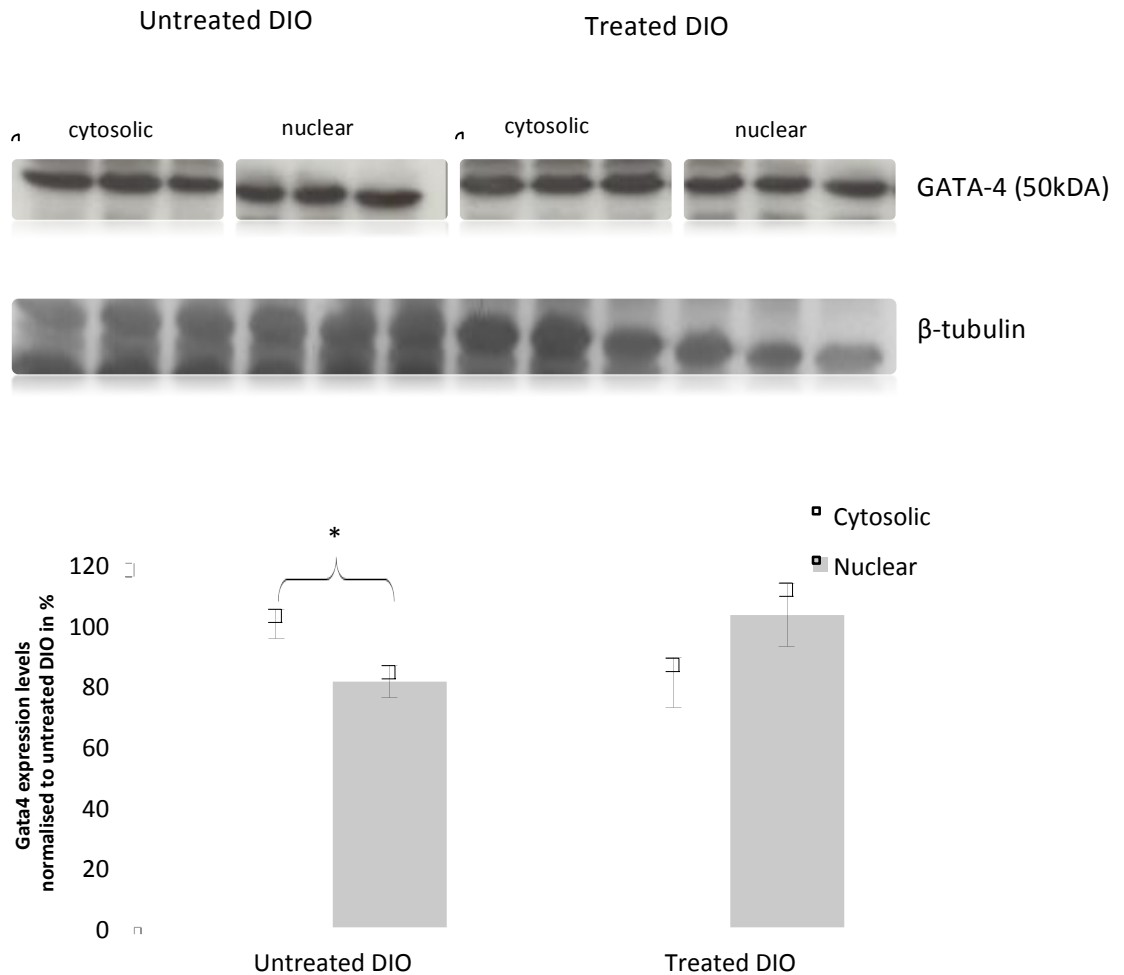
Figure 33: *GATA-4 expression levels in the cytosolic and nuclear fraction of hearts from untreated vs. treated DIO animals. All values expressed as mean ± SEM; *p<0.05; n=7-9*

The total GATA-4 expression levels were significantly higher in the cytosolic fraction than in the nuclear fraction in the hearts from untreated DIO animals (untreated cytosolic DIO 100±4.8 % vs. untreated nuclear DIO 81.0±5.3 %; *p<0.05). In hearts from the treated DIO animals total GATA-4 expression levels were decreased in the cytosolic fraction and increased in the nuclear fraction (treated cytosolic DIO 80.5±8.2 % vs. treated nuclear DIO 103.0±10.5 %), however, this nuclear import of GATA-4 was not significant.

3.7 Immunofluorescence
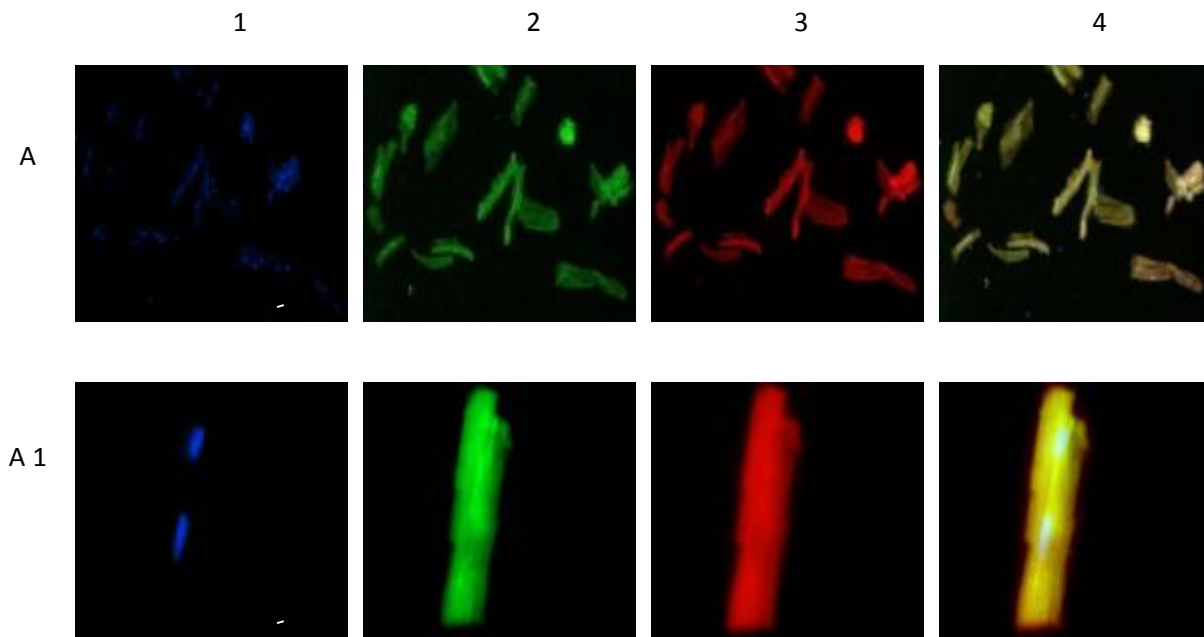
Figure 34: *Images of cardiomyocytes were acquired with a 20 x (A) and 60 x (A 1) oil immersion objective (scale bar, 200µm and 20µm respectively). Figure A shows the low magnification (scale bar 200µm) and A1 shows the high magnification (20µm) of cardiomyocytes from untreated control animals. The images show the signal from: (1) Hoescht, a nuclear stain (2) NFATc3 coupled to FITC, displayed in green, (3) GATA-4 coupled to Texas Red, displayed in red and (4) co localisation are NFATc3 and GATA-4, displayed in yellow. The images given are representative of experiments on 3 individual hearts in each group.*

In cardiomyocytes from the untreated controls both NFATc3 and GATA-4 were evenly distributed in the cytoplasm as shown in figure 34.
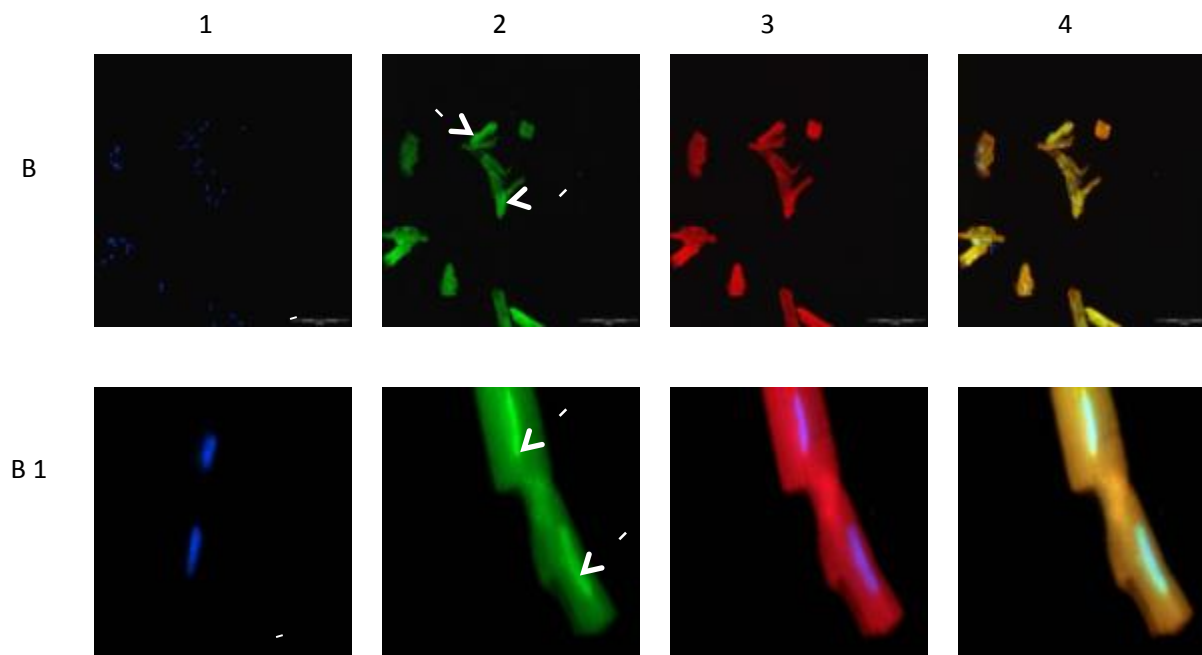
Figure 35: *Images of cardiomyocytes were acquired with a 20 x (B) and 60 x (B 1) oil immersion objective (scale bar, 200μm and 20μm respectively). Figure B shows the low magnification (scale bar 200μm) and B1 shows the high magnification (20μm) of cardiomyocytes from untreated DIO animals. The images show the signal from: (1) Hoescht, a nuclear stain (2) NFATc3 coupled to FITC, displayed in green, (3) GATA-4 coupled to Texas Red, displayed in red and (4) co localisation are NFATc3 and GATA-4, displayed in yellow. The images given are representative of experiments on 3 individual hearts in each group. The white arrows indicate nuclear localization of NFATc3.*

In cardiomyocytes from the untreated DIO animals, both at low and at high magnification, NFATc3 was localized in the perinuclear area of the cytoplasm as indicated by the white arrows, but this phenomenon was only seen in some cells. GATA-4 was once again more evenly distributed in the cytoplasm as shown in figure 35.
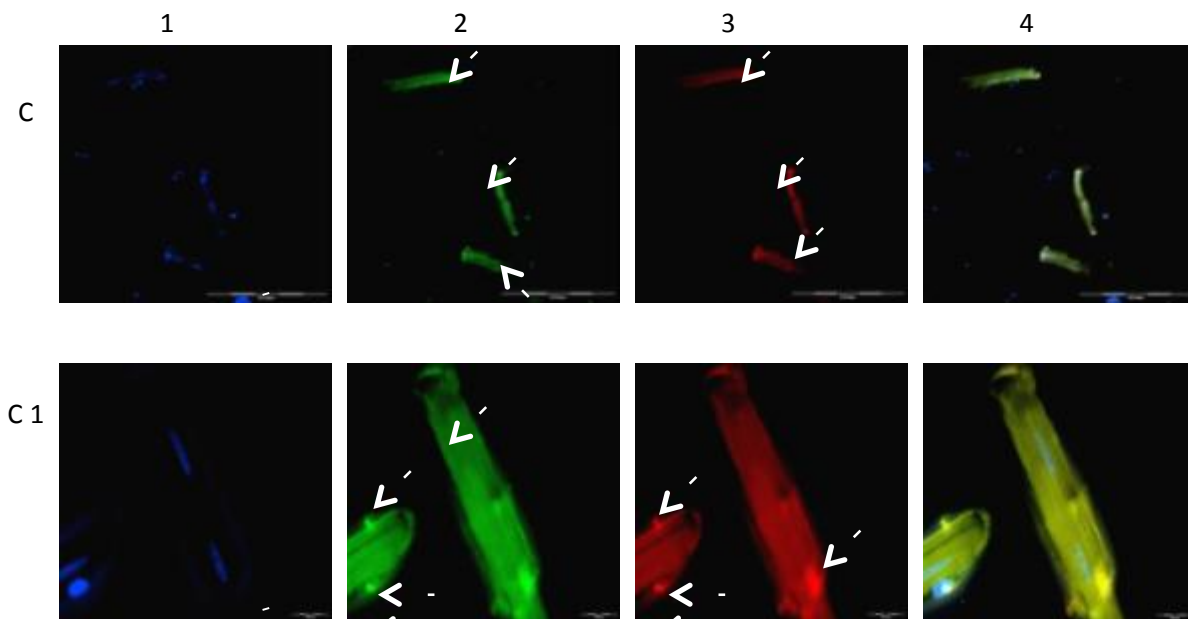
Figure 36: *Images of cardiomyocytes were acquired with a 20 x (C) and 60 x (C 1) oil immersion objective (scale bar, 200μm and 20μm respectively). Figure C shows the low magnification (scale bar 200μm) and C1 shows the high magnification (20μm) of cardiomyocytes from treated control animals. The images show the signal from: (1) Hoescht, a nuclear stain (2) NFATc3 coupled to FITC, displayed in green, (3) GATA-4 coupled to Texas Red, displayed in red and (4) co localisation are NFATc3 and GATA-4, displayed in yellow. The images given are representative of experiments on 3 individual hearts in each group. The white arrows indicate nuclear localization of NFATc3 and GATA-4.*

In the cardiomyocytes from treated control animals, both at low and at high magnification, NFATc3 and GATA-4 were localized in the perinuclear area of the cytoplasm as indicated by the white arrows, but this phenomenon was only seen in some cells as shown in figure 36.
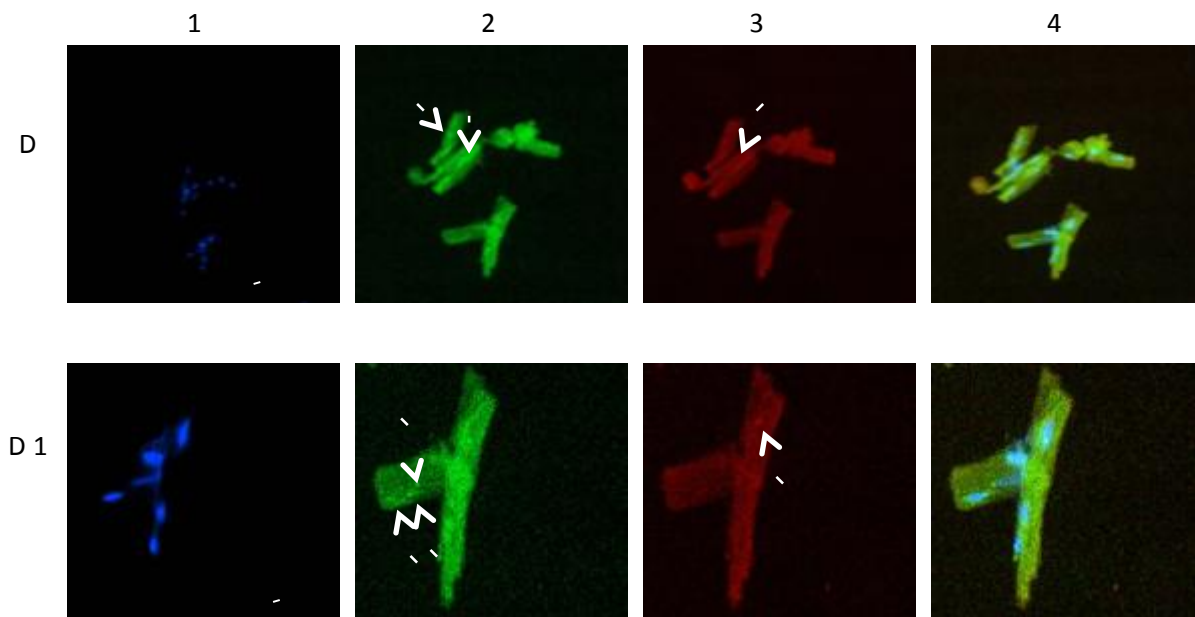
***Figure 37*:** *Images of cardiomyocytes were acquired with a 20 x (D) and 60 x (D 1) oil immersion objective (scale bar, 200μm and 20μm respectively). Figure D shows the low magnification (scale bar 200μm) and C1 shows the high magnification (20μm) of cardiomyocytes from treated DIO animals. The images show the signal from: (1) Hoescht, a nuclear stain (2) NFATc3 coupled to FITC, displayed in green, (3) GATA-4 coupled to Texas Red, displayed in red and (4) co localisation are NFATc3 and GATA-4, displayed in yellow. The images given are representative of experiments on 3 individual hearts in each group. The white arrows indicate nuclear localization of NFATc3 and GATA-4.*

In the cardiomyocytes from treated DIO animals, both at low and at high magnification, NFATc3 and GATA-4 were localized in the perinuclear area of the cytoplasm as indicated by the white arrows, but this phenomenon was only seen in some cells as shown in figure 37.

3.8 Light microscopy: determination of cell width
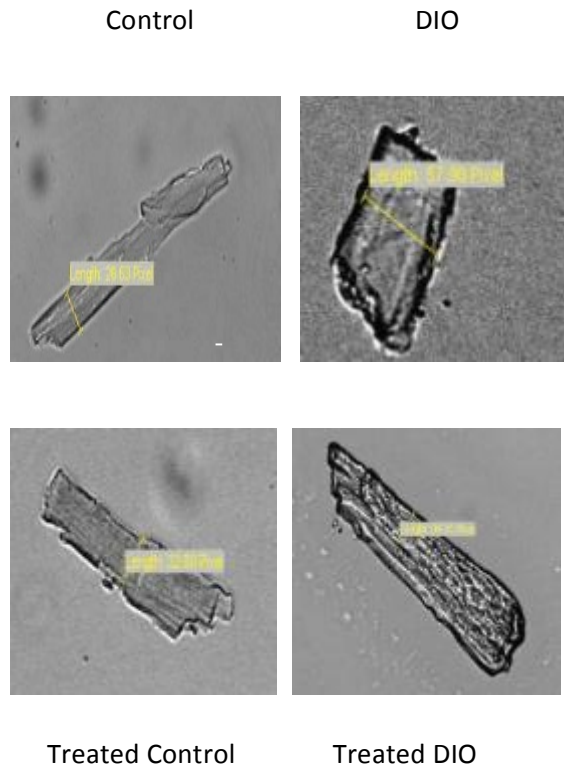
Control   DIO

Figure 38: Representative cardiomyocytes images showing cell width as determined by light microscopy from control, DIO, treated control and treated DIO hearts. The images were acquired with a 60 x oil immersion objective (scale bar 20µm). 40-50 cells, on 3 different planes were selected from each group.

Treated Control   Treated DIO
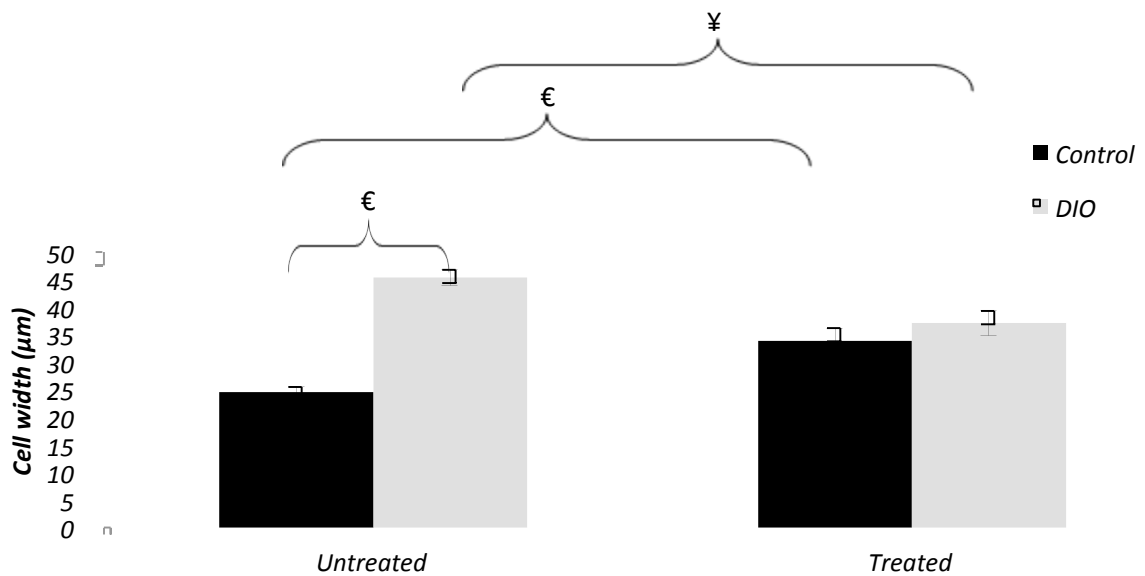
Figure 39: *Cell width (µm) of cardiomyocytes isolated from Control vs. DIO animals and the effect of treatment. All values are expressed as mean ±SEM. ¥p<0.01; €p<0.0001; n=2-3 individual preparations*

There was a significant increase (figure 39) in the cardiomyocyte cell width (µm) of control vs. DIO rats (24.55±0.97 µm vs. 45.37±2.31 µm; [€]p<0.0001), indicating concentric hypertrophy. The GSK-3 inhibitor treatment also increased cardiomyocyte cell width significantly in the control animals (treated control 33.89±1.42 µm vs. untreated control 24.55±0.97 µm; [€]p<0.0001). The cell width in the treated DIO animals was significantly decreased compared to the untreated DIO animals (treated DIO 37.12±2.19 µm vs. untreated DIO 45.37±2.31 µm; [¥]p<0.01).

CHAPTER 4: DISCUSSION

4.1 Characterisation of the model

The primary aims of the current study were to document the progression of myocardial hypertrophy induced in a rat model of diet induced obesity leading to pre-diabetes and to assess how inhibition of the GSK-3 protein affects this process in both the normal and pre-diabetic animals. We successfully utilized the model of diet induced obesity, which is characterized by "hyperphagia, increased thermogenesis, hyperleptinaemia and mild insulin resistance" (Pickavance LC *et al.,* 1999). This model has been characterized in our laboratory and shown to be physiologically relevant and comparable to the human equivalent of insulin resistance as a result of obesity (Du Toit EF *et al.,* 2005). The choice of a non-diabetic model was based on the premise that in the diabetic state, a difference in glycemic control between placebo and drug-treated animals constitutes a confounding factor for food intake and plasma volume regulation.

4.2 Effect of the diet

4.2.1 Biometric and metabolic data

A feeding period of 20 weeks was chosen, as opposed to the 16 weeks usually employed in our laboratory, in order to document the progression of obesity on certain biometric and metabolic parameters. Furthermore, this time period was chosen in order to ensure that hypertrophy was well pronounced in our model of diet induced obesity.

The main findings on the biometric and metabolic parameters were as follows: The high caloric diet (HCD) used in this present study was of sufficient intensity and duration to promote obesity in the DIO rats. These rats had a significant increase in body weight (table 4) and intra-peritoneal fat mass (table 4) compared to their control litter mates. Moreover, we also observed complications associated with obesity, such as impaired glucose tolerance (table 4) and hyperinsulinemia (table 4), which are associated with the insulin resistant state. These results are in agreement with other studies where obesity was induced in rats using a high caloric diet. Cerf ME *et al*. (2007) found that prolonged feeding with fat-enriched diets induces an increase in body weight in susceptible rats in the range of 10% to 20% over standard rat chow (SRC) controls. Furthermore, Du Toit EF *et al.* (2005) found that the HCD animals consumed more energy per day (table 1) compared to their age matched control counterparts. The increase in food intake between the HCD and SRC fed rats could be due to the increased palatability of the HCD, which promotes hyperphagia (Cerf ME *et al.,* 2005; Du Toit EF *et al.,* 2005), as the HCD consists of moist, sweet pellets, while the SRC, received by the control animals, is made up of dry pellets. As a measure of obesity, the intraperitoneal fat mass was used. The measurement of this adipose tissue has been used previously as a measure of body fat (De Freitas Mathias PC *et al*., 2007). An increase in intraperitoneal fat has been shown to play a significant role in the development of insulin resistance.

The proposed mechanism is that large visceral fat masses imply hypertrophy of the adipose tissue. These adipose tissues then release excessive amounts of FFA (Hutley L and Prins JB, 2005) and adipocyte-derived peptides (Vázquez-Vela ME, 2008) in the circulation, which incites lipotoxicity (Hutley L and Prins JB, 2005). The resulting lipotoxicity affects adipose as well as non-adipose tissue, resulting in excess fat being deposited in ectopic tissue such as liver, skeletal muscle, pancreas and the heart.

This contributes to the development of hypertriglyceridemia and hyperglycemia in the liver, muscle and pancreas and results in insulin resistance in the heart (Boden G *et al.,* 1994; Pan DA *et al.,* 1997; Eckel J and Reinauer H, 1990; Eckel RH *et al.,* 2005; Unger RH, 1995; Belfort R *et al.,* 2005). The observed complications associated with obesity, such as hyperinsulinemia, were also reported by Hallfrisch J *et al*. (1981), where they found that sucrose and high-fat feeding for eight to nine weeks resulted in euglycemia, but with increased circulating insulin concentrations. Obese individuals may exhibit euglycemia due to the sufficient production of insulin, but suffer from insulin resistance in the peripheral tissues such as muscle, liver and adipose tissue (Sesti G, 2006). Hyperglycemia arises at a later stage, when the pancreas reaches its capacity to overproduce insulin, and this then leads to elevated fasting blood glucose concentrations and impaired glucose tolerance (Sesti G, 2006; Thévenod F, 2008). The HOMA-IR model for the assessment of insulin resistance is commonly used as a tool for measuring the degree of insulin resistance. A low HOMA-IR value indicates high insulin sensitivity, while a high HOMA-IR value indicates low insulin sensitivity and insulin resistance (Bonora E *et al*., 2002). We found that the HOMA-IR values (table 4) were greater in the DIO animals than in the control animals. Mendoza J *et al.* (2008) also reported an increase in the HOMA-IR index as a result of high caloric feeding. The biometric and metabolic parameters thus show that the high caloric diet used in this present study was of sufficient duration and intensity to induce insulin resistance but not hyperglycemia in the DIO animals.

4.2.2 Glucose uptake

At a low concentration, deoxy-glucose is taken up by tissues in the body at the same rate as glucose (Utriainen T *et al*., 2000). The deoxy-glucose is, however, not metabolized by the cells, therefore it accumulates intra-cellularly (Chadwick WA *et al*., 2007).

Radioactive labelled 2-deoxy-[^{3}H]-D-glucose can thus serve as a tool in measuring glucose uptake (Chadwick WA *et al*., 2007). At basal level the diet had no significant effect on glucose uptake, as measured by 2-deoxy-[^{3}H]-D-glucose in cardiomyocytes prepared from Langendorff perfused hearts, in the control and DIO animals (figure 12). This result is in agreement with those reported by Carroll R *et al.* (2005), where they demonstrated that basal deoxyglucose uptake in 6-8 week diabetic db/db cardiomyocytes was unchanged relative to cardiomyocytes from control db/+ mice. Glucose transporter 1 (GLUT1) and glucose transporter 4 (GLUT4) are the two main glucose transporters present in cardiomyocytes. At basal levels, GLUT4 resides in intracellular, cytoplasmic vesicles, however, during insulin stimulation GLUT4 translocates to the plasma membrane where it transports postprandial glucose from the extracellular environment into cells (Huang S and Czech MP, 2007). If there are no differences in glucose uptake under basal conditions, this would imply that the GLUT1 transporter concentration in the membranes is similar in the control and the DIO animals.

When the cardiomyocytes were stimulated with 1nM of insulin we found no significant differences between the controls and DIO animals. It is possible that this low concentration of glucose uptake could not discern the differences between the sensitivity of the cells prepared from control vs DIO animals. We did, however, note that the DIO animals had a significantly impaired response to insulin, when 10nM and 100nM of insulin was used (figure 12). These results are in agreement with what other groups found. Carroll R *et al.* (2005) demonstrated that 10nM of insulin produced a marked stimulation of deoxyglucose uptake by control db/+ cardiomyocytes from mice. Huisamen B *et al*. (2001) also found in two rat models of noninsulin-dependent diabetes mellitus (NIDDM) that the insulin-stimulated values of glucose uptake were severely impaired in the NIDDM animals compared to the controls.

This reduction in glucose uptake in the DIO animals is consistent with peripheral insulin resistance as demonstrated by the biometric and metabolic parameters assessed in this study. The proposed mechanism for this defect in the DIO animals is that it could be as a result of defects located at the level of the glucose transporter (Carroll R *et al.,* 2005). Further, it is proposed that there is reduced PKB/Akt activation by insulin, which could also contribute to cardiac GLUT-4 translocation defects (Shao J *et al.,* 2000).

4.2.3   Insulin signalling pathway

In the insulin signalling pathway, insulin binds to its receptor and activates IRS-1 or IRS-2, which then leads to PKB/Akt phosphorylation and activation (Saltiel AR and Pessin JE, 2003; Shepherd PR, 2005). The activated PKB/Akt protein is known to directly phosphorylate GSK-3α and β protein on its serine 21/9 residues respectively, thus inhibiting its activity (Lawrence JC and Roach PJ, 1997). In the DIO animals we found that total PKB/Akt was significantly up-regulated. Phosphorylated PKB/Akt was down-regulated (figure 16) and the phospho/total ratio (figure 17) was significantly reduced, indicating that less PKB/Akt was in the phosphorylated state in this group under basal conditions. With respect to the GSK-3 protein, we found no significant differences in total GSK-3β expression levels in the DIO animals. The phospho GSK-3β (Ser^9) was significantly decreased (figure 22) and the phospho/total ratio (figure 23) was also decreased in these DIO animals, however, the latter was not significant as a result of the large standard error. These results are consistent with what Shulman GI *et al.* (1990) and Cline GW *et al.* (1994) found in the muscle tissue from type 2 diabetic patients. They reported that GSK-3 is up-regulated, and that this up-regulation correlated with decreased glycogen synthase activity and impaired insulin responsiveness. The latter is also in agreement with what we found in the biometric and metabolic parameters, and it is also consistent with the demonstration of lower insulin-stimulated glucose uptake in the DIO animals.

4.2.4   The development of myocardial hypertrophy

In this study we have used ventricular mass, VW/BW ratio, VW/TL ratio, echocardiography, protein expression levels, indirect fluorescent microscopy and light microscopy to quantify myocardial hypertrophy. In the DIO animals we found an increase in ventricular weight (table 4), but the VW/BW ratio (figure 13) was decreased due to the marked increase in body mass in the DIO animals. Iyer SN and Katovich MJ (1996) have, however, reported no differences in VW/BW ratio in fructose-fed male Sprague-Dawley rats. As a result, VW/TL ratio is used in addition to the VW/BW ratio, as the former is regarded as a more accurate and stable index for quantifying myocardial hypertrophy, especially when there are fluctuations in weight gain, as is evident in our study (Yin FC *et al.,* 1982). Our results show that the VW/TL ratio (figure 14) was increased.

Excess adiposity and body size have been cited as proposed mechanisms of how obesity may result in the development of myocardial hypertrophy (Lauer MS *et al.,* 1991; Urbina EM *et al.,* 1995; Lorber R *et al.,* 2003). The prevailing hypothesis is that increases in body size augment heart size through changes in loading conditions on the heart. The increases in blood volume associated with excess adiposity result in an enhanced cardiac output and stroke volume (Stoddard MF *et al.,* 1992; Messerli FH *et al., 1983*). The chronic volume overload mediated by obesity results in an increase in LV filling, which in turn leads to chamber dilation, and thus enhances preload and myocardial oxygen demand (Peterson LR *et al.,* 2004). These changes promote cardiomyocyte growth, which is intended to reduce wall stress and myocardial oxygen demand by increasing the wall thickness of the heart. If the wall thickness does not increase sufficiently in keeping up with the increments in filling volumes, LV wall stress may increase (Zarich SW *et al.,* 1991; Alpert MA *et al.,* 1995; Berkalp B *et al.,* 1995), the consequence potentially being heart failure.

Trans-thoracic echocardiography has become one of the most frequently used non-invasive tools of assessing LV contractile performance, dimensions and hypertrophy in small animal research (Reffelmann T and Kloner RA, 2003). We found no significant differences in LV end systolic diameter (ESD), however, we observed a significant increase in LV end diastolic diameter (EDD) in the DIO animals (table 5). Messerli *et al.* (1983) conducted echocardiographic analysis on lean and obese patients that were either hypertensive or normotensive. Obesity was seen to be associated with an increase in LV diameter, which is considered to be indicative of eccentric LV hypertrophy, while hypertension was associated with concentric hypertrophy. Fractional shortening (FS), the traditional index of systolic function, was used as a parameter of cardiac contractile performance. We found no significant differences in FS in the control vs. DIO animals. This result is in agreement with that of Rennison JH *et al.* (2007). They reported that administration of a high saturated fat diet did not adversely affect LV contractile function or the progression of LV remodelling. In the current study, these findings may be attributed to the fact that too few parameters were used to quantify diastolic dysfunction. Alternatively, the ability to observe subtle differences in myocardial function may have been limited by the small sample size used (n=6).

4.2.5   Proteins implicated in the hypertrophic response

We investigated NFAT-3 and GATA-4 transcription factors as markers of myocardial hypertrophy. Calcium signalling mediates the effects of NFAT-3 and GATA-4 proteins, but a number of parallel signalling pathways can also regulate these transcription factors. In the insulin signalling pathway, GSK-3 phosphorylates NFAT proteins, inhibiting both their nuclear localization and DNA-binding activity (Graef IA *et al.*, 1999), hence attenuating the hypertrophic response. Additionally, GSK-3 negatively regulates GATA-4's transcriptional activity through N-terminal phosphorylation (Morisco C *et al.,* 2001). This phosphorylation subsequently promotes nuclear export of GATA-4.

We found that total NFAT-3 expression levels were higher in the cytosolic fraction of both the control and the DIO animals (figure 28). Similarly, we found that total GATA-4 expression levels were lower in the nuclear fraction in both control and DIO animals (figure 31). We cannot conclude whether these transcription factors were activated to initiate the transcription of hypertrophic genes, because the phosphorylation status of these proteins was not determined. Despite this, previous data from our laboratory has revealed the presence of myocardial hypertrophy in the DIO animals after 16 weeks on the HCD (Du Toit *et al.,* 2005).

To address the fact that the phosphorylation status of NFAT-3 and GATA-4 was not determined, we used indirect immunofluorescence to visualise NFATc3 and GATA-4 distribution and localisation in cardiomyocytes. These results confirmed the presence of myocardial hypertrophy in the DIO animals, as both NFATc3 and GATA-4 were localised in the perinuclear area of the cytoplasm (figure 34, 35). However, this phenomenon was only seen in some cells. This finding could be attributed to the difficulty of optimising the protocol. One of the challenges experienced was cardiomyocyte adherence. We did not culture these cells, thus the isolation and staining protocols were all performed in one day, in order to avoid contamination. The time frame used to allow these cells to adhere might not have been optimal. There are no other studies which use the same model as the one used in this present study with which we could confirm the present findings. The findings of this present study should, however, not be discredited, as Oliveira RSF *et al.* (2009) also reported this perinuclear localisation. The latter was shown in a knock-in mouse model of heart failure, therefore indicating that upon induction of hypertrophic stimuli these transcription factors are activated to participate in the transcription of genes which promote hypertrophy.

Light microscopy was used to determine cardiomyocyte cell width, another marker of myocardial hypertrophy. We found a significant increase in cardiomyocyte cell width in the DIO animals (figure 38, 39) indicating concentric hypertrophy. This finding is not what we expected to find, as earlier studies suggest that the predominant effect of obesity on LV structure is eccentric LV hypertrophy (LV end diastolic diameter increases in proportion to wall thickness with no change in relative wall thickness) (Messerli FH *et al.,* 1983; Lauer MS *et al.,* 1992; Gottdiener JS *et al.,* 1994; De Simone G *et al.,* 1994). This notion has been supported by some recent studies which show the lack of impact of body size on relative wall thickness despite an increase in LV mass (Kizer JR *et al.,* 2004; Fox E *et al.,* 2004). However, other recent studies indicate that adiposity may be associated with a relatively greater increase in LV wall thickness as compared to LV end diastolic diameter, with an increased relative wall thickness (concentric LV remodelling and concentric LV hypertrophy) being the primary consequence (Mensah GA *et al.,* 1999; Gutin B *et al.,* 1998; Avelar E *et al.,* 2007; Woodiwiss AJ *et al.,* 2008). The uncertainty as to whether obesity promotes primarily eccentric or concentric LV hypertrophy in these studies may be attributed to the use of small study samples (Messerli FH *et al.,* 1983; Gutin B *et al.,* 1998; Wong CY *et al.,* 2004), non-random recruitment approaches (Messerli FH *et al.,* 1983, De Simone G *et al.,* 1994) and the assessment of study groups with a limited blood pressure range (Lauer MS *et al.,* 1992). All these factors thus show that there are many reasons to explain the uncertainty that exists regarding the impact of obesity on LV geometry.

4.2.6 Lung fluid content

Accumulation of fluid in the lungs is used as an indicator of heart failure; this phenomenon is referred to as cardiogenic pulmonary edema (Ware LB and Matthay MA, 2005). Our results therefore show that both the diet and the GSK-3 inhibitor treatment did not induce heart failure in the animals (figure 15).

4.3   Effects of GSK-3 inhibitor treatment

4.3.1   Biometric and metabolic parameters

In the current study we treated the animals with the GSK-3 inhibitor CHIR118637 (CT20026) supplied by Novartis. This GSK-3 inhibitor inhibits target protein kinases in an ATP competitive manner and has been shown to target both the GSK-3α and β isoforms (Cline GW *et al.,* 2002; Meijer L *et al.,* 2004). The main findings on the biometric and metabolic parameters were as follows: In the control animals, the GSK-3 inhibitor treatment increased the body weight, but it had no significant effect on the intraperitoneal fat mass. This increase in body weight was also associated with an increase in serum insulin levels and HOMA-IR value. However, blood glucose levels were within the normal range (table 4). This data indicates that the treatment had an adverse effect on the controls, as these animals show signs of whole body insulin resistance with normoglycemia (table 4). However, the effect does not seem to be as severe as the effect of the diet. In contrast to the control animals, we found no significant differences in body weight or intraperitoneal fat mass in the treated DIO animals. These animals displayed normal blood glucose levels, significantly decreased serum insulin concentration values and no significant differences in the HOMA-IR index (table 4). The results from the treated DIO animals are in agreement with other studies. In a study published by Henriksen EJ and Dokken BB (2006), where they also investigated the effects of chronic GSK-3 inhibition in prediabetic obese Zucker rats, they found no change in body weight. Additionally, they found that fasting plasma glucose was not affected by chronic GSK-3 inhibitor treatment, however, they did report that the fasting serum insulin levels were significantly lowered. In the same study the HOMA-IR values were also significantly reduced in these animals. The latter finding is not in agreement with our results, as we found no significant differences in the HOMA-IR index.

In another independent study Henriksen EJ *et al*. (2003) also demonstrated in Zucker diabetic fatty (ZDF) rat that acute (4h) oral treatment with aminopyrimidine-based GSK-3 inhibitors enhanced oral glucose tolerance and whole body insulin sensitivity. All these results are in agreement with what we are reporting. Our results are novel in that they indicate that chronic GSK-3 inhibitor treatment enhanced fasting whole body insulin sensitivity specifically in the DIO animals. However, in the control animals, chronic GSK-3 inhibition may have adverse effects, as it may promote insulin resistance. We argue that in the pathological state of insulin resistance and downregulation of the phosphorylation of GSK-3, therefore overactive GSK-3, inhibition of GSK-3 will normalise signalling and response in these hearts. However, in the control animals with a normal level of expression and phosphorylation of GSK-3 and a normal response to insulin, inhibition of GSK-3 will lead to pathology, as indicated by our results and discussed in 4.3.3.

4.3.2 Glucose uptake

In the control and DIO animals the GSK-3 inhibitor treatment had no significant effect on glucose uptake at basal level and upon stimulation with 1nM of insulin (figure 12). In both groups a 2-way ANOVA showed a significant overall effect of the treatment upon stimulation with 10nM and 100nM of insulin. Additionally, a paired student t-test showed a significant increase in glucose uptake upon stimulation with 100nM of insulin in the treated DIO animals. The treatment thus normalized glucose uptake in these animals to a similar levels as seen in the untreated control animals. This corroborates other studies that showed that GSK-3 inhibition promotes glucose uptake into cultured human muscle cells (Nikoulina SE *et al.,* 2000), and isolated diabetic rat muscle cells (Ring D *et al.,* 2001). In contrast, Cline GW *et al.* (2002), found no effect of GSK-3 inhibition on insulin stimulation rates of whole body glucose disposal in ZDF (*fa/fa*) rats.

4.3.3 Insulin signalling pathway

In the treated control animals we found no significant differences in total PKB/Akt expression, however, phosphorylated PKB/Akt was down-regulated (figure 18) and the phospho/total ratio (figure 19) was significantly reduced, indicating that less PKB/Akt was phosphorylated in this group. In the treated DIO animals we found no significant differences in total, phospho PKB/Akt and the phospho/total ratio (figure 20, 21).

The lower PKB/Akt activity in the treated control animals ties in well with the conclusion that the treatment seemed to induce insulin resistance in these animals. With respect to the GSK-3 protein we found a significant decrease in total GSK-3β expression levels in the treated control animals. The phospho GSK-3β (Ser^9) was, however, significantly increased (figure 24) and the phospho/total ratio was also increased (figure 25) in these animals, indicating overall inhibition of the kinase. In the treated DIO animals we found no significant differences in total GSK-3β expression levels. The phospho GSK-3β (Ser^9) was significantly decreased (figure 26) and the phospho/total ratio was also decreased (figure 27) in these animals. One explanation for the higher level of phosphorylation of GSK-3 in the hearts of the treated control animals can be that other kinases are involved besides PKB/Akt. Inhibition of GSK-3 will lead to an accumulation of glycogen in these hearts. According to Derave W *et al.* (2000), a high level of glycogen will lead to lower glucose uptake, lower GLUT-4 translocation as well as lower levels of phosphorylation of PKB/Akt, especially after stimulation with insulin. In addition, this increased phosphorylation and inhibition may be responsible for the larger cell size in the cardiomyocytes from treated control animals.

In a study published by Gao HK *et al.* (2008) they also showed that the GSK-3 inhibitor 4-benzyl-2-methyl-1, 2, 4-thiadiazolidine-3, 5-dione (TDZD-8) increased GSK-3 serine-9 phosphorylation and that this was consistent with inactivation of the kinase. In another study, Nikoulina SE *et al.* (2001), reported that following treatment with GSK-3 inhibitor, PKB/Akt expression was unaltered. In the DIO animals we cannot draw any clear conclusions on the effects of the inhibitor on PKB/Akt and GSK-3. In contrast, a lower phospho/total ratio of GSK-3 was documented in the control animals. This would indicate that the kinase was more active in the phase of inhibition. It must be kept in mind that the hearts of the DIO animals were insulin resistant before the onset of the treatment regime.

4.3.4   The development of myocardial hypertrophy

In the treated animals we found a significant increase in ventricular weight in the treated controls, compared to untreated controls, but found no differences in the treated DIO animals, compared to untreated DIO (table 4). Additionally, both the VW/BW and VW/TL ratios revealed no differences in these groups (figure 13, 14). Yin FC *et al.* (1982), proposed that VW/BW ratio may show no differences as a result of age related fluctuations in weight gain and he further proposed that VW/TL ratio be used. These parameters thus indicate that chronic GSK-3 inhibition did not obviously promote myocardial hypertrophy in the treated DIO rats.

The echocardiography data also revealed no significant differences in left ventricular diameters in systole in both groups, however, we observed a significant increase during diastole in the treated control animals (table 5), coinciding with the other documented changes in this group. We found no significant differences in FS in any of the groups, indicating no effect of the treatment on myocardial function. Tissue Doppler Imaging might thus be of use, as it uses more sensitive parameters to quantify both systolic and diastolic dysfunction.

4.3.5   Proteins implicated in the hypertrophic response

Regarding the expression of NFAT-3 and GATA-4 transcription factors we found no significant differences in total NFAT-3 expression levels in the treated control (figure 29) or treated DIO animals (figure 30). However, the significant nuclear export that was observed in the untreated animals (figure 28) was absent, indicating that a higher proportion of NFAT-3 was in the nucleus. We also found no significant differences in total GATA-4 expression levels in the treated control (figure 32) and treated DIO animals (figure 33). But again, the proportional distribution of cytosolic vs. nuclear protein was in favour of a higher proportion of the protein in the nucleus. Total expression levels of these proteins were measured, not their phosphorylation status.

Indirect immunofluorescence was also used to visualise NFATc3 and GATA-4 distribution and localisation in cardiomyocytes. These results confirmed the presence of myocardial hypertrophy both in the treated control and treated DIO animals as both NFATc3 and GATA-4 were localised in the perinuclear area of the cytoplasm (figure 36, 37). Interestingly, this phenomenon was only seen in some cells. Once again this could be as a result of the time frame used to allow these cells to adhere. This might not have been optimal. Unfortunately, there are no other studies which used the same model and treatment regimen as the one used in this present study with which we could confirm our findings.

Light microscopy was used to determine cardiomyocyte cell width, a marker of myocardial hypertrophy. The GSK-3 inhibitor treatment increased cardiomyocyte cell width significantly in the controls, however, in the DIO animals it significantly decreased the cell width (figure 38, 39). This would imply that the treated DIO animals had eccentric hypertrophy. There are no other studies which use the same model and treatment regiment as the one used in this present study with which we could compare our results to.

CHAPTER 5: CONCLUSION

The primary aims of the current study were to document the progression of myocardial hypertrophy in a rat model of pre-diabetes and insulin resistance, and to assess the role of inhibition of the GSK-3 protein on this hypertrophic response. We successfully showed that the high caloric diet promotes the development of insulin resistance and myocardial hypertrophy. We also showed that this insulin resistant state was accompanied by a disruption of the insulin signalling pathway, characterized by alterations in involved proteins, such as PKB/Akt and GSK-3. Regarding the effect of the inhibitor, we observed signs of insulin resistance in control animals, while inhibition of GSK-3 improved the glycemic control in the DIO animals. In addition, treatment of normal control rats with the GSK-3 inhibitor resulted in clear signs of the beginning of myocardial hypertrophy, but did not exacerbate the hypertrophic state in the pre-diabetic animals.

In view of the fact that GSK-3 inhibitors are currently developed for clinical utilization in disease states not associated with obesity, insulin resistance or cardiovascular disease (e.g. muscle hypertrophy, Alzheimer's disease, certain types of cancer and bipolar- and mood disorders, as discussed on page 31), the results from this study is deemed very important as it highlights the possible side effects of such treatment. Interventions targeting protein kinases should therefore be subject to further investigations to establish unknown interactions.

Limitations of this study:

There are many pathways implicated in the development of myocardial hypertrophy, and the current study was limited to focus on the insulin signalling pathway, especially on the role of the GSK-3 protein. Unfortunately, a limited amount of inhibitor for *in vivo* studies was supplied, therefore we were unable to investigate the effect of GSK-3 protein on downstream substrates.

5.1 Future studies

To confirm the effectiveness of the inhibitor *in vivo*, we will investigate the expression and phosphorylation of glycogen synthase protein. Glycogen synthase is a downstream substrate of GSK-3, which plays a role in regulation of glycogen synthesis (MacAulay et al., 2005). We expect to find decreased insulin stimulated phosphorylation. Since we cannot exclude the participation of other pathways we would like to look at key proteins in the Wnt pathway that promote hypertrophy. We also wish to determine the phosphorylation status of NFAT-3 and GATA-4. We would also like to perform Tissue Doppler echocardiography, as this method has been shown to be more sensitive and will allow us to determine more specific parameters for systolic and diastolic dysfunction. Additionally we would like to increase the sample number, as our results show that there are subtle differences, and the small sample number might have been a confounding factor for observing any differences.

CHAPTER 6: REFERENCES

1. ACC/AHA 2005 Guideline Update for the Diagnosis and Management of Chronic Heart Failure in the Adult Summary Article A Report of the American College of Cardiology/ American Heart Association Task Force on Practice Guidelines (Writing Committee to Update the 2001 Guidelines for the Evaluation and Management of Heart Failure). *J Am Coll Cardiol.* 2005; 46: 1116-43.

2. Abel ED. Insulin signaling in heart muscle: lessons from genetically engineered mouse models. *Curr Hypertens Rep*. 2004; 6: 416-423.

3. Abel ED, Litwin SE, Sweeney G. Cardiac remodelling in obesity. *Physiological Reviews*. 2008; 88(2): 389-419.

4. Agrawal R, Agrawal N, Koyani CN, Singh R. Molecular targets and regulators of cardiac hypertrophy. *Pharmacological Research.* 2010; 61: 269-80.

5. Alexander JK. The cardiomyopathy of obesity. *Prog. Cardiovasc Dis*. 1985; 27: 325-334.

6. Alpert MA, Lambert CR, Panayiotou H, Terry BE, Cohen MV, Massey CV, Hashimi MW, Mukerji V. Relation of duration of morbid obesity to left ventricular mass, systolic function, and diastolic filling, and effect of weight loss. *Am J Cardiol*. 1995; 76: 1194-1197.

7. Asai T, Kushiro T, Fujita H, Kanmatsuse K. Different effects on inhibition of cardiac hypertrophy in spontaneously hypertensive rats by monotherapy and combination therapy of adrenergic receptor antagonists and/or the angiotensin II type 1 receptor blocker under comparable blood pressure reduction. *Hypertens Res*. 2005; 28(1): 79-87.

8. Avelar E, Cloward TV, Walker JM, Farney RJ, Strong M, Pendleton RC, Segerson N, Adams TD, Gress RE, Hunt SC, Litwin SE. Left ventricular hypertrophy in severe obesity: interactions among blood pressure, nocturnal hypoxemia, and body mass. *Hypertension*. 2007; 49: 34-39.

9. Baumann CA, Ribon V, Kanzaki M, Thurmond DC, *et al*. CAP defines a second signalling pathway required for insulin-stimulated glucose transport. *Nature*. 2000; 407: 202-207.

10. Belfort R, Mandarino L, Kashyap S, Wirfel K, Pratipanawatr T, Berria R, Defronzo RA, Cusi K. Dose-response effect of elevated plasma free fatty acid on insulin signaling. *Diabetes*. 2005; 54: 1640-1648.

11. Berkalp B, Cesurb V, Corapcioglub D, Erola C, Baskal N. Obesity and left ventricular diastolic dysfunction. *Int J Cardiol*. 1995; 52: 23-26.

12. Bernardo BC, Weeks KL, Pretorius L, McMullen JR. Molecular distinction between physiological and pathological cardiac hypertrophy: Experimental findings and therapeutic strategies. *Pharmacology & Therapeutics*. 2010; 128: 191-227.

13. Bird SD, Doevendans PA, van Rooijen MA, Brutel de la Riviere A, Hassink RJ, Passier R, Mummery CL. The human adult cardiomyocyte phenotype. *Cardiovascular Research*. 2003; 58: 423-434.

14. Björntorp P. The associations between obesity, adipose tissue distribution and disease. *Acta Med Scand Suppl*. 1988; 723: 121-34.

15. Boden G, Chen X, Ruiz J, White JV, Rossetti L. Mechanisms of fatty acid-induced inhibition of glucose uptake. *J Clin Invest*. 1994; 93: 2438-2446.

16. Bogardus C, Lillioja S, Mott DM, Hollenbeck C, Reaven G. Relationship between degree of obesity and in vivo insulin action in man. *Am J Physiol*. 1985; 248: 286-291.

17. Bonora E, Formentini G, Calcaterra F, Lombardi S, Marini F, Zenari L, Saggiani F, Poli M, Perbellini S, Raffaelli A, Cacciatori V, Santi L, Targher, Bonadonna R and Muggeo M. HOMA-estimated insulin resistance is an independent predictor of cardiovascular disease in type 2 diabetic subjects. *Diabetes Care*. 2002; 25: 1135-1141.

18. Boulton TG, Nye SH, Robbins DJ, Ip NY, Radziejewska E, Morgenbesser SD, *et al*. ERKs: a family of protein-serine/threonine kinases that are activated and tyrosine phosphorylated in response to insulin and NGF. *Cell*. 1991; 65: 663-675.

19. Bradford MM. Rapid sensitive method for quantion of microgram quantities of protein utilizing the principle of protein-dye binding. *Analytical Biochemistry*. 1976; 71: 248-254.

20. Brede M, Roell W, Ritter O, Wiesmann F, Jahns R, Haase A, Fleischmann BK, Hein L. Cardiac hypertrophy is associated with decreased eNOS expression in angiotensin AT2 receptor-deficient mice. *Hypertension*. 2003; 42(6): 1177-82.

21. Brownsey RW, Boone AN, Allard MF. Actions of insulin on the mammalian heart: metabolism, pathology and biochemical mechanisms. *Cardiovasc Res*. 1997; 34: 3-24.

22. Brunning JC, Michael MD, Winnay JN, Hayashi T, Horsch D, Accili D et al. A muscle-specific insulin receptor knockout exhibits features of the metabolic syndrome of NIDDM without altered glucose tolerance. *Mol. Cell*. 1998; 2: 559-569.

23. Carroll R, Carley AN, Dyck JRB, Severson D. Metabolic effects of insulin in cardiomyocytes from contrl and diabetic db/db mouse hearts. *Am J Physiol Endocrinol Metab*. 2005; 288: 900-906.

24. Cerf ME, Williams K, Nkomo XI, Muller CJ, Du Toit DF, Louw J and Wolfe-Coote SA. Islet cell response in the neonatal rat after exposure to a high-fat diet during pregnancy. *American Journal of Physiology. Regulatory, Integrative and Comparative Physiology*. 2005; 288: 1122-1128.

25. Cerf ME. High fat diet modulation of glucose sensing in the β-cell. Medical Science. *Monitor*. 2007; 13(1): 13-17.

26. Chadwick WA, Roux S, van der Venter M, Louw J and Oelofsen W. Anti-diabetic effects of Sutherlandia frutescens in Wistar rats fed a diabetogenic diet. *Journal of Ethnophamocology*. 2007; 109: 121-127.

27. Cheatham B, Kahn CR. Insulin action and insulin signalling network. *Endocr Rev.* 1995; 16: 117-142.

28. Ciaraldi TP, Carter L, Mudaliar S, Henry RR. GSK-3beta and control of glucose metabolism and insulin action in human skeletal muscle. *Mol Cell Endocrinol*. 2010; 315(1-2): 153-158.

29. Ciaraldi TP, Nikoulina SE, Bandukwala RA, Carter L, Henry RR. Role of glycogen synthase kinase-3 alpha in insulin action in cultured human skeletal muscle cells. *Endocrinology.* 2007; 148(9): 4393-9.

30. Cline GW, Johnson K, Regittnig W, Perret P, Tozzo E, Xiao L, Damico C and. Shulman GI. Effects of a Novel Glycogen Synthase Kinase-3 Inhibitor on Insulin-Stimulated Glucose Metabolism in Zucker Diabetic Fatty (fa/fa) Rats. *Diabetes.* 2002; 51: 2903-2910.

31. Cline GW, Rothman DL, Magnusson I, Katz LD, Shulman GI. 13C-nuclear magnetic resonance spectroscopy studies of hepatic glucose metabolism in normal subjects and subjects with insulin-dependent diabetes mellitus. *J Clin Invest*. 1994; 94(6): 2369-76.

32. Coffer PJ, Jin J, Woodgett JR. Protein kinase B (c-Akt): a multifunctional mediator of phosphatidylinositol 3-kinase activation. *Biochem J*. 1998; 335 (1): 1-13.

33. Condorelli G, Drusco A, Stassi G, Bellacosa A, Roncarati R, Iaccarino G, Russo MA, Gu Y, Dalton N, Chung C, Latronico MV, Napoli C, Sadoshima J, Croce CM, Ross J Jr. Akt induces enhanced myocardial contractility and cell size in vivo in transgenic mice. *Proc Natl Acad Sci USA*. 2002; 99: 12333-12338.

34. Cross DA, Alessi DR, Cohan P, Andjelkovich M, Hemmings BA. Inhibition of glycogen synthase kinase-3 by insulin mediated protein kinase B. *Nature*. 1995; 378: 785-789.

35. De Freitas Mathias PC, Grassiolli S, Rocha DN, Scomparin DX and Gravena C. Transplantation of pancreatic islets from hyperthalamic obese rats corrects hyperglycemia of diabetic rats. *Transplantation Proceedings*. 2007; 39: 193-195.

36. De Simone G, Daniels SR, Devereux RB, Meyer RA, Roman MJ, de Divitiis O, Alderman MH. Left ventricular mass and body size in normotensive children and adults: assessment of allometric relations and impact of overweight. *J Am Coll Cardiol*. 1992; 20: 1251-1260.

37. Deborah J. Burks and Morris F. White. Section 4: β-Cell Mass and Function in Type 2 Diabetes IRS Proteins and β-Cell Function. *Diabetes*. 2001; 50 (1): 140-145

38. Derave W, Hansen BF, Lund S, Kristiansen S, Richter EA. Muscle glycogen content affects insulin-stimulated glucose transport and protein kinase B activity. *Am J Physiol Endocrinol Metab*. 2000; 279(5): 947-55.

39. Diehl JA, Cheng M, Roussel MF, Sherr CJ. Glycogen synthase kinase-3beta regulates cyclin D1 proteolysis and subcellular localization. *Genes Dev*. 1998; 12(22): 3499-511.

40. Dobbelsteyn CJ, Joffres MR, MacLean DR, Flowerdew G and The Canadian Heart Health Surveys Research Group. A comparative evaluation of waist circumference, waist-to-hip ratio and body mass index as indicators of cardiovascular risk factors. The Canadian Heart Health Surveys. *International Journal of Obesity*. 2001, 25: 652-661.

41. Donthi RV, Huisamen B and Lochner A. Effect of Vanadate and Insulin on Glucose Transport in Isolated Adult Rat Cardiomyocytes. *Cardiovascular Drugs and Therapy 2* 2000; 14: 463-470.

42. Du Toit EF, Nabben M and Lochner A. A potential role for angiotensin ll in obesity induced cardiac hypertrophy and ischaemic/reperfusion injury. *Basic Research in Cardiology.* 2005; 100: 346-354.

43. Du Toit EF, Smith W, Muller C, Strijdom H, Stouthammer B, Woodiwiss AJ, Norton GR, Lochner A. Myocardial susceptibility to ischemic-reperfusion injury in a prediabetic model of dietary-induced obesity. *Am J Physiol Heart Circ Physiol.* 2008; 294(5): 2336-2343.

44. Du X, Edelstein D, Obici S, Higham N, ZouMH, BrownleeM. Insulin resistance reduces arterial prostacyclin synthase and eNOS activities by increasing endothelial fatty acid oxidation. *J Clin Invest.* 2006; 116: 1071-1080.

45. Duflou J, Virmani R, Rabin I, Burke A, Farb A, Smialek J. Sudden death as a result of heart disease in morbid obesity. *Am Heart J.* 1995; 130: 306-313.

46. Dwyer EM, Asif M, Ippolito T, Gillespie M. Role of hypertension, diabetes, obesity, and race in the development of symptomatic myocardial dysfunction in a predominantly minority population with normal coronary arteries. *Am Heart J.* 2000; 139: 297-304.

47. Eckel J, Reinauer H. Insulin action on glucose transport in isolated cardiac myocytes: signaling pathways and diabetes-induced alterations. *Biochemical Society Transaction* 1990; 18: 1125-1127.

48. Eckel RH, Grundy SM, Zimmet PZ. The metabolic syndrome. *Lancet.* 2005; 365: 1415-1428.

49. Eldar-Finkelman H, Krebs EG. Phosphorylation of insulin receptor substrate 1 by glycogen synthase kinase 3 impairs insulin action. *Proc Natl Acad Sci U S A.* 1997; 94(18): 9660-4.

50. Eldar-Finkelman H, Licht-Murava A, Pietrokovski S, Eisenstein M. Substrate competitive GSK-3 inhibitors - strategy and implications. *Biochim Biophys Acta*. 2010; 1804(3): 598-603.

51. Eldar-Finkelman H. Glycogen synthase kinase 3: an emerging therapeutic target. *Trends Mol Med.* 2002; 8(3): 126-32.

52. Eldar-Finkelman H, Schreyer SA, Shinohara MM, LeBoeuf RC, Krebs EG. Increased Glycogen Synthase Kinase-3 Activity in Diabetes- and Obesity-Prone C57BL/6J Mice. *Diabetes.* 1999; 48: 1-5.

53. Fischer Y, Rose H and Kammermeier H. Highly insulin-responsive isolated rat heart muscle cells yielded by a modified isolation method. *Life Sciences* 1991; 49(23): 1679-1688.

54. Fox E, Taylor H, Andrew M, Han H, Mohamed E, Garrison R, Skelton T. Body mass index and blood pressure influences on left ventricular mass and geometry in African Americans. The Atherosclerotic Risk in Communities (ARIC) Study. *Hypertension*. 2004; 44: 55-60.

55. Fruman DA, Cantley LC. Phosphoinositide 3-kinase in immunological systems. *Semin Immunol.* 2002; 14(1): 7-18.

56. Galassi A, Reynolds K, He J. Metabolic syndrome and risk of cardiovascular disease: a meta-analysis. *Am J Med*. 2006; 119(10): 812-9.

57. Gao HK, Yin Z, Zhou N, Feng XY, Gao F, Wang HC. Glycogen synthase kinase 3 inhibition protects the heart from acute ischemia-reperfusion injury via inhibition of inflammation and apoptosis. *J Cardiovasc Pharmacol*. 2008; 52(3): 286-92.

58. Garavaglia GE, Messerli, FH, Nunez BD, Schmieder RE, Grossman E. Myocardial contractility and left ventricular function in obese patients with essential hypertension. *The American Journal of Cardiology*. 1988; 62(9): 594-597.

59. Gottdiener JS, Reda DJ, Materson BJ, Massie BM, Notargiacomo A, Hamburger RJ, Williams DW, Henderson WG. Importance of obesity, race and age to the cardiac structural and functional effects of hypertension. The Department of Veterans Affairs Cooperative Study Group on Antihypertensive Agents. *J Am Coll Cardiol*. 1994; 24: 1492-1498.

60. Graef IA, Mermelstein PG, Stankunas K, Neilson JR, Deisseroth K, Tsien RW, Crabtree GR. L-type calcium channels and GSK-3 regulate the activity of NFATc4 in hippocampal. *Nature*. 1999; 401: 703-8.

61. Gregor MF, Hotamisligil GS. Inflammatory mechanisms in obesity. *Annu Rev Immunol*. 2011; 29: 415-45.

62. Grossman W, Jones, McLaurin LP. Wall stress and patterns of hypertrophy in the human left ventricle. *J Clin Invest*. 1975; 56(1): 56-64.

63. Grundy SM. Obesity, metabolic syndrome, and cardiovascular disease. *J Clin Endocrinol Metab*. 2004; 89(6): 2595-600.

64. Gual P, Le Marchand-Brustel Y, Tanti JF. Positive and negative regulation of insulin signaling through IRS-1 phosphorylation. *Biochimie*. 2005; 87(1): 99-109.

65. Gutin B, Treiber F, Owens S, Mensah GA. Relations of body composition to left ventricular geometry and function in children. *J Paediatr*. 1998; 132: 1023-1027.

66. Hajduch E, Litherland GJ, Hundal HS. Protein kinase B (PKB/Akt)-a key regulator of glucose transport? *FEBS Lett*. 2001; 492(3): 199-203.

67. Hallfrisch J, Cohen L and Reiser S. Effects of feeding rats sucrose in a high fat diet. *The Journal of Nutrition*. 1981; 111: 531-536.

68. Haq S, Choukroun G, Kang ZB, Ranu H, Matsui T, Rosenzweig A, Molkentin JD, Alessandrini A, Woodgett J, Hajjar R, Michael A, Force T. Glycogen synthase kinase-3beta is a negative regulator of cardiomyocyte hypertrophy. *J Cell Biol*. 2000; 151(1): 117-30.

69. Henriksen EJ, Dokken BB. Role of glycogen synthase kinase-3 in insulin resistance and type 2 diabetes. *Curr Drug Targets*. 2006; 7(11): 1435-41.

70. Henriksen EJ, Kinnick TR, Teachey MK, O'Keefe MP, Ring D, Johnson KW, Harrison SD. Modulation of muscle insulin resistance by selective inhibition of GSK-3 in Zucker diabetic fatty rats. *Am J Physiol Endocrinol Metab*. 2003; 284(5): 892-900.

71. Hicks R. Combating childhood obesity. *Health*. 2006.

72. Hirashima Y, Tsuruzoe K, Kodama S, Igata M, Toyonanga T, Ueki K et al. Insulin down-regulates insulin receptor substrate-2 expression through the phosphatidylinositol 3-kinase/Akt pathway. *J. Endocrinol*. 2003; 179: 253-266.

73. Hoeflich KP, Luo J, Rubie EA, Tsao MS, Jin O, Woodgett JR. Requirement for glycogen synthase kinase-3beta in cell survival and NF-kappaB activation. *Nature*. 2000; 406(6791): 86-90.

74. Hogan PG, Chen L, Nardone J, Rao A. Transcriptional regulation by calcium, calcineurin, and NFAT. *Genes Dev*. 2003; 17: 2205-32.

75. Huang S and Czech MP. The GLUT4 glucose transporter. *Cell Metabolism*. 2007; 5: 237–252.

76. Hubert HB, Feinleib M, McNamara PM and Castelli WP. Obesity as an independent risk factor for cardiovascular disease: a 26-year follow-up of participants in the Framingham Heart Study. *Circulation*. 1983; 67: 968-977.

77. Huisamen B, Donthi RV and Lochner A. Insulin in Combination with Vanadate Stimulates Glucose Transport in Isolated Cardiomyocytes from Obese Zucker Rats. *Cardiovascular Drugs and Therapy*. 2001; 15: 445-452.

78. Huisamen B, Genis A, Marais E, Lochner A. Pre-treatment with a DPP-4 inhibitor is infarct sparing in hearts from obese, pre-diabetic rats. *Cardiovasc Drugs Ther*. 2011; 25(1): 13-20.

79. Hutley L, Prins JB. Fat as an endocrine organ: relationship to the metabolic syndrome. *Am J. Med. Sci.* 2005; 330: 280-289.

80. Iyer SN, Katovich MJ. Fructose feeding in rats is not associated with sodium retention. *Am J Hypertens.* 1996; 9(10 Pt 1): 1018-23.

81. Ichida M and Finkel T. Ras regulates NFAT3 activity in cardiac myocytes. *J Biol Chem.* 2001; 276: 3524-30

82. Jacob R, Gulch RW. The functional significance of ventricular geometry for the transition from hypertrophy to cardiac failure. Does a critical degree of structural dilatation exist? *Basic Res Cardiol*. 1998; 93: 423-9.

83. Jacobs S, Cuatrecasas P. Insulin receptor: structure and function. *Endocr Rev.* 1981; 2: 251-263.

84. James PT, Rigby N and Leach R. International obesity task force. The obesity epidemic, metabolic syndrome and future prevention strategies. *Eur. J. Cardiovasc. Prev. Rehabil*. 2004; 11: 3-8.

85. Jope RS and Johnson GVW. The glamour and gloom of glycogen synthase kinase -3. *Trends in Biochemical Sciences*. 2004; 29(2): 95-102.

86. Kelly T, Yang W, Chen CS, Reynolds K, He J. Global burden of obesity in 2005 and projections to 2030. *Int J Obes (Lond)*. 2008; 32(9): 1431-7.

87. Kenchaiah S, Evans JC, Levy D, Wilson PW, Benjamin EJ, Larson MG, Kannel WB, Vasan RS. Obesity and the risk of heart failure. *N Engl J Med* 2002; 347: 305-313.

88. Khan AH, Pessin JE. Insulin regulation of glucose uptake: a complex interplay of intracellular signalling pathways. *Diabetologia.* 2002; 45: 1475-1483.

89. Kido Y, Nakae J, Accili D. The insulin receptor and its cellular targets. *J. Clin. Endocrinol Metab*. 2001; 86: 972-9.

90. Kim WY, Wang X, Wu Y *et al*. GSK-3 is a master regulator of neural progenitor homeostasis. *Nature Neuroscience*. 2009; 12(11): 1390-1397.

91. Kizer JR, Arnett DK, Bella JN, Paranicas M, Rao DC, Province MA, Oberman A, Kitzman DW, Hopkins PN, Liu JE, Devereux RB. Differences in left ventricular structure between black and white hypertensive adults: the Hypertension Genetic Epidemiology Network study. *Hypertension*. 2004; 43: 1182-1188.

92. Klein L, O'Connor CM, Gattis WA, Zampino M, de Luca L, Vitarelli A, Fedele F, Gheoghiade M. Pharmacologic therapy for patients with chronic heart failure and reduced systolic function: review of trials and practical considerations. *Am J Cardiol*, 2003; 91: 18-40.

93. Klein PS, Melton DA. A molecular mechanism for the effect of lithium on development. *Proc Natl Acad Sci U S A*. 1996; 93(16): 8455-9.

94. Klinzing S, Lesser T, Schubert H, Bartel M, Klein U. Wet-to-dry ratio of lung tissue and surfactant outwash after one-lung flooding. *Res Exp Med*. 2000; 200(1): 27-33.

95. Laemmli UK. Cleavage of structural proteins during the assembly of the head of bacteriophage T4. *Nature*. 1970; 227: 680-685.

96. Lauer MS, Anderson KM, Kannel WB, Levy D. The impact of obesity on left ventricular mass and geometry. The Framingham Heart Study. *JAMA*. 1991; 266: 231-236.

97. Lauer MS, Anderson KM, Levy D. Separate and joint influences of obesity and mild hypertension on left ventricular mass and geometry: The Framingham Heart Study. *J Am Coll Cardiol*. 1992; 19: 130-134.

98. Lawrence JC Jr, Roach PJ. New insights into the role and mechanism of glycogen synthase activation by insulin. *Diabetes*. 1997; 46(4): 541-7.

99. Lee J, Kim MS. The role of GSK3 in glucose homeostasis and the development of insulin resistance. *Diabetes Res Clin Pract*. 2007; 77 Suppl 1: S49-57.

100.   Lewis GF, Carpentier A, Adeli K, Giacca A. Disordered fat storage and mobilization in the pathogenesis of insulin resistance and type 2 diabetes. *Endocr Rev*. 2002; 23(2): 201-229.

101.   Licata G, Scaglione R, Barbagallo M, Parrinello G, Capuana G, Lipari R, Merlino G, Ganguzza A. Effect of obesity on left ventricular functional studies by radionuclide angiocardiography. *Int. J. Obes*. 1991; 15: 295-302.

102.   Lopaschuck GD, Folmes CDL, Stanley WC. Cardiac energy metabolism in obesity. *Circ Res*. 2007; 101: 335-47.

103.   Lorber R, Gidding SS, Daviglus ML, Colangelo LA, Liu K, Gardin JM. Influence of systolic blood pressure and body mass index on left ventricular structure in healthy African-American and white young adults: the CARDIA study. *J Am Coll Cardiol*. 2003; 41: 955-960.

104.   Lowry OH, Rosenbrough NJ, Farr AL and Randall RJ. Protein measurement with the Folin phenol reagent. *Journal of Biological Chemistry*. 1951; 193: 265-275.

105.   MacAulay K, Blair AS, Hajduch E, Terashima T, Baba O, Sutherland C, Hundal HS. Constitutive activation of GSK3 down-regulates glycogen synthase abundance and glycogen deposition in rat skeletal muscle cells. *J Biol Chem*. 2005; 280(10): 9509-18.

106. Maier S, Aulbach F, Simm A, Lange V, Langenfeld H, Behre H, Kersting U, Walter U, KirsteinM. Stimulation of L-type Ca2+ current in human atrial myocytes by insulin. Cardiovasc Res. 1999; 44: 390-397.

107. Manning BD, Cantley LC. AKT/PKB signaling: navigating downstream. *Cell.* 2007; 129(7): 1261-74.

108. Markou T, Cullingford TE, Giraldo A, Weiss SC, Alsafi A, Fuller SJ, Clerk A, Sugden PH. Glycogen synthase kinases 3alpha and 3beta in cardiac myocytes: regulation and consequences of their inhibition. *Cell Signal.* 2008; 20(1): 206-18.

109. Matthews DR, Hosker JP, Rudenski AS, Naylor BA, Treacher DF, Turner RC: Homeostasis model assessment: Insulin resistance and beta-cell function from fasting plasma glucose and insulin concentrations in man. *Diabetologia.* 1985; 28: 412-419.

110. Meijer L, Flajolet M, Greengard P. Pharmacological inhibitors of glycogen synthase kinase 3. *Trends in Pharmacological Science.* 2004; 25(9): 472-480.

111. Mendoza J, Pévet P, Challet E. High-fat feeding alters the clock synchronization of light. *J Physiol.* 2008; 586(24): 5901-5910.

112. Mensah GA, Treiber FA, Kapuku GK, Davis H, Barnes VA, Strong WB. Patterns of body fat deposition in youth and their relation to left ventricular markers of adverse cardiovascular prognosis. *Am J Cardiol.* 1999; 84: 583-588.

113. Messerli FH, Sundgaard-Riise K, Reisin ED, Dreslinski GR, Ventura HO, Oigman W, Frohlich ED, Dunn FG. Dimorphic cardiac adaptation to obesity and arterial hypertension. *Ann Intern Med.* 983; 99: 757-761.

114. Messerli FH, Ventura HO, Reisin E, Dreslinki GR, Dunn FG, Mac Phee AA, Frohlich ED. Borderline hypertension and obesity: two prehypertensive states with elevated cardiac output. *Cirrulation.* 1982; 66(1): 55-60.

115.   Michael A, Haq S, Chen X, Hsich E, Cui L, Walters B, Shao Z, Bhattacharya K, Kilter H, Huggins G, Andreucci M, Periasamy M, Solomon RN, Liao R, Patten R, Molkentin JD, Force T. Glycogen synthase kinase-3beta regulates growth, calcium homeostasis, and diastolic function in the heart. *J Biol Chem*. 2004. 279(20): 21383-93.

116.   Mlinar B, Marc J, Janez A, Pfeifer M. Molecular mechanisms of insulin resistance and associated diseases. *Clin Chim Acta*. 2007; 375(1-2): 20-35.

117.   Mokdad AH, Bowman BA, Ford BA, Ford ES, Vinicor F, Marks JS and Koplan JP. The continuing epidemics of obesity and diabetes in the United States. *JAMA*. 2001; 286: 1195-1200.

118.   Molkentin JD, Lu JR, Antos CL, Markham B, Richardson J, Robbins J, Grant SR, Olson EN. A calcineurin-dependent transcriptional pathway for cardiac hypertrophy. *Cell*. 1998; 93: 215-228.

119.   Molkentin JD. The zinc finger-containing transcription factors GATA-4, -5, and -6: ubiquitously expressed regulators of tissue-specific gene expression. *J Biol Chem.* 2000; 275: 38949-52.

120.   Morisco C, Lembo G, Trimarco B. Insulin resistance and cardiovascular risk: New insights from molecular and cellular biology. *Trends Cardiovasc Med*. 2006; 16(6): 183-8.

121.   Morisco C, Seta K, Hardt SE, Lee Y, Vatner SF, Sadoshima J. Glycogen synthase kinase 3*beta* regulates GATA-4 in cardiac myocytes. *J Biol Chem*. 2001; 276: 28586-97.

122.   Morisco C, Zebrowski D, Condorelli G, Tsichlis P, Vatner SF, Sadoshima J. The Akt-glycogen synthase kinase 3beta pathway regulates transcription of atrial natriuretic factor induced by beta-adrenergic receptor stimulation in cardiac myocytes. *J Biol Chem.* 2000; 275: 14466-75.

123. Mukai F, Ishiguro K, Sano Y, Fujita SC. Alternative splicing isoforms of tau protein kinase I/glycogen synthase kinase 3β is targeted to growing neuritis and growth cones. *Molecular and Cellular Neurochemistry.* 2010; 42(3): 184-194.

124. Muniyappa R, Montagnani M, Koh KK, Quon MJ. Cardiovascular actions of insulin. *Endocr Rev.* 2007; 28: 463-491.

125. Murphy E, Steenbergen C. Inhibition of GSK-3beta as a target for cardioprotection: the importance of timing, location, duration and degree of inhibition. *Expert Opin Ther Targets*. 2005; 9(3): 447-56.

126. Nadal-Ginard B, Kajstura J, Leri A, Anversa P. Myocyte death, growth and regeneration in cardiac hypertrophy and failure. *Circ Res*. 2003; 92: 139–50.

127. National institute of health (NIH) PUBLICATION NO. 98-4083. The Evidence Report. SEPTEMBER 1998;

http://www.nhlbi.nih.gov./nhlbi/cardio/obes/prof/guidelns/ob_home. Accessed May 2011

128. Nikoulina SE, Ciaraldi TP, Carter L, Cha B-S, Johnson K, Henry RR: Role of glycogen synthase kinase-3 in regulation of glucose metabolism and insulin action in human skeletal muscle cells (Abstract). *Diabetes*. 2000; 49 (1).

129. Nikoulina SE, Ciaraldi TP, Carter L, Mudaliar S, Park KS, Henry RR. Impaired muscle glycogen synthase in type 2 diabetes is associated with diminished phosphatidylinositol 3-kinase activation. *J Clin Endocrinol Metab*. 2001; 86(9): 4307-14.

130. Ogden CL, Carroll MD, Curtin LR, McDowell MA, Tabak CJ and Flegal KM. Prevalence of overweight and obesity in the United States, 1999-2004. *JAMA*. 2006; 295: 1549-1555.

131. Okamoto H, Nakae J, Kitamuru T, Park BC, Dragatsis I, Accili D. Transgenic rescue of insulin receptor deficient mice. *J. Clin Invest*. 2004; 114: 214-223.

132.   Oliveira RSF , Ferreira1 JCB, Gomes ERM, Paix̃ao NA, Rolim NPL, Medeiros A, Guatimosim S Brum PC. Cardiac anti-remodelling effect of aerobic training is associated with a reduction in the calcineurin/NFAT signalling pathway in heart failure mice. *J Physiol*. 2009; 587.15: 3899–3910.

133.   Olshansky SJ, Passaro DJ, Hershow RC, Layden J, Carnes BA, Brody J, Hayflick L, Butler RN, Allison DB and Ludwig DS. A potential decline in life expectancy in the United States in the 21st century. *N Engl J. Med*. 2005; 352(11): 1138-45.

134.   Opie L.H. The heart: Physiology from cell to circulation. Second edition. New York. Raven Press. 1991; p184-185, p396-400.

135.   Pan DA, Lillioja S, Kriketos AD, Milner MR, Baur LA, et al. Skeletal muscle triglyceride levels are inversely related to insulin action. *Diabetes*. 1997; 46: 983-988.

136.   Parizkova J, Chin M-K, Chia M and Yang J. An international perspective on obesity, health and physical activity: current trends and challenges in China and Asia. *Exerc Sci Fit*. 2007; 5(1): 7-23.

137.   Park KW, Yang HM, Youn SW, Yang HJ, Chae IH, Oh BH, Lee MM, Park YB, Choi YS, Kim HS, Walsh K. Constitutively active glycogen synthase kinase-3beta gene transfer sustains apoptosis, inhibits proliferation of vascular smooth muscle cells, and reduces neointima formation after balloon injury in rats. *Arterioscler Thromb Vasc Biol*. 2003; 23(8): 1364-9.

138.   Pascual M, Pascual DA, Soria F et al. Effects of isolated obesity on systolic and diastolic left ventricular function. *Heart (British Cardiac Society)*. 2003; 89(10): 1152-1156.

139.   Passier R, Zeng H, Frey N, Naya FJ, Nicol RL, McKinsey TA, Overbeek P, Richardson JA, Grant SR, Olson EN. CaM kinase signaling induces cardiac hypertrophy and activates the MEF2 transcription factor in vivo. *J Clin Invest*. 2000; 105: 1395-1406.

140.   Patient RK, McGhee JD. The GATA family (vertebrates and invertebrates). *Curr Opin Genet Dev*. 2002; 12: 416-22.

141.   Peterson LR, Herrero P, Schechtman KB, Racette SB, Waggoner AD, Kisrieva-Ware Z, Dence C, Klein S, Marsala J, Meyer T, Gropler RJ. Effect of obesity and insulin resistance on myocardial substrate metabolism and efficiency in young women. *Circulation*. 2004; 109: 2191-2196.

142.   Pickavance LC, Tadayyon M, Widdowson PS, Buckingham RE and Wilding JP. Therapeutic index for rosiglitazone in dietary obese rats: separation of efficacy and haemodilution. *British Journal of Pharmacology*. 1999; 128: 1570-1576.

143.   Pikkarainen S, Tokola H, Kerkela R, Ruskoaho H. GATA transcription factors in the developing and adult heart *Cardiovas Res*. 2004; 63: 196-207.

144.   Pittas AG, Joseph NA and Greenberg AS. Adipocytokines and Insulin Resistance. *Journal of Clinical Endocrinology & Metabolism.* 2004; 89: 447-452.

145.   Pluim BM, Zwinderman AH, van der Laarse A, van der Wall EE. The athlete's heart. A meta-analysis of cardiac structure and function. *Circulation*. 2000; 101(3): 336-344.

146.   Puoane T, Steyn K, Bradshaw D, Laubscher R, Fourie J, Lambert V, Mbananga N. Obesity in South Africa: the South African demographic and health survey. *Obes Res*. 2002; 10(10):1038-48.

147.   Ramirez MT, Zhao XL, Schulman H, Brown JH. The nuclear B isoform of Ca2+/calmodulin-dependent protein kinase II regulates atrial natriuretic factor gene expression in ventricular myocytes. *J Biol Chem*. 1997; 272: 31203-31208.

148.   Rayasam GV, Tulasi VK, Sodhi R, Davis JA and Ray A. Glycogen synthase kinase 3: more than a namesake. *British Journal of Pharmacology*. 2009; 156: 885-898.

149.   Reaven GM. Banting lecture 1988. Role of insulin resistance in human disease. *Diabetes*. 1988; 37: 1595-607.

150.	Reffelmann T and Kloner RA. Transthoracic echocardiography in rats. Evaluation of commonly used indices of left ventricular dimensions, contractile performance, and hypertrophy in a genetic model of hypertrophic heart failure (SHHF-Mcc-facp-Rats) in comparison with Wistar rats during aging. *Basic Res Cardiol*. 2003; 98 (5): 275-284.

151.	Rennison JH, McElfresh TA, Okere IC, Vazquez EJ, Patel HV, Foster AB, Patel KK, Chen Q, Hoit BD, Tserng KY, Hassan MO, Hoppel CL, Chandler MP. High-fat diet postinfarction enhances mitochondrial function and does not exacerbate left ventricular dysfunction. *AJP-Heart Circ Physiol*. 2007; 292: 1498-1506.

152.	Ring D, Johnson K, Henricksen E, Nuss J, Goff D, Kinnick T, Ma S, Reeder J, Samuels I, Slabiak T, Wagman A, Wernette-Hammond ME, Harrison SD: Glycogen synthase kinase-3 (GSK3) inhibitors potentiate glucose tolerance and muscle glycogen synthase activity and glucose uptake in the Zucker Diabetic Fatty (ZDF) rat (Abstract). *Diabetes.* 2001: 50 (2).

153.	Rosendal S and Black FT. Direct and Indirect Immunofluorescence of Unfixed and Fixed Mycoplasma Colonies. *Acta Pathologica Microbiologica Scandinavica Section B Microbiology and Immunology* 1972; 4(80B): 615-622.

154.	Saltiel AR and Kahn R. Insulin signaling and the regulation of glucose and lipid metabolism. *Nature.* 2001; 414: 799-806.

155.	Saltiel AR, Pessin JE. Insulin signaling in microdomains of the plasma membrane. *Traffic*. 2003; 4(11): 711-6.

156.	Saltiel AR. New perspectives into the molecular pathogenesis and treatment of type 2 diabetes. *Cell*. 2001; 104, 517-529.

157.	Saupe KW, Sobol SC, Koh SG, Apstein CS. Effects of AT1 receptor block begun late in life on normal cardiac aging in rats. *J Cardiovasc Pharmacol*. 2003; 42(4): 573-80.

158. Sesti G. Pathophysiology of insulin resistance. Best Practice and Research. *Clinical Endocrinology and Metabolism* 2006; 20 (4): 665-679.

159. Sethi JK, Vidal-Puig AJ. Thematic review series: adipocyte biology. Adipose tissue function and plasticity orchestrate nutritional adaptation. *J Lipid Res*. 2007; 48(6):1253-1262.

160. Seufert J. Leptin effects on pancreatic (beta)-cell gene expression and function. *Diabetes* 2004; 53:152-158.

161. Shao J, Yamashita H, Qiao I, Friedman L. Deceased Akt kinase activity and insulin resistance in C57BL/KsJ-Lepr db/db mice. *J Endocrinol*. 2000; 167: 107-115.

162. Shepherd PR. Mechanisms regulating phosphoinositide 3-kinase signalling in insulin-sensitive tissues. *Acta Physiol Scand*. 2005; 183(1): 3-12.

163. Shoelson SE, Boni-Schnetzler M, Pilch PF, Kahn CR. Autophosphorylation within insulin receptor beta-subunits can occur as an intramolecular process. *Biochemistry*. 1991; 30(31): 7740-6.

164. Shulman GI, Rothman DL, Jue T, Stein P, DeFronzo RA, Shulman RG. Quantitation of muscle glycogen synthesis in normal subjects and subjects with non-insulin-dependent diabetes by 13C nuclear magnetic resonance spectroscopy. *N Engl J Med*. 1990; 322(4): 223-8.

165. Skoumal R, Seres L, Soós P, Balogh E, Kovàts T, Rysa J, Ruskoaho H, Tóth M, Horkay F. Endothelin levels in experimental diabetes combined with cardiac hypertrophy. *J Cardiovasc Pharmacol*. 2004; 44: S195-S197.

166. Stepniakowski KT, Goodfriend TL, Egan BM**.** Fatty acids enhance vascular _-adrenergic sensitivity. *Hypertension*. 1995; 25: 774-778.

167. Stoddard MF, Tseuda K, Thomas M, Dillon S, Kupersmith J. The influence of obesity on left ventricular filling and systolic function. *Am Heart J*. 1992; 124: 694-699.

168. Sutherland C. What Are the *bona fide* GSK3 Substrates? *International Journal of Alzheimer's Disease*. 2011; 2011: 1-23.

169. Thévenod F. Pathophysiology of diabetes mellitus type 2: roles of obesity, insulin resistance and β-cell dysfunction, In Masur K, Thévenod F, Zänker KS (Eds). *Diabetes and Cancer*. 2008; 19: 1-18.

170. Tokudome T, Horio T, Kishimoto I, Soeki T, Mori K, Kawano Y, Kohno M, Garbers DL, Nakao K, Kangawa K. Calcineurin–Nuclear Factor of Activated T Cells Pathway–Dependent Cardiac Remodeling in Mice Deficient in Guanylyl Cyclase A, a Receptor for Atrial and Brain Natriuretic Peptides. *Circulation*. 2005; 111: 3095-3104.

171. Tschöp M, Heiman ML. Rodent obesity models: an overview. *Exp Clin Endocrinol Diabetes* 2001;109:307–319.

172. Unger RH. Lipotoxicity in the pathogenesis of obesity-dependent NIDDM: Genetic and clinical implications. *Diabetes*. 1995; 44: 863-870.

173. Urbina EM, Gidding SS, Bao W, Pickoff AS, Berdusis K, Berenson GS. Effect of body size, ponderosity, and blood pressure on left ventricular growth in children and young adults in the bogalusa heart study. *Circulation*. 1995; 91: 2400-2406.

174. Utriainen T, Lovisatti S, Mäkimattila S, Bertoldo A, Weintraub S, DeFronzo R, Cobelli C and Yki-Järvinen H. Direct measurement of the lumped constant for 2-deoxy-[1-14C] glucose in vivo in human skeletal muscle. *American Journal of Physiology. Endocrinology and Metabolism*. 2000; 279: 228-233.

175. van Obberghen E, Baron V, Delahaye L, Emanuelli B, Filippa N, Giorgetti-Peraldi S, Lebrun P, Mothe-Satney I, Peraldi P, Rocchi S, Sawka-Verhelle D, Tartare-Deckert S, Giudicelli J. Surfing the insulin signaling web. *Eur J Clin Invest*. 2001; 31(11): 966-77.

176. van Wauwe J, Haefner B. Glycogen synthase kinase-3 as drug target: from wallflower to center of attention. *Drug News Perspect*. 2003; 16(9): 557-65.

177.   Vázquez-Vela ME, Torres N, Tovar AR. White adipose tissue as endocrine organ and its role in obesity. *Arch Med Res*. 2008; 39(8): 715-28.

178.   von Lewinski D, Bruns S, Walther S, Kogler H, Pieske B. Insulin causes [Ca2+]i-dependent and [Ca2+i-independent positive inotropic effects in failing human myocardium. *Circulation.* 2005; 111: 2588–2595.

179.   Wang X, Ren B, Liu S, Sentex E, Tappia PS, Dhalla NS. Characterization of cardiac hypertrophy and heart failure due to volume overload in the rat. *J Appl Physiol*. 2003; 94(2): 752-63.

180.   Ware LB, Matthay MA. Clinical practice. Acute pulmonary edema. *N Engl J Med*. 2005; 353(26): 2788-96.

181.   Watanabe S, Tagawa T, Yamakawa K, Shimabukuro M, Ueda S**.** Inhibition of the renin-angiotensin system prevents free fatty acid-induced acute endothelial dysfunction in humans. *Arterioscler Thromb Vasc Biol*. 2005; 25: 2376–2380.

182.   Watson RT and Pessin JE. Subcellular compartmentalization and trafficking of the insulin-responsive glucose transporter, GLUT4. *Exp. Cell Res.* 2001; 271: 75-83.

183.   Watson RT, Saltiel AR, Pessin JE, Kanzaki M (2007). Mechanisms of insulin action: Subcellular compartmentalization of insulin signalling processes and GLUT4 trafficking events. New York: Springer Science and Landes Bioscience.

184.   Welsh GI, Proud CG. Glycogen synthase kinase-3 is rapidly inactivated in response to insulin and phosphorylates eukaryotic initiation factor eIF-2B. *Biochem J.* 1993; 294 (Pt 3): 625-9.

185.   Welsh GI, Stokes CM, Wang X, Sakaue H, Ogawa W, Kasuga M, Proud CG. Activation of translation initiation factor eIF2B by insulin requires phosphatidyl inositol 3-kinase. *FEBS Lett.* 1997; 410(2-3): 418-22.

186.   White MF. IRS proteins and the common path to diabetes. *Am J Physiol Endocrinol Metab*. 2002; 283(3) 413-22.

187.   Wilkins BJ, De Windt LJ, Bueno OF, Braz JC, Glascock BJ, Kimball TF, Molkentin JD. Targeted disruption of NFATc3, but not NFATc4, reveals an intrinsic defect in calcineurin-mediated cardiac hypertrophic growth. *Mol Cell Biol*. 2002; 22: 7603-13.

188.   Wojtaszwewski JF, Higaki Y, Hirshman MF, Michael MD, Dufresne SD, Kahn CR et al. Exercise modulates postreceptor insulin signalling and glucose transport in muscle-specific insulin receptor knock-out mice. *J. Clin. Invest*. 1999; 104: 1257-1264.

189.   Wong CY, O'Moore-Sullivan T, Leano R, Byrne N, Beller E, Marwick TH. Alterations of left ventricular myocardial characteristics associated with obesity. *Circulation*. 2004; 110(19): 3081-3087.

190.   Woodgett JR, Cohen P. Multisite phosphorylation of glycogen synthase. Molecular basis for the substrate specificity of glycogen synthase kinase-3 and casein kinase-II (glycogen synthase kinase-5). *Biochim Biophys Acta*. 1984; 788(3): 339-47.

191.   Woodgett JR. Judging a protein by more than its name: GSK-3. *Sci STKE*. 2001; 2001(100):re12.

192.   Woodgett JR. Molecular cloning and expression of glycogen synthase kinase-3/factor A. *EMBO J*. 1990; 9(8): 2431-8.

193.   Woodgett JR. Regulation and functions of the glycogen synthase kinase-3 subfamily. *Semin Cancer Biol*. 1994; 5(4): 269-75.

194.   Woodiwiss AJ, Libhaber CD, Majane OHI, Libhaber E, Maseko M, Norton GR. Obesity promotes left ventricular concentric rather than eccentric geometric remodeling and hypertrophy independent of blood pressure. *Am J Hypertens*. 2008; 21: 1144-1151.

195. World Health Organization (WHO). Obesity: Prevention and managing the global epidemic. Report of a WHO Consultation. WHO Technical Report Series 894. World Health Organization, Geneva, Switzerland, 2000.

196. World Health Organization: Overweight and obesity; fact sheet 311. Available at http://www.who.int/mediacentre/fact-sheet/fs311/en/index.html. Accessed May 20, 2011.

197. Wu X and Garvey WT (2011). Textbook of diabetes: Insulin action. (4th edition). West Sussex United Kingdom: Blackwell Publishing Ltd.

198. Yin FC, Spurgeon HA, Rakusan K, Weisfeldt ML, Lakatta EG. Use of tibia length to quantify cardiac hypertrophy: application in the aging rat. Am J Physiol 1982; 243(6): H941-7.

199. Zarich SW, Kowalchuk GJ, McGuire MP, Benotti PN, Mascioli EA, Nesto RW. Left ventricular filling abnormalities in asymptomatic morbid obesity. *Am J Cardiol*. 1991; 68: 377-381.

200. Zeng G, Quon MJ. Insulin-stimulated production of nitric oxide is inhibited by wortmannin. Direct measurement in vascular endothelial cells. J Clin Invest. 1996; 98: 894–898.

201. Zhuang GQ, Wu W, Liu F, Ma JL, Luo YX, Xiao ZX, Liu Y, Wang W, He Y. SNAP-25 (1-180) enhances insulin secretion by blocking Kv2.1 channels in rat pancreatic islet beta-cells. *Biochem Biophys Res Commun*. 2009; 379(4): 812-6.